sciendo

Journal of Environmental Geography 14 (1–2), 1–14.

DOI: 10.2478/jengeo-2021-0001
ISSN 2060-467X

ENVIRONMENTAL HISTORY OF RICE PLANTATIONS IN THE EARLY MODERN OTTOMAN EMPIRE BETWEEN THE 15TH AND 19TH CENTURIES AND ITS POTENTIAL FOR CLIMATE RESEARCH

Özlem Sert[1]*

[1]Department of History and Urban Studies Center, Hacettepe University Ankara,
06800 Beytepe, Ankara, Turkey
Tel.: +90 (542) 3032275 ORCiD ID: 0000-0002-5759-1089
*Corresponding author, e-mail: oezlemsert@gmail.com

Research article, received 25 November 2020, accepted 15 January 2021

Abstract

Historians readily discuss the effect of climate change on the 21st century, but Ottomanists rarely reference palaeoclimatology data. This research compares palaeoclimatological data with documentary evidence from institutionalized rice plantations in the Ottoman Empire. Between the 15th and 19th centuries, the empire employed a group of experts for the cultivation of rice in the vast region between the Tigris and the Danube. Extensive registers exist from this period in archives that give documentary evidence about the organization of plantations, yields, prices and destructive floods. The objective of the study, as presented in this article, is to find rice-related phenological data in Ottoman Archive registers. It utilizes a comparative analysis of the Old World Drought Atlas (OWDA) summer precipitation data reconstructed by Cook et al. (2015), temperature changes, documentary evidence about seasonal extremes and archival evidence. The comparison shows that palaeoclimatology proxies are important sources of information regarding changes in rice cultivation. It also indicates that the Ottoman archive is a valuable source of possible phenological data. Thus, research sources from nature and societies complement one another. The comparison also demonstrates that climate change during the Ottoman Empire's reign showed regional differences, and a local comparison of phenological data and palaeoclimatological data can explain more about the effects of the Little Ice Age (LIA) on the empire.

Keywords: Climate History, Environmental History, Ottoman History, Rice Farming, Phenology, Palaeoclimatology

INTRODUCTION

The climate extremes of the Little Ice Age were a trigger for the development of the modern state's institutional structure (Parker, 2013). After the so-called early-modern gunpowder revolution of the 16th century, anthropogenic intrusions into the environment grew significantly all over the world (Ágoston, 2009). New institutional bodies in absolutist states enforced the large-scale displacement of plants, animals, human beings and raw materials. Empires employed plant breeders, who experimented with new hybrid forms to increase crop yields and enhance variation. The early modern era was a period of agronomic challenges (Murphy, 2007). The appropriate location of plantations, using the right varieties, coordinating the workforce and ensuring sustainable production was a great institutional challenge at a time of climate change. Cash crops such as sugar cane, rice, coffee, cacao, tea and tobacco had a substantial social and environmental impact in the regions where they were planted. Rice was one of the products that transformed the socio-ecological landscapes in its foodway from China and India to the Middle East, Europe and the Americas. Sugar cane and rice were among those plants diffused westwards from South Asia to the Middle East and Europe during the Arab Agricultural Revolution between the 8th and 13th centuries (Watson, 1981; Canard, 1959). Rice, the main staple of Indian and Chinese cuisines, first entered the courts of Middle Eastern sultans on its way from Persia and the Mamluk Empire to Ottoman lands. The demand for rice as a luxury cash crop in growing local markets rose hand in hand with the increasing specialization of production activities in Ottoman cities. Although rice production was known in Southeast Europe before the 14th century, there was no extensive production before the Ottomans founded institutionalized rice plantations in the 14th and 15th centuries (İnalcık, 1982). The Ottoman Empire was one of the empires that introduced agronomic challenges and experienced fundamental institutional changes in the early modern era.

Rice plantations in the Ottoman Empire have drawn the attention of many scholars for their political and economic importance (Gökbilgin, 1952; Barkan, 1963; Beldiceanu et al., 1978; İnalcık, 1982; Arıkan, 1990; Venzke, 1992; Andreev et al., 2003; Karagöz, 2004, Evered et al., 2015; Amedosky, 2017; Kul, 2017). Promitzer (2010), Evered et al. (2015) and Gratien (2017) introduced an environmental perspective to the study of 19th and early 20th century rice plantations. Shopov (2020) draws attention to early modern intrusions on the landscape, deforestation and the societal effects of rice plantations in Plovdiv, Bulgaria. However, in the above studies, climate change has

received little attention. Amedosky (2017) relates the fluctuations in rice harvests to the environmental conditions of the Little Ice Age in the Balkans. She refers to Tabak (2008), connecting the humid conditions of the Little Ice Age with the introduction of aquatic crops. Andreev et al. (2003) mention drought and revenue problems in the 17th and 18th centuries. In these studies, neither proxy data from archives of nature (i.e., tree rings) nor speleothem or pollen analysis have been used.

The present article aims to compare palaeoclimatology data with documentary evidence about institutionalized rice plantations of the Ottoman state, thus it is a first attempt to find rice-related phenological data in Ottoman sources as potential material for the identification of climate history. The study addresses the effect of climate variability on rice plantations. Available phenological data is compared with regional tree ring data. The June-July-August drought index (PDSI) reconstruction maps by Cook et al. (2015), research on temperature changes and historical data on climate extremes are compared with available yields, prices and other historical evidence about rice plantations.

STUDY AREA

Ottoman rice plantations were situated in the river valleys of the region between the Tigris and the Danube, between 30°–46° latitude and 19°–43° longitude, where temperatures were over 20 °C in the growing season and water scarcity was rare. Figure 1 shows the distribution of Ottoman rice plantations in relation to: a) May-June-July mean temperatures; and b) annual mean precipitation values. The location of plantations has been ascertained from studying documentary evidence in decrees, cadastres, rice tax office books and the rice paddy tax registers.

The survey mainly focuses on areas where both documentary evidence and palaeoclimatology data are sufficient; therefore, it includes the region of Anatolia and the Balkans but does not cover Iraq and Egypt.

This large study area has a variety of very different climatic conditions. The strong influence of the East Atlantic/Western Russia's seesaw teleconnection pattern is sometimes evident between Anatolia and the Balkans (Roberts et al., 2012). At times, while Central Anatolia is dry, Western Europe has higher precipitation rates. Constantinidou et al. (2019) define six climatic regions (Anatolia, Balkans, Western, Central and Eastern Mediterranean, and Mesopotamia) depending on the Radiative Index of Dryness, the Fuel Dryness Index and the Water-limited Yield of winter wheat. However, even in this differentiated regional model, both Anatolia and the Balkans have sub-climatic regions as shown below (Fig. 2).

Anatolia

While Central Anatolia is often hit by extreme drought, the Black Sea Region and the Aegean coasts of Western Anatolia are not influenced as much. The parallel mountain chains in the east-west direction of the Mediterranean and the Black Sea Region build a barrier, thus rain clouds transform humid air into rainfall on the slopes (Akkemik et al., 2005). Whereas the mean annual rainfall in continental Central Anatolia is only about 300 mm, the western and eastern Black Sea measures 1,000 mm and the western Mediterranean coasts 800 mm (Türkeş, 1996; Akkemik et al., 2005). Based on annual precipitation totals from 96 stations in Turkey, Türkeş et al. (2011) have defined seven rainfall regime regions in the country: the Black Sea, Marmara Transition, the Mediterranean, Mediterranean Transition, Continental Mediterranean, Continental Central Anatolia and Continental Eastern Anatolia. Moreover, by using spectral clustering of precipitation values, Türkeş et al. (2011) have defined 800 mm in eight resultant subregions: the Black Sea, Northwest Turkey, the Southern Aegean and Western Mediterranean, the Mediterranean, West Continental Central Anatolia, East Continental Central Anatolia, Continental Eastern and Southeastern Anatolia. Since the rainfall regime is very important across the breadth of this study, the simplified climate region definition derived by Türkeş et al. (2011) is considered an appropriate categorization tool.

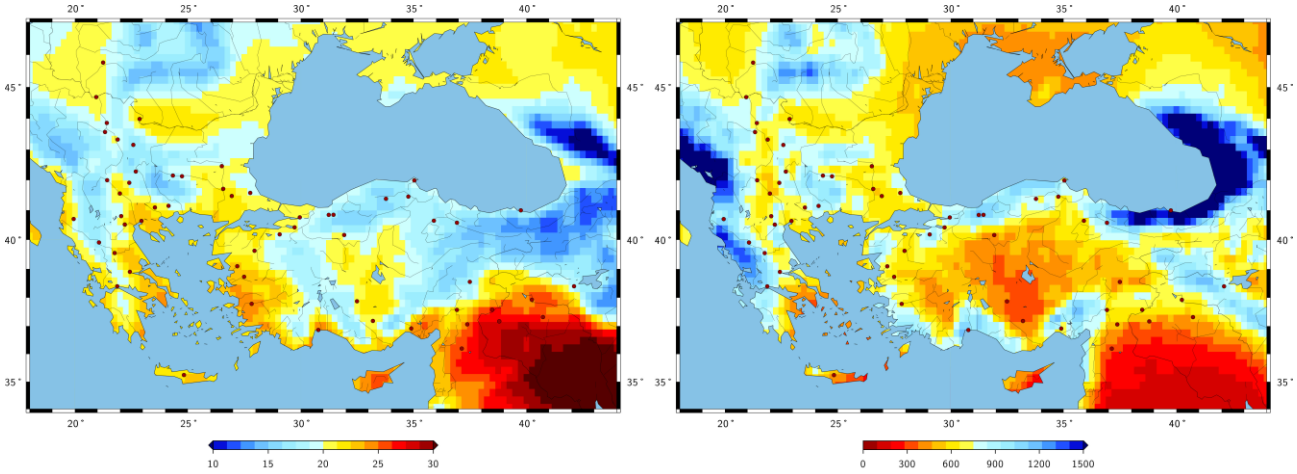

Fig. 1 Actual May-June-July mean temperatures [°C] (left) and annual mean precipitation [mm] (right) of the study area according to Hersbach et al. (2020) and the location of studied Ottoman plantations

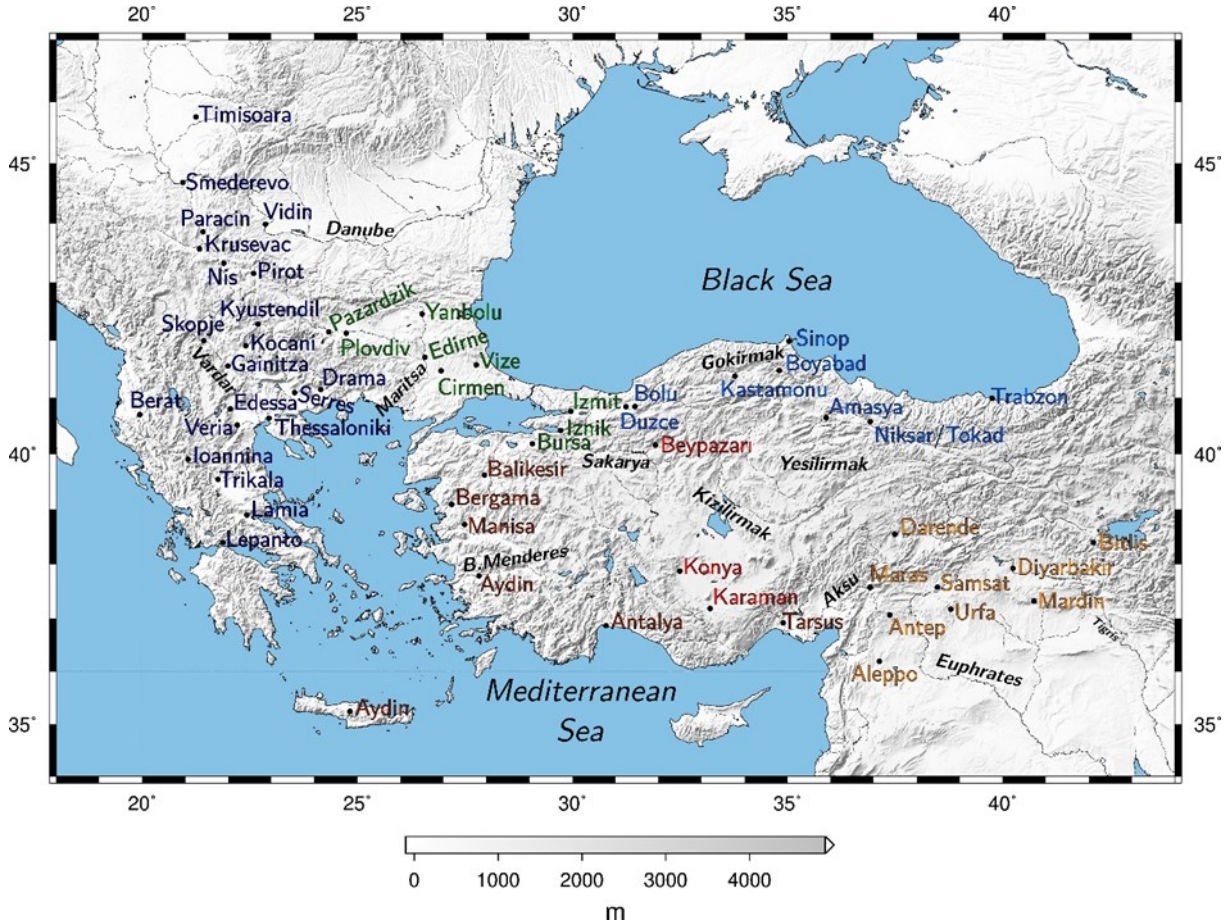

Fig. 2 Major rivers and locations discussed in the results section.
Colour coding of the locations: Continental Central Anatolia (red), the Black Sea Region (blue), the Mediterranean (burgundy), Southeastern Anatolia (orange), Southeastern Europe (navy blue) and Marmara Transition (green)

The Balkans

The Köppen-Geiger climate classification for the Balkans (Peel et al., 2007) is not sufficient to show the study area's regional climatic differences. The Balkans also have sub-climatic regions: Popov (2018), for example, modified the Köppen-Geiger classification for the Vardar, Struma and Mesta valleys. Similarly, using contemporary data and projections, Beck et al. (2018) drew a new Köppen-Geiger climate classification using a 1 km resolution map for 1980–2016. This map shows regional differences better than the Köppen map. Beck et al. (2018) also made another projection map for 2071–2100. The two maps show a great change in climate zones, which is a suitable warning against using current data for historical studies. In this study, the entire region is called Southeastern Europe.

The comparison of documentary evidence and palaeoclimatology data focuses on seven regions: Continental Central Anatolia, the Black Sea Region, the Mediterranean, Southeastern Anatolia, Southeastern Europe and Marmara Transition. The locations that have comparable data is restricted. Fig. 2 shows the major rivers and the locations discussed in the results section via a colour code. Since data that provide indications about annual yield and price variability are restricted, not all locations are discussed in the study.

DATA AND TERMINOLOGY

The Ottoman government gave particular importance to the production of rice as a cash crop. The administration of rice plantations required great organizational capacity for building canals and repairing them in case they were damaged by floods. New plantation areas were often allocated to *waqfs*, Islamic charitable foundations. In Southeastern Anatolia, the previous Mamluk system of rice growing was assimilated. The resultant Ottoman system was a challenging system that depended on waqfs to open new land for plantations. Waqfization also provided the cash flow that the gunpowder empire needed for its armies. High-ranking statesmen and affluent people donated income from revenue-generating sources to uphold the public good and simultaneously entrust their estates to family members. After Mehmed II's reign (1444–1446 and 1451–1481), the state employed a group of cultivation experts (*çeltikçi*) to implement and rehabilitate rice farming, organize the workforce and ensure sustainable production (İnalcık, 1982; Emecan, 1993). Waqfization went hand in hand with the spread of rice plantations in the Balkans (Shopov, 2020). The branches of the rivers were allocated to a tax farmers.

Each river and creek, which was used for rice production, were listed in registers.

The terminology in these registers gives an indication about the organizational principles that were used. To guarantee that correct varieties were used, the administration often supplied seeds to start plantations. Controlling the rice variety not only secured higher revenues but also prevented losses caused by planting mixed varieties. Controlling the varities was so important, that *tohum*, which literally means "seed", became a measurement unit for production lots. Rice plantations were so highly regarded by the state that there is an immense volume of data.

The use of archival data as historical evidence requires available documents to be classified and their potential analyzed.

Decrees

Important events, changes in production or changes in the organization of production were recorded in decrees called *Mühimme*. The data in these decrees provide evidence of weather extremes such as floods and droughts that resulted in reduced yield. The decrees also include information about geographical distribution. However, they are not useful for tracing gradual changes in rice production.

Cadastres

Cadastres (*Tapu Tahrir* and *İcmal* registers) are valuable because they give data about local production and the distribution of lots to tax farmers (*mukataa*) for 2–3 years. However, the data is not adequate enough to compare annual yields with climate variability.

Rice Tax Office Books

The Anatolian Fiscal Office kept separate registers for cash crops such as silk, tobacco, coffee and rice. The first Rice Tax Office Book (*Çeltik Rüsumu Kalemi or Vâridât-i Şikk-i Sânî Kalemi*) was started in 1524 and ended in 1532 defining the annual allocation of river branches to tax farmers (BOA D.ÇRS.D.25994). This book is valuable because it shows that the branches of the rivers were registered as early as the first half of the 16th century (Fig. 3).

Although these entries do not give data about the climate, similar register books could be beneficial for future land surveys. The documentation of each branch of the river from the 15th to 20th centuries is vast and the registers become more elaborate from the 16th century onwards.

The second Rice Tax Office Book dated up until 1551, which originated from Skopje (Üsküp), lists the allocation of lots (BOA D.ÇRS.D.25995). The third book is from Plovdiv (Filibe) and Pazardzhik (Tatarpazarı) (from now on modern names will be used). There are various entries from 1659, 1664–1665 and 1673. (BOA D.ÇRS.D.25996) The fourth register is also from Plovdiv and Pazardzhik for 1674 (BOA D.ÇRS.D.25997). The fifth is also from the same region and is dated 1684–1688 (D.ÇRS.D.25998). The sixth is from Pazardzhik and is dated up to 1780 (Karagöz, 2004; D.ÇRS.d.25999). The last book is from Düzce dated 1829 (BOA D.ÇRS.d.26000). The seventh Rice Tax Office Books show the allocation of river branches in Skopje on the Vardar River, Plovdiv and Pazardzhik on the Maritsa River, and Düzce on the Sakarya River in Anatolia (Fig. 2).

Rice Paddy Tax Register Documents

Rice Paddy Tax Register Documents (*Çeltik Rüsümu Evrakı*, Fig. 4) are records about the allocation of paddy fields, the changes to tax farmers' lots (*mukataa*) and their administration. There are four books, the first dating from 1688 to 1728 (BOA D.ÇRS.1), the second from 1734 to 1761 (BOA D.ÇRS.2), the third from 1762 to 1776 (BOA D.ÇRS.3) and the fourth from 1777 to 1792 (BOA D.ÇRS.4). All four books are related to the rice paddies in Pazardzhik and Plovdiv. The data are almost continuous from 1688 to 1792 covering more than 100 years of changes in the allocation of paddy lots on various river branches, except for five years between 1728 and 1734.

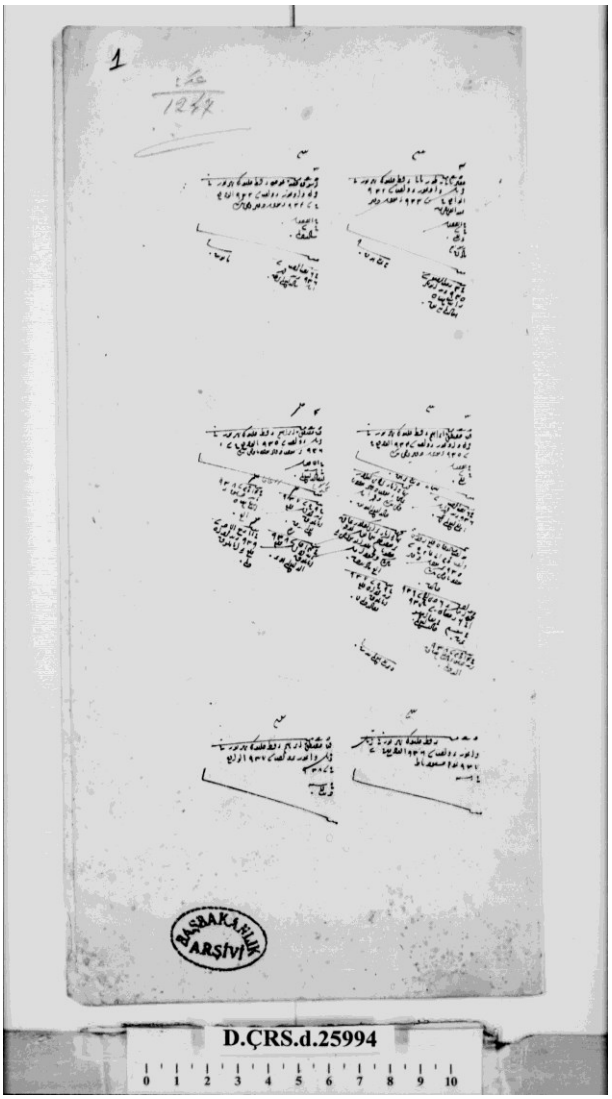

Fig. 3 Example of a Rice Tax Office Book from the first half of the 16th century (Image courtesy of the Prime Ministry's Ottoman Archive, Istanbul, BOA D.ÇRS.D.25994)

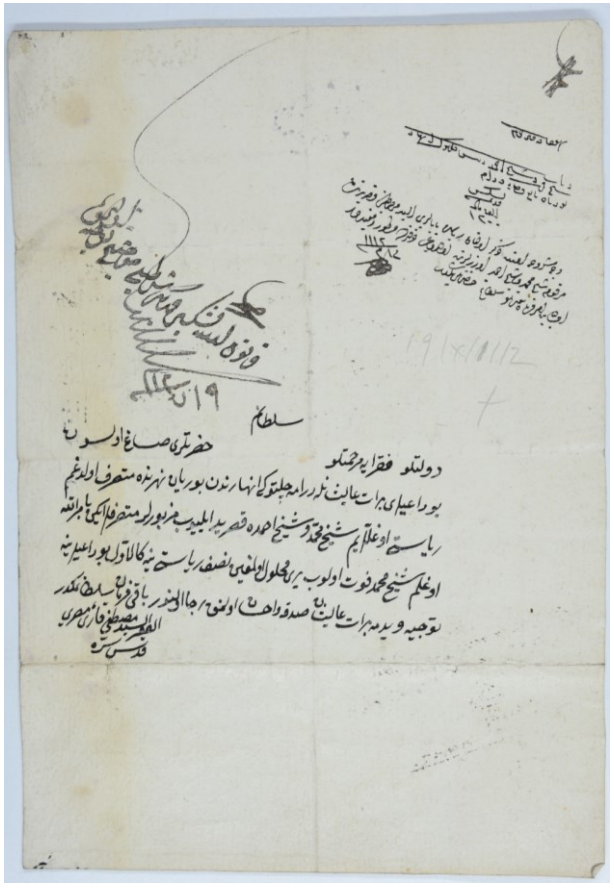

Fig. 4 Example of a Rice Paddy Tax Register Document from the early 18th century (Image courtesy of the Ottoman Archive, Istanbul, BOA D.ÇRS1, 29. ÇRS 1, 29)

The data about the allocation of the paddy fields is not adequate to compare yield quantity with climate variability, since they do not offer annual accounts. Despite these shortcomings, analysis of these documents may give important results about the anthropogenic intrusions on the land. When compared with the pollen data of rice in future studies, new perspectives may be gained.

Waqf Account Books

One critical type of regional document may help to provide evidence of climate variability and its effect on yield: the Waqf Account Books (*Vakıf Muhasebe Defterleri*) record yearly revenues from foundation budgets. Annual changes to the quantity of yield and price fluctuations are appropriate for a comparison with climate variability. However, the data are seldom continuous.

METHODS

Climate variability is not the only controlling factor of rice yield variability. Dry spells, changing cloud cover (and solar radiation), wind speed, seasonality and the timing of heat stress, water scarcity, pest and pathogen infestations, agronomic challenges, and economic and political or social factors can also affect yields. Among the many factors influencing rice production, yield fluctuations caused by climate variability can only be traced in high accuracy matches. This study offers a comparison of contemporary sources with regional climate data. It uses only contemporary sources that enable analysis of the change in rice yield. Since there is no one-to-one matching palaeoclimatology data for each plantation location, the definition of the regions is crucial to the analysis. The study defines regions which show similar climatic characteristics and uses the reconstruction of the June-July-August Palmer Drought Severity Index (JJA PDSI) series of the Old World Drought Atlas (OWDA) produced by Cook et al. (2015). Their OWDA reconstruction depends on data derived from tree rings and historical and archaeological data. It uses the point-by-point method, and yet, for some locations, the data's sensitivity is weak since it uses a proxy search radius of 1,000 km around each location. All in all, for this long-term review, the single year maps and decadal mean summer precipitation values show a regional differentiation in the distribution of droughts and are useful for understanding yield decreases caused by long-term drought and consequent water scarcity in the rice growing season.

Rice grows and matures in approximately 150 to 200 days. Seeds start to be planted as temperatures increase after April in South Anatolia, in early May in Thrace and in late May or early June in the north Balkan Peninsula. During the first 60 days, at the vegetative stage of germination, seedling and tillering, scorching temperatures and water deficits are detrimental to growth. The ideal temperature for germination is 20–35 °C (Maclean et al., 2013). Water scarcity in the crop-growing season reduces yield (Altinsoy et al. 2013) and the need for water in June and July increases, thus the reduced depths of water in rice fields decreased yield (Kara et al. 2013). Decadal droughts may cause water scarcity and lead to less water being allocated to the branch canals.

Phenological data from rice plantations in the Central Anatolian, Black Sea, Mediterranean, Southeastern Anatolian, Southeastern European and Marmara Transition regions will be compared with the reconstructed OWDA summer precipitation data (Cook et al. 2015), temperature changes and weather extremes. Important changes to the organization of plantations from decrees and revenue changes from cadasters offer partial comparison. Available yearly records of yield and rice price data in waqf account books provide year on year changes.

RESULTS

Central Anatolia, the Black Sea Region, the Mediterranean, Southeastern Anatolia, Southeastern Europe and Marmara Transition regions show dissimilar climatic characteristics. For each region, changes in summer PDSI values are indicated with yellow boxes and periods when the summer PDSI extremes increased with blue boxes.

Continental Central Anatolia

In Continental Central Anatolia, production was located in temperate lower regions (Fig. 1a). Three locations can be identified from archival evidence: Beypazarı, Konya and Karaman (BOA, MAD.d.10249, BOA, MAD.d.12168, BOA, MAD.d.3120; Coşkun 2010).

Although plantations in the Kızılırmak and Sakarya River valleys depended on irrigation, the annual mean precipitation values are very low and the region was vulnerable to decadal droughts. The tree ring-based hydroclimate reconstruction of the OWDA (Cook et al., 2015) shows that there were extreme drought years and an important decrease in the mean summer PDSI values by the end of the 16th century (Fig. 5). The small yellow box shows a short high precipitation era in the early 16th century. The long yellow box shows that the region had experienced a long low precipitation period, in which the mean JJA PDSI values were under -1. Nar Lake high-resolution data confirm that there was also a dry period between AD 1400–1950 (Jones et al., 2006).

The change in mean summer precipitation, and the length and intensity of the drought in these years may have caused water scarcity, resulting in an overall trend toward desiccation and decreased water depth in some paddy fields. For example, in Konya and Karaman, active plantations existed before the end of the 16th century. The Karaman pious foundations' regional revenue book from 1483 mentions two rice grinding mills (Coşkun, 2010). Historical evidence from Konya also shows that rice was planted there in the 16th century (Orbay, 2012). In both locations, the production of rice had decreased by the end of the century.

The account books of Selim II's and Mevlânâ Celâleddîn-i Rûmî's waqfs in the Konya region provide some annual comparable price data (Orbay, 2012). According to this data, rice was listed among both the revenues and expenditures of the foundation between 1594 and 1597; however, it had disappeared from revenues by 1597. This probably means that rice production in the lands that the foundation owned no longer returned revenues or production stopped.

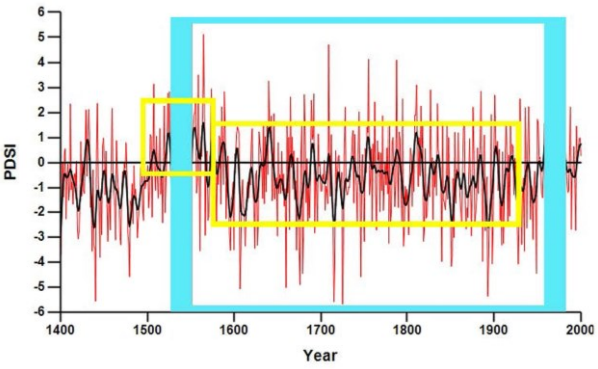

Fig. 5 Reconstructed June-July-August Palmer Drought Severity Index (PDSI) values of the OWDA (Cook et al., 2015) for Continental Central Anatolia between 1400–2000

Table 1 Rice prices in the account books of Selim II's and Mevlânâ Celâleddîn-i Rûmî's foundations (Orbay, 2012) and their comparison to reconstructed OWDA June-July-August Palmer Drought Severity Index (PDSI) values (Cook et al., 2015) for Continental Central Anatolia at Konya between 1594 and 1602.

Year	Reconstructed JJA		Selim II.'s Waqf		Mevlânâ Celâleddîn-i Rûmî's Waqf
	PDSI	10-Year Spline	Revenues	Expenditures	Expenditures
1594	-1,4054	-2,257	1,73	2,6	
1595	-2,8337	-2,339	2,3	3,18	
1596	-3,4746	-2,301	2,3	2,59	3,23
1597	-1,5316	-2,106		3,27	3,46
1598	-1,2798	-1,834		3,76	3,56
1599	-0,7683	-1,525		4,16	4,33
1600	-3,3649	-1,125		3,62	3,75
1601	0,2699	-0,545		3,42	4,33
1602	0,4688	0,112			4,79

A comparison with the reconstructed OWDA summer precipitation data (Cook et al., 2015) shows that this may be related to water scarcity. Table 1 compares rice prices in the account books of Selim II's and Mevlânâ Celâleddîn-i Rûmî's waqfs and reconstructed OWDA June-July-August PDSI values (Cook et al., 2015) between 1594 and 1602.

Ten-year spline summer PDSI values point to water scarcity in 1594, 1595 and 1596. The drought intensified from 1595 to 1596 and summer precipitation values fell from PDSI -2.8337 to -3.4746. In the same years, rice prices in the revenue section of the accounting book increase from 1.73 *akçes* to 2.3 *akçes*. After 1596, the rice revenue record was no longer in use and summer precipitation values were under zero.

Moreover, according to the Cook et al. OWDA reconstruction (2015), an extreme drought occurred in 1600. Rice prices listed as waqf expenses increased from 2.6 *akçes* in 1594 to 3.42 *akçes* in 1601. Although climate stress may not have been the only factor to cause such a price increase, this partial data shows a negative correlation between summer PDSI values and rice prices in waqfs revenues. Many other factors may have been causal in this decline and the disappearance of rice revenues, but dry June-July-August conditions are one probable trigger for this decline, as suggested by the OWDA reconstruction (Cook et al., 2015).

This fragmentary data from the revenue records reveals little in itself about water scarcity's effect on rice production. Therefore, it is highly important to find data more appropriate for comparison. Future studies may fill in the gaps and produce continuous results. Historical studies by Griswold (1993) and White (2011) relate peasant rebellions in Continental Central Anatolia to climate variability. There were also extreme fluctuations in the grain yield revenues

of the region's waqfs. Orbay (2012) relates the financial difficulties of Sadreddîn-i Konevî and the Mevlevî waqf with June-July-August precipitation fluctuations in Southwestern Anatolia, as described by Touchan et al. (2005). More documentary evidence from the grain yield revenue registers of the account books can provide a better understanding of the effect of the Little Ice Age droughts in Central Anatolia by using palaeoclimatology data produced in the last decade.

Documentary evidence from the revenue books shows that northern parts of Central Anatolia were more active in production. The mean precipitation rates are slightly higher in the area (Fig. 1 right). According to an edict dating back to 1546, Beypazarı, a town northwest of Ankara, had rice fields on the Sakarya catchment (BOA, İE.ML.1/29). In 1580, a decree ordered villagers to give their tax revenue as hulled rice to bolster the Halil Paşa Waqf's revenue and avoid losses (BOA, A.DVNSMHM.d.41/1031). A decree dating back to 26 November 1609 states that those who worked the Hasan Paşa Waqf in Beypazarı but had left their village because of bandits should not experience problems returning to Beypazarı (BOA, A.DVNSMHM.d.78/2104). Two months later, another decree stated that new revenues from Bursa and Ankara should be added to the waqf's revenues. The decree book also mentions other security problems in the region (BOA, A.DVNSMHM.d.78/2104). At present, it is not possible to analyze the specific effect of the drought on the fields; production may have stopped because of bandits or drought, or both. In 1802, a decree ordered that rice from Beypazarı be sent to Hacı Bayram-ı Veli Order in Ankara (BOA, AE.SSLM.III/197, 11831). Thus, although there may have been ruptures in production by the end of the 19th century, rice production continued in areas north of Ankara. The blue box shows the period where precipitation extremes also occurred after the mid-16th century. Future phenological study may provide more data about the influence of these summer extremes.

According to the OWDA reconstruction (Cook et al., 2015), the low mean summer precipitation period started at the end of the 16th century and lasted until the late 20th century. In this four-hundred-year period, the mean precipitation rates during droughts were under -1 and the region experienced a significant change in its flora. Agricultural areas also suffered subsurface water problems and high salinization, as shown by the long yellow box in Figure 5. Some areas are still experiencing desertification today. Studying the early effects of droughts and previous conditions in the region makes the effect of climate change more evident. Water scarcity will likely be the most important issue to affect the region in the future (Sen et al., 2012).

Black Sea Region

There were once plantations on the Sakarya and Yeşilırmak Rivers at locations where temperatures were adequate. Other rice plantations were cultivated in Düzce, Kastamonu, Boyabad on the Gökırmak River, a tributary of the Sakarya River, and in Amasya within the Yeşilırmak River valley (BOA, AE.SSÜL.I.2; BOA, MAD.d.141; BOA, MAD.d.9507; BOA, İE.ML.1/29; BOA, İE.DH.2/109; BOA, İE.ML.12/1035; BOA, İE.ML.24/2327; BOA, AE.SMMD.IV.56/6501; BOA, İE.ML.16/1532; BOA, AE.SMMD.IV.101/11751; Evliya II, 98). The annual precipitation in the Black Sea Region is much higher than in other areas of Continental Central Anatolia (Fig. 1b). Türkeş (1996) and Akkemik et al. (2005) calculated 300 mm mean annual rainfall for Continental Central Anatolia and 1,000 mm for the Black Sea Region. The OWDA June-July-August PDSI values (Cook et al., 2015) also show that summer droughts were less effective in the Black Sea Region than in Continental Central Anatolia. Rice production in the Black Sea catchment of the Sakarya River continues to this day.

Historical evidence about revenue collection and security problems draws our attention to drought years and their possible impact. For example, according to the OWDA reconstruction (Cook et al., 2015), there was a drought in 1701 and subsequent problems with the collection of rice revenues, as recorded in March 1702 in Boyabad (BOA, A.DVNSMHM.d.112/6109). After the drought year of 1708, as shown by the OWDA reconstruction (Cook et al., 2015), another revenue collection and subsequent security problem occured (BOA, İE.ŞKRT.2/170). However, many other factors may play a role and better analysis would require the study of yearly yield data from the waqf account books.

Mediterranean Coastline

The west coasts of the Anatolian peninsula usually receive more precipitation than Continental Central Anatolia even in the scorching summers (Fig. 1 right). Rice production existed as early as 1480 in Aydın on the Büyük Menderes River (BOA, MAD.d.7387). The decrease in JJA PDSI after the 17th century did not fall below zero until the end of the 20th century (Fig. 6).

As seen in the second yellow box, JJA PDSI values declined at the end of the 16th century. The blue box shows an increase in the extreme values and also betterment in the low precipitation that started at the end of the 16th century and continued until the mid-17th century. After this betterment of precipitation value, mean JJA PDSI in the growing season did not fall below zero. However, as these data derive from the trees that lay higher in the mountains, they may not directly reflect the precipitation for lower agricultural regions. Historical evidence shows that rice production was undertaken sporadically due to water scarcity. For example, in Manisa, on some of the sultan's plantations, certain fields were left unfarmed for 10–15 years (Emecan, 1993). There are numerous registers, mentioning changes to tax farmer rice plantation lots. As in other locations, rice yield data may be found in single waqf account books and historical evidence about climatic extremes and their effect on plants may be documented.

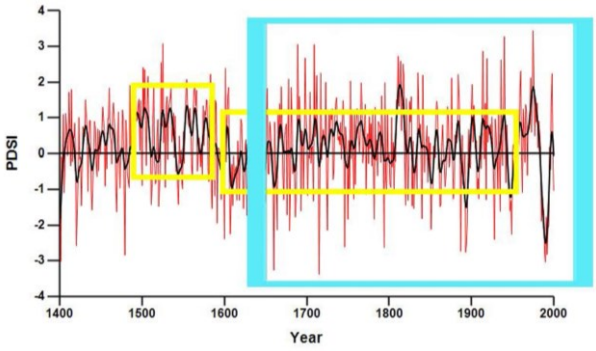

Fig. 6 June-July-August Palmer Drought Severity Index (PDSI) from the OWDA reconstruction (Cook et al., 2015) for the Mediterranean between 1400 and 2000

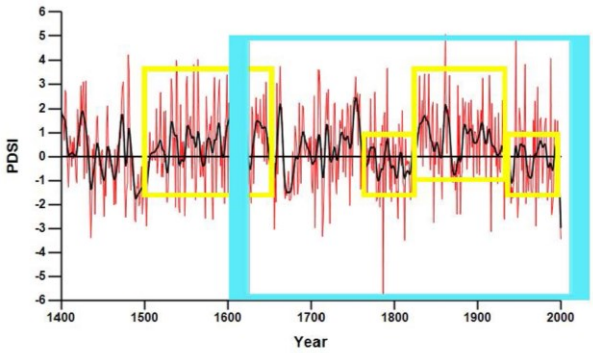

Fig. 7 June-July-August Palmer Drought Severity Index (PDSI) from the OWDA reconstruction (Cook et al., 2015) for Southeast Anatolia between 1400 and 2000

Southeastern Anatolia

There were rice plantations in Mardin, Urfa, Samsat and Darende on the Euphrates River (BOA, TS.MA.d4391), Bitlis and Siirt on the Tigris River (BOA, MAD.d.10280; Evliya III: 95, 97) and in the region between Maraş and Ayıntab on the Aksu River (Evliya III, 100). Registers were kept from 1519 about tax farmer changes in Darende on the Tohma River, a branch of the Euphrates (BOA, MAD.d.15450).

A decree dating back to 1595 informs about tax farmer changes in Diyarbakır (BOA, A.DVNS.MHM.d.73/33, 81). Unfortunately, the data do not include yearly yield or price data that would allow any comparison. Pehlivan (2020) provides documentary evidence on animal deaths, especially in the years of drought that followed extremely cold winters in the 19th century. JJA PDSI values are lower in years from the late 18th century (Fig. 7). Available proxy data show that there are two crucial decreased mean summer precipitation periods: one between the late 18th and early 19th centuries and a second that began in the early 20th century. Moreover, the region's summer precipitation extremes began in the middle of the 17th century, as shown within the blue box. Future regional studies may provide more data about the fluctuations of rice harvests and other effects of climate variability. Since proxy data from tree rings are also very rare for the region, the Cook et al. 2015 OWDA JJA PDSI mean values probably have low resolution. All in all, phenological data for this region would be very valuable.

Southeastern Europe

15th century censuses show that the Ottomans started cultivating rice in the Osum and Seman River Deltas even when JJA PDSI values were low. Rice tax was mentioned among the revenues of some villages near Berat, Albania, as early as 1432 in the area's first revenue registers (İnalcık, 1987). The Seman River Delta in present-day Albania is favorable for building rice paddies: the area's mean May-June-July temperatures are over 20ºC (Fig. 1 left) and the yearly mean precipitation is high (Fig. 1 right). According to Cook et al. (2015), JJA PDSI mean summer precipitation values were also high when the Ottomans organized plantations there in the 16th century (shown within the first yellow box in Figure 8).

Southeastern European river valleys in Macedonia, Thessaly and Thrace were also appropriate for rice farming. Other revenue registers show that in 1516 the area between Niš and Pirot (in present-day Serbia) and northern regions like Kruševac also had rice plantations (Amedosky, 2017). Drought data from the OWDA and historical evidence show that weather extremes started in the mid-16th century and ended in the mid-18th century. During these extreme weather conditions, floods disrupted some rice paddies in the 17th century. In Lamia, floods filled the paddies with stones in 1629 and 1630 (BOA, A.DVNSMHM.d.85/297). Between 1714 and 1718, very severe conditions affected the paddies in Thrace and, in 1716, floods ruined rice paddies on the Peloponnes, causing villagers to leave their homes (Amedosky, 2017). Weather extremes are especially relevant to cash crops like rice and sugar cane since they require mills in their production process, which are operated using water energy or working animals that are both stressed by extreme levels of water. Floods that damage mills also negatively impact rice production.

Rice production existed in Niš before the Ottomans arrived in the region, but production increased under their reign. The crop was one item among several doubling Niš' revenues from 1498 to 1516 (Amedosky, 2017). Temperatures fell in the 17th century (Luterbacher et al., 2004) and weather extremes started mid-century. By the 18th century, some Niš plantations became meadows and were used for animal farming (Amedosky, 2017). On 21 February 1739, a decree ordered rice to be sent from Plovdiv to Niš for the army (BOA, İE.ML.45/4373), which may indicate that production was not even enough for local use or the increased army needs in the region at the time.

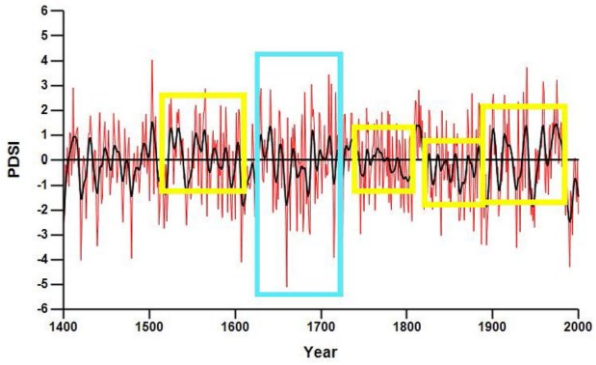

Fig. 8 June-July-August Palmer Drought Severity Index (PDSI) from the OWDA reconstruction (Cook et al., 2015) for Albania between 1400 and 2000

The effect of 18th century extremes changed crop preferences in the region. Since rice leaches the soil and makes it suitable for other crops (Maclean et al., 2013), people often substituted rice with less labour-intensive corn (Warman, 2003). The decline in rice production may have been due to insecurity, deteriorating workforce availability, energy problems, deteriorating climate conditions and/or the incompatibility of rice varieties.

The Ottomans started plantations at Timişoara, the most northern-known plantation location. Five decrees between 1572 and 1579 mentioned rice cultivation. The first, from 7 April 1572, regards a request for rice plantation experts (çeltikçis) (BOA, A.DVNSMHM.d.16/399; BOA, A.DVNSMHM.d. 16/400). The second, from 12 September 1573, mentions a decline in revenue (BOA A.DVNSMHM.d.22/683). On 25 June 1578, a decree ordered the administrators to check whether the region was appropriate for rice growing or not (BOA, A.DVNSMHM.d.35/33). In the following year, problems in the collection of rice revenues were mentioned again (BOA, A.DVNSMHM.d.36/577). European summer temperatures decreased in the 17th century (Luterbacher et al., 2004), which might have resulted in the reduction of rice plantations at the northern limit of the natural rice cultivation zone.

Historical evidence from Franciscan monastery chronicles mentioned by Mrgić (2011) shows that weather extremes influenced the region's agriculture in the 17th and 18th centuries. While droughts were recorded in 1660, 1664 and from 1686 to 1687, heavy snowfall was also mentioned in 1683, 1687–1690, 1731, 1737–38, 1741, 1743, 1749–50, 1753, 1759–60, 1762, 1764–65, 1767, and 1769–70. These extreme weather years correspond to wars (Mrgić, 2011; 2018), including the Long War (1593–1606) in the Western Balkans, followed by the Morea War (1684–1699) in the south of the Balkan Peninsula and, finally, the War of the Holy League (1683–1699). Weather extremes and wars decreased the workforce and caused insecurity in plantation areas. In the Balkans, the number of *çeltikçis* had decreased by the beginning of the 18th century (Kul, 2017). But, as long as the workforce was available, the canals were repaired and there were still numerous paddies producing rice throughout the century. Evliya Çelebi mentions Serres, Thessaloniki, Crete, Lepanto and Ioannina as places where good rice was produced in the 17th century (Evliya VIII, 59, 73, 240-241, 271, 289). The influence of weather extremes both on the production process at mills and agriculture would be a very important topic for future studies.

Marmara Transition

The OWDA reconstruction (Cook et al., 2015) shows that the mean summer precipitation values in the Maritsa River catchment at Plovdiv were much higher than they are today. The yellow boxes in Figure 9 indicate periods of change in mean summer precipitation values. According to these values, the region experienced a two-step decrease in mean summer precipitation from the early 19th century. As a result of these gradual long-term decreases in precipitation and the high use of water sources for mass agricultural production, the region experiences significant water resource problems today.

In the Ottoman Plovdiv, rice paddies were registered as early as 1480 (Boykov et al., 2000). Plovdiv and Pazardzhik produced large amounts of rice (Shopov, 2020). This agricultural organization for large-scale production relied on the existence of large estates. These estates that fed Istanbul belonged to the waqfs of the sultans and high statesman. The organization of the workforce was the most critical factor for labour-intensive rice plantations. The number of workers known as *kürekçi*, involved in rice production, who were responsible for the technical organization of the canals, increased from 19 in 1480 to 55 in 1570–71 (Shopov, 2020).

The OWDA reconstruction (Cook et al., 2015) shows that the mean summer precipitation values decreased by the end of the 16th century, as seen in the second yellow box in Figure 9. Scorching summers and water stress meant harder conditions for workers and animals, and less water for the mills. Historical evidence shows that workers sometimes fled from hard working conditions in the fields and from malaria, which was rampant in rice fields. In 1583, a malaria outbreak was recorded (Sert, 2020a; Shopov, 2020; BOA, A.DVNSMHM.d.49/137). Conditions became harder by the end of the 16th century. In 1597, some villagers could not pay their taxes and fled (BOA, AE.SMMD.III.1/31). Commercial production continued in Eastern Europe despite reduced wages and worsening labour conditions (Wiesner, 2013); when workers left, new ones replaced them and production continued. Migrants supplied the labour-intensive workforce in the Plovdiv paddies. After extreme droughts and extraordinarily cold winters in the Crimean Peninsula that resulted in animals and people perishing, many moved to Ottoman lands in the 15th century and later in 1560 (Veinstein, 2001). Moreover, demographic studies (Stoianovich, 1992; Kiel, 1997) show that decreasing temperatures in the 17th century affected many people living in mountainous areas of the Balkans who moved to lower altitude settlements like Plovdiv.

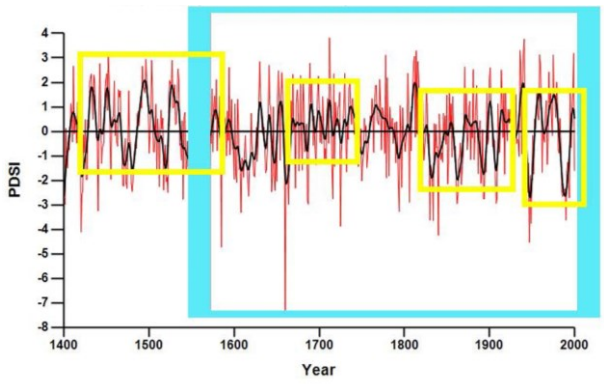

Fig. 9 June-July-August Palmer Drought Severity Index (PDSI) from the OWDA reconstruction (Cook et al., 2015) for Plovdiv between 1400 and 2000

Waqf account books published by Oruç et al. (2014) give a snapshot from five years between 1635 and 1641 and allows a comparison of yearly yield fluctuation with June-July-August PDSI changes. In Table 2 annual rice revenue entries of the Şahabeddin Paşa Waqf account books are compared with the June-July-August PDSI values from the OWDA.

Yield amounts show a negative correlation with OWDA summer precipitation values and decadal spline values. The approximate production amounts compared with June-July-August PDSI values show that PDSI values were -0.2539 in 1634, 0.0924 in 1635 and -0.6714 in 1636 and that production was approximately 456 kg (14 *müd*) in those years. It dropped to 391 kg (12 *müd*) in 1637 and 1638 when June-July-August PDSI decreased to -2.436 in 1637 and -2.2904 in 1638. There is no yield data for 1639 when the June-July-August PDSI was -1.4531. Although the June-July-August PDSI was 0.9276 in 1640, ten-year spline values were still negative. After the long dry years, yield dropped to 293 kg (9 müd). In 1641, the June-July-August PDSI increased to 2.084 and yield increased to 489 kg (15 *müd*) (Oruç et al., 2014). The same negative correlation was seen in Konya. However, a long series of data is needed to fully understand the influence of climate variability.

For Plovdiv, other revenue books of the Şehabeddin Paşa Waqf are available in the Sofia Archive for 1613–1614, 1672–1673 and 1679–1680, but the series of documents does not continue. The fluctuations of yields in other waqfs can also be a good source of information for determining climate history. Quite a few waqfs had rice plantations in Plovdiv. Even in low precipitation years such as in 1540 (Cook et al., 2015), the amount of rice carried by camel caravans from Plovdiv to Istanbul was around 513 tons (Shopov, 2020). This means that data regarding the Şahabeddin Paşa Waqf indicate only a very small part of the production. In future, the waqf account book series may show the relationship between yearly yield and precipitation changes for more extended periods.

All in all, droughts have been effective. Andreev et al. (2003) mention issues regarding rice revenues from 1698 to 1700 and water supply in 1708.

Table 2 Comparison of reconstructed OWDA June-July-August Palmer Drought Severity Index (PDSI) values (Cook et al., 2015) to the yield amounts according to Şahabeddin Paşa Waqf account books (Oruç et al. 2014) for the area of Plovdiv.

	Reconstructed JJA		Crop yield	
Year	PDSI	10-Year Spline	Production in kg	müd
1634	-0,2539	-0,176	456	14
1635	0,0924	-0,622	456	14
1636	-0,6714	-0,993	456	14
1637	-2,436	-1,176	391	12
1638	-2,2904	-1,04	391	12
1639	-1,4531	-0,607		
1640	0,9276	-0,085	293	9
1641	2,084	0,224	489	15

Moreover, historical evidence highlights the 1718 drought when villagers applied for a tax reduction and help to repair canals. However, officials declined their request and instead ordered them to pay 60 *akçes* for each kilo of rice they failed to deliver. People left their villages in Plovdiv and Pazarcık after this event (Andreev et al. 2003). Andreev et al. (2003) describe how the 1730s were even worse, whereby there was almost no rice revenue in 1735.

This coincides with accounts of Kelemen Mikes (1690–1761), the famous Hungarian essayist and political figure, who lived in exile with the Transylvanian Prince Ferenc Rákóczi in Tekirdagh. Kelemen Mikes described extraordinarily hot temperatures in March 1735 (Sert, 2007). As March is the germination period for rice seed and the ideal temperature for germination is 20–35ºC, scorching temperatures and water deficits would have been detrimental at this vegetative stage. This may be a reason why there were no rice revenues.

Kelemen Mikes mentions a significantly cold spell in 1740. That year, spring came late. It was even cold in May. In addition, December of the same year was extraordinarily hot. It was as if the seasons had changed place (Sert, 2007). There is a decree dating back to 27 March 1742 that includes the complaint that villagers did not seed their rice in March (BOA AE.SMHD.I.158/11923); since 1740's spring was so cold and farmers lost their seed, it is possible that they were behaving cautiously. Kelemen Mikes also mentions a devastating amount of snow, which started in October 1751 before the harvest of cotton and grapes (Sert, 2007).

According to Cook et al. (2015), the OWDA 19th century mean summer precipitation values fell and extreme drought years were experienced in 1806, 1830, 1832–1834, 1840, 1851, 1861–1863, 1887 and 1893–1894 (Fig. 9). Droughts probably made working conditions harder. In May 1844, the center sent help to rice workers (BOA, A.MKT.12/13, 01). Before this date, all relevant records refer to the punishment of workers who fled or peasants who did not pay their

taxes. Perhaps conditions were more demanding and the workforce had diminished to such an extent after the long Balkan Wars that state authorities realized coercion might not work this time. This is the first mention of help being sent to workers so far identified by this study. In the course of the 19th century, the Ottoman Empire lost its plantations in the Balkans. The supply of rice decreased so much that demand in the Ottoman market could only be met with imported rice (Emecan, 1993). The state gave priority to resettling rice farmers who migrated from the Balkans to places that were convenient for rice farming in Anatolia, for example, and rice farmers from Plovdiv continued rice cultivation in Bursa.

DISCUSSION

The Little Ice Age was the period in which mean temperatures declined by up to 2ºC. Like global warming today, the change in mean temperatures meant very hot and very cold extremes, floods and extreme seasonal changes. Its effects were divergent and showed regional differences. While in Continental Central Anatolia, the Little Ice Age brought drought years, which reduced agricultural production, and caused migration and rebellion (White, 2011), its effects on Europe were asynchronous and diverse.

Ottoman historians have asked (Griswold, 1993; Orbay, 2007; Sert, 2007, 2020b; White, 2011; Kolovos et al., 2018; Kuru, 2018) whether or not the Little Ice Age and other climate changes influenced the Ottoman Empire. To answer this question, institutional changes should be first mapped and then these changes should be related to the environmental and socio-economic conditions that the institutions faced. The present study shows partial effects of climate variability on rice yields, labour relations, rice mills, the health of inhabitants and population movements. The regional variability demonstrates the importance of using appropriate palaeoclimatology data in historical studies. Paleoclimatogic proxy data can advance discussions about the impact of climate variability in Ottoman historiography. Both the regional differences in climate variability and the influence of weather extremes are significant for discussions about the Little Ice Age in Ottoman history.

The Ottoman Empire experienced profound institutional changes after the second half of the 16th century (Kunt, 1983; Tezcan, 2010). An increase in the capacity of supplying food to cities and the capacity of intrusion into the environment draw some attention. However, the effect of climate is an underestimated topic in this anthropocentric historiography. The effects of the Little Ice Age have been introduced as a trigger for the decline of the Ottoman Empire (White, 2011) but have never been examined as a factor for institutional advancement even when the decline theory was rejected. The Little Ice Age droughts, which started at the end of the 16th century and continuing into the 17th century, were destructive in Central Anatolia. Due to the teleconnections of climate, an east-west bipolar climate seesaw operated in the Mediterranean. While Inner Anatolia was dry, West Europe and Western Anatolia had higher precipitation rates (Roberts et al., 2012). While in Continental Anatolia the Little Ice Age brought drought years, which decreased agricultural production and caused migration and rebellion in the 17th century (White, 2011), the Aegean islands and southern Balkans saw an increase in the olive harvest during the very same century (Kolovos et al., 2018). Likewise, in the coastal regions of Anatolia, where climate conditions were different, population movements and production conditions were not like those in Central Anatolia (Kuru, 2018). Due to these conflicting conditions, Ottoman scholars have discussed whether the Little Ice Age was effective on the Ottoman Empire at all. The present study asserts that a better acquaintance of the Ottomanist with palaeoclimatology data is vital to understand the teleconnections of climate and society.

Instead of focusing only on the destructive effects of the Little Ice Age, recognizing its institutional challenges may overcome dualistic discourse in this scholarly discussion. Orbay (2007) shows that waqfs undertook important institutional transformations to overcome the problems caused by increased food prices (e.g., waqfs introduced cash aid to students instead of providing free food from their kitchens). He highlights regional differences in the transportation of food from other regions, exemption of tax revenues and refutes the idea that the 17th century was a crisis era triggered by climate change that led to the empire's decline. Although I agree with Orbay (2007) about the importance of institutional measures and organizational changes and agree with Kolovos et al. (2018) and Kuru (2018) that climate conditions were different in other regions, there was a regional crisis in Central Anatolia that started at the end of the 16th century and continued during the 17th century. Moreover, the effects of the Little Ice Age in the Balkans still needs to be studied, especially as this study and Mrgić (2018) show that the 18th century climate extremes influenced the region. Moreover, the effect of 19th century droughts were more influential than the 16th century in Istanbul (Sert, 2020b).

CONCLUSION

This study has introduced the importance of Ottoman rice plantations in the environmental reconstruction of the region between the Tigris and the Danube. It has classified available archival documents about plantations and compared palaeoclimatology data with archival evidence. This comparison shows partial historical evidence about the effects of precipitation and temperature variability and climate extremes on rice yields and the research potential of Ottoman archival documents for climate history.

Results show that decadal low summer PDSI values coincided with a decrease in rice yields or an increase in rice prices in Plovdiv and Central Anatolia. Weather extremes such as the cold May in 1740 resulted in a fatal decrease in yield in Plovdiv. The piecemeal information about the effects of climate

variability prove that the account books of waqfs are an important source type that can give yearly yield data. Nature provides useful evidence to help understand the archives of societies (White et. al, 2018).

Questions about the influence of the Little Ice Age on the Ottoman Empire will find answers in line with an increase in palaeoclimatology data. In 2007, when Orbay (2007) was writing about grain yields and climate relation, available palaeoclimatology proxy data was limited. Future works on account books may answer some of the questions raised here if prices and yearly revenues are compared with palaeoclimatology proxy data. Moreover, a group of scholars in Paleo-Science and History at the Max Planck Institute for the Science of Human History in Jena, including Ottomanists Georgios Liakopoulus and Elias Kolovos, are working on phenological data about grain to reveal information about the relation between climate and institutional changes. The present study aims to contribute to the debate.

ACKNOWLEDGEMENT

I would like to thank Onur İnal, Florian Riedler and Yavuz Köse for their comments and suggestions on earlier versions of this article. I want to express my gratitude to Andrea Kiss, Zeki Bora Ön, Ozan Mert Göktürk, Adam Izdebsky and Georgious Liakopoulus for their support and guidance regarding climate history. Zeki Bora Ön, Maya Gül Sandfuchs and Haluk Zelef gave their precious time to help me develop my figures. Elçin Arabacı shared valuable data about Bursa. Kayhan Orbay discussed climate influence and LIA since 2007. An Ottoman database for climate events was planned with him and Günhan Börekçi. I thank Umut Soysal for his guidance on the diplomatic features of Rice Tax Office Books (Çeltik Rüsumu Kalemi). I am greatful to Sarah Waring, whose thorough editing has helped me express my ideas more precisely. I also thank Nurten Akarsu for her support. I am grateful to two institutions: the Research Council of Hacettepe University, which supported my studies at Vienna University for three months, and the Department of Near Eastern Studies of Vienna University, which hosted my project for one year.

References

Ágoston, G. 2009. Where environmental and frontier studies meet: rivers, forests, marshes, and fortifications along the Ottoman-Hapsburg frontier in Hungary. In: Peacock, A. (ed.) The frontiers of the Ottoman world Oxford University Press, Oxford and New York, 57–79.

Akdağ, M. 1963. Celâlî isyanları (1550-1603). Ankara Üniversitesi Basımevi, Ankara.

Altinsoy, H., Kurt, C., Kurnaz, L. 2013. Analysis of the Effect of Climate Change on the Yield of Crops in Turkey Using a Statistical Approach. In: Helmis C., Nastos P. (eds.) Advances in Meteorology, Climatology and Atmospheric Physics. Springer Atmospheric Sciences. Springer, Berlin, Heidelberg, 379–384. DOI: 10.1007/978-3-642-29172-2_53

Amedosky, D. 2017. Introduction of Rice Culture in the Central Balkans. In: Rudic, S. and Aslantaş, S. (ed.) State and Society in the Balkans Before and After the Establishment of Ottoman Rule. The Institute of History Belgrade, Belgrad, 235–255.

Andreev, S., Grozdanova, E. 2003. Reisanbau und Reisgewinner (çeltükçi) im mittleren und östlichen Teil des Balkans (15. bis 18.Jh.). *Bulgarian Historical Review / Revue Bulgare d'Histoire* III (4), 54–76.

Arıkan, Z. 1990. XV-XVI. Yüzyıllarda Anadolu'da Çeltik Üretimi. In: V. Milletlerarası Türkiye Sosyal ve İktisat Tarihi Kongresi, Tebliğler (İstanbul 21-25 Ağustos 1989). Ankara, 477–481.

Beck, H. E., Zimmermann, N. E., McVicar, T. R., Vergopolan, N., Berg, A., Wood, E. F. 2018. Present and future Köppen-Geiger climate classification maps at 1-km resolution. *Scientific data* 5, 180214. DOI: 10.1038/sdata.2018.214

Beldiceanu, N., Beldiceanu-Steinherr, I. 1978. Riziculture dans l'Empire ottoman (XIVe-XVe siècle). Turcica IX (2–10), 9–28.

Barkan, Ö. L. 1963. Osmanlı İmparatorluğunda Zirai Ekonominin Hukuki ve Mali Esasları. İstanbul

Bloschl, G., Kiss, A., Viglione, A., Barriendos, M., Bohm, O., Brázdil, R., Coeur, D. 2020. Current European flood-rich period exceptional compared with past 500 years. *Nature* 583, 560–566. DOI: 10.1038/s41586-020-2478-3

Başbakanlık Osmanlı Arşivi (Hereafter BOA), A.DVNSMHM.d.16/399; 16/400; 22/683; 35/33; 36/577; 41/1031; 49/137; 73/33, 81; 78/2104; 85/297; 112/6109.

BOA A.MKT.12/13, 01.

BOA AE.SMMD.III.1/31; IV.56/6501; IV.101/11751.

BOA AE.SSLM.III/197, 11831.

BOA AE.SSÜL.I.2.

BOA, D.ÇRS.1; 2; 3; 4.

BOA, D.ÇRS.D.25994; 25995; 25996; 25997; 25998; 25999; 26000.

BOA İE.DH.2/109.

BOA İE.ML.1/29; 12/1035; 16/1532; 24/2327; 45/4373.

BOA İE.ŞKRT.2/170.

BOA MAD.d.141; 3120; 7387; 10249; 10280; 12168; 15450.

BOA TS.MA.d4391.

Boykov, G., Kiprovska, M. 2000. The Ottoman Philippopolis (Filibe) During the Second Half of the 15th century. *Bulgarian Historical Review* 3–4, 112–139.

Brázdil, R., Glaser, R., Pfister, C., Dobrovolny, P., Antoine, J.M., Barriendos Vallve, M., Camuffo, D., Deutsch, M., Enzi, S., Guidoboni, E., Kotyza, O., Sanchez, R.F. 1999. Flood events of selected European rivers in the sixteenth century. *Climatic Change* 43 (1), 239 – 285. DOI: 10.1023/A:1005550401857

Brázdil, R., Wanner H., von Storch, H., Luterbacher, J. 2005. Historical climatology in Europe– The state of the art. *Climatic Change* 70 (3), 363–430. DOI: 10.1007/s10584-005-5924-1

Brázdil, R., Zahradniček, P., Dobrovolny, P., Kotyza, O., Valašek, H. 2008. Historical and recent viticulture as a source of climatological knowledge in the Czech Republic. *Geografie* 113 (4), 351–371. DOI: 10.37040/geografie2008113040351

Canard, M. 1959. Le riz dans le Proche Orient aux premiers siècles de l'Islam. *Arabica* VI (2): 111–131. DOI: 10.1163/157005859X00299

Constantinidou, K., Zittis, G., Hadjinicolaou, P. 2019. Variations in the Simulation of Climate Change Impact Indices due to Different Land Surface Schemes over the Mediterranean, Middle East and Northern Africa. *Atmosphere* 10(1), 26. DOI: 10.3390/atmos10010026

Cook, E.R., Seager, R., Kushnir, Y., Briffa, K.R., Büntgen, U. , Frank, D., Krusic, P.J., Tegel, W., van der Schrier, G., Andreu-Hayles, L., Baillie, M., Baittinger, C., Bleicher, N., Bonde, N., Brown, D., Carrer, M., Cooper, R., Čufar, K., Dittmar, C., Esper, J., Griggs, C., Gunnarson, B., Günther, B., Gutierrez, E., Haneca, K., Helama, S., Herzig, F., Heussner, K.-U., Hofmann, J., Janda, P., Kontic, R., Köse, N., Kyncl, T., Levanič, T., Linderholm, H., Manning, S., Melvin, T. M., Miles, D., Neuwirth, B., Nicolussi, K., Nola, P., Panayotov, M., Popa, I., Rothe, A., Seftigen, K., Seim, A., Svarva, H., Svoboda, M., Thun, T., Timonen, M., Touchan, R., Trotsiuk, V., Trouet, V., Walder, F., Ważny, T., Wilson, R., Zang, C. 2015. Old World megadroughts and pluvials during the Common Era. *Science Advances* 1, e1500561. DOI: 10.1126/sciadv.1500561

Coşkun, F. 2010. 888/1483 Tarihli Karaman Eyaleti Vakıf Tahrir Defteri. *Vakıflar Dergisi* 33, 15–52.

Emecan, F.M. 1993. Çeltik. TDV İslâm Ansiklopedisi. Türk Diyanet Vakfı, İstanbul, 265–266.

Evered, K.T., Evered, E.Ö. 2015. A Conquest of Rice: Agricultural Expansion, Impoverishment, and Malaria in Turkey. *Historia Agraria* 68, 103–36.

Evliya Çelebi. 2006. Evliya Çelebi Seyahatnâmesi: Topkapı Sarayı Bağdat 304 Yazmasının Transkripsiyonu, Dizini. 10 Vols. In: Gökyay, O. S. (ed.). Yapı Kredi Yayınları, İstanbul.

Gökbilgin, T. 1952. XV ve XVI. Asırlarda Edirne ve Pâşâ Livası. Istanbul.

Gratien, C. 2017. The Ottoman Quagmire: Malaria, Swamps, and Settlement in the Late Ottoman Mediterranean. *International Journal of Middle East Studies* 49 (4), 583–604. DOI: 10.1017/S0020743817000605

Griswold, W.J. 1993. Climatic Change: A Possible Factor in the Social Unrest of Seventeenth-Century Anatolia. In: Lowry, Jr. H.W., Lowry, H.W., Quataert, D. (eds.) Humanist and Scholar. Gorgias Press, Piscataway (NJ), DOI: 10.31826/9781463230081-005

Hersbach, H., Bell, B., Berrisford, P., Hirahara, S., Horányi, A., Muñoz-Sabater, J., Nicolas, J., Peubey, C., Radu, R., Schepers, D., Simmons, A., Soci, C., Abdalla, S., Abellan, X., Balsamo, G., Bechtold, P., Biavati, G., Bidlot, J., Bonavita, M., De Chiara, G., Dahlgren, P., Dee, D., Diamantakis, M., Dragani, R., Flemming, J., Forbes, R., Fuentes, M., Geer, A., Haimberger, L., Healy, S., Hogan, R.J., Hólm, E., Janisková, M., Keeley, S., Laloyaux, P., Lopez, P., Lupu, C., Radnoti, G., de Rosnay, P., Rozum, I., Vamborg, F., Villaume, S., Thépaut, J. 2020. The ERA5 global reanalysis. *Quarterly Journal of the Royal Meteorological Society* 146 (730), 1999–2049. DOI: 10.1002/qj.3803

İnalcık, H. 1982. Rice Cultivation and the Çeltükci-Re' âyâ System in the Ottoman Empire. *Turcica* XIV, 69–141.

İnalcık, H. 1987. Fatih devri üzerinde tetkikler ve vesikalar. Türk Tarih Kurumu, Ankara.

Jones, M.D., Roberts, C.N., Leng, M.J., Türkes, M. 2006. A high-resolution late Holocene lake isotope record from Turkey and links to North Atlantic and monsoon climate. *Geology* 34, 361–364. DOI: 10.1130/G22407.1

Kara, T., Gürel, C. 2013. Farklı Su Derinliklerinin Çeltik Verimine Etkisi. *Anadolu Tarım Bilim Dergisi* 28 (2), 82–86. DOI: 10.7161/anajas.2013.282.82

Karagöz, M. 2004. 1193/1779 Senesi Rüsum Defterine göre Bazarcık-Tatarpazarı'nda Pirinç Üretimi. *Fırat Üniversitesi Sosyal Bilimleri Dergisi* XIV (1), 275–299.

Kiel, M. 1997. Tatar Pazarcik — The development of an Ottoman town in central Bulgaria or the story of how the Bulgarians conquered Upper Thrace without firing a shot. In: Kreiser, K., Neumann, C. (eds.) Das osmanische Reich und seinen Archivalien und Chroniken, Nejat Göyünç zu Ehren. Franz Steiner Verlag, Stuttgart, 31–67.

Kolovos, Ē., Kotzageorgis, P. 2018. Searching for the 'Little Ice Age' Effects in the Ottoman Greek Lands: The Cases of Salonica and Crete. In: İnal, O., Köse, Y. (eds.) Seeds of Power: Explorations in Ottoman Environmental History. The White Horse Press, Winwick, Cambridgeshire, 17–34.

Köse, N., Akkemik, Ü., Dalfes, H.N, Özerenc, M.S. 2011. Tree-ring reconstructions of May–June precipitation for western Anatolia. *Quaternary Research* 75 (3), 438–450. DOI: 10.1016/j.yqres.2010.12.005

Kul, E. 2017. The Derbendcis, The Köprücüs and the Çeltikcis in the Province of Rumeli (in the Beginning of the 18th Century). *Гласник* 1: 91–106.

Kunt, İ.M. 1983. The sultan's servants: The transformation of Ottoman provincial government, 1550–1650. Columbia University Press, New York.

Kuru, M. 2018. A 'Magnificant' Climate: Demography, Land and Labour in Sixteenth-Century Anatolia. In: İnal, O., Köse, Y. (eds.) Seeds of Power: Explorations in Ottoman Environmental History. The White Horse Press, Winwick, Cambridgeshire, 35–57.

Luterbacher, J., Dietrich, D., Xoplaki, E., Grosjean, E., Wanner, H. 2004. European Seasonal and Annual Temperature Variability, Trends, and Extremes Since 1500. *Science* 303 (5663), 1499–1503. DOI: 10.1126/science.1093877

Maclean, J., Hardy, B., Hettel, G. 2013. Rice Almanac: Source Book for One of the Most Important Economic Activities on Earth 4th ed. International Rice Research Institut, Los Baños, Philippines.

Mrgić, J. 2011. Wine or *Raki* – The Interplay of Climate and Society in Early Modern Ottoman Bosnia. *Environment and History* 17(4), 613–637. DOI: 10.3197/096734011x13150366551652

Mrgić, J. 2018. Intemperate weather in violent times – narratives from the Western Balkans during the Little Ice Age (17–18th centuries). *Cuadernos de Investigación Geográfica* 44(1), 137–169. DOI: 10.18172/cig.3380

Murphy, D.J. 2007. Imperial botany and the early scientific breeders. In: Murphy, D.J. (ed.) People, Plants and Genes: The Story of Crops and Humanity. Oxford, Oxford University Press. DOI: 10.1093/acprof:oso/9780199207145.003.0015

Nesbitt, M., Simpson, J., Svanberg. I. 2010. History of Rice in Western and Central Asia. In: Sharma, S.D. (ed.) Rice: Origin, Antiquity and History. Science Publishers, Enfield, DOI: 10.1201/EBK1578086801-c10

Nicault, A., Alleaume, S., Brewer, S., Carrer, M., Nola, P., Guiot, J. 2008. Mediterranean drought fluctuation during the last 500 years based on tree-ring data. *Climate Dynamics* 31, 227–245. DOI: 10.1007/s00382-007-0349-3

Orbay, K. 2007 Osmanlı Topraklarında "Küçük Buzul Çağı"nın Etkileri Hakkında Bazı Notlar. *Kebikeç Tarım Tarihi Dosyası 1.* 23, 85–93.

Orbay, K. 2012. Financial Development of the Waqfs in Konya and the Agricultural Economy in the Central Anatolia (Late Sixteenth-Early Seventeenth Centuries). *Journal of the Economic and Social History of the Orient* 55, 74–116. DOI: 10.1163/156852012X628509

Oruç, H., Orbay K. 2014. Şehabettin Paşa'nın Felibe'deki Vakfına Ait Kaynaklar: Muhasebe Defterleri. *Belgeler* XXXV/39, 1–144.

Parker, G. 2013. Global Crisis: War, Climate Change and Catastrophe in the Seventeenth Century. Yale University Press, New Haven

Peel, M.C., Finlayson, B.L., McMahon, T.A. 2007. Updated world map of the Köppen-Geiger climate classification. *Hydrology and Earth System Sciences* 11, 1633–1644. DOI: 10.5194/hess-11-1633-2007

Pehlivan, Z. 2020. El Niño and the Nomads: Global Climate, Local Environment, and the Crisis of Pastoralism in Late Ottoman Kurdistan. *Journal of the Economic and Social History of the Orient*, 63(3), 316–356. DOI: 10.1163/15685209-12341513

Popov, H. 2018. Local climates of Vardar, Struma and Mesta valleys (Balkan peninsula) according to the modified Köppen climate classification. *Glasnik Srpskog geografskog drustva* 98, 79–90. DOI: 10.2298/GSGD180428005P

Promitzer, C., Troumpeta, S., Turda, M. 2010. Health, hygiene, and eugenics in southeastern Europe to 1945. Central European University Press, Budapest.

Roberts, N., Moreno, A., Valero-Garcés, B.L., Corella, J.P., Jones, M., Allcock, S., Woodbridge, J., Morellón, M., Luterbacher, J., Xoplaki, E., Türkeş, M. 2012. Palaeolimnological evidence for an east-west climate see-saw in the Mediterranean since AD 900. *Global and Planetary Change* 84–85, 23–34. DOI: 10.1016/j.gloplacha.2011.11.002

Sert, Ö. 2007. Kelemen Mikes'in Mektuplarına Göre 1716-1758 Yılları Mevsim Takvimi; Osmanlı Topraklarında Küçük Buzul Çağının Etkileri Hakkında Bazı Notlar [Effects of Little Ice Age According to the Letters of Kelemen Mikes 1716-1758]. *Kebikeç Tarım Tarihi Dosyası 1.* 23, 79–83.

Sert, Ö. 2018. 1549, Rodosçuk'ta Bir Yıl. (1549, A year in Rodosçuk). Süleymanpaşa Belediyesi Yayınları. Tekirdağ.

Sert, Ö. 2020a. Effects of Ottoman Rice Plantations in South-eastern European Landscape: Climate Change, Hydrology and Disease. EGU General Assembly 2020, Online, 4–8 May 2020. EGU2020–22271, DOI: 10.5194/egusphere-egu2020-22271.

Sert, Ö. 2020b. Water, Firewood, and Disease in Nineteenth Century Istanbul. Environment & Society Portal, Arcadia Rachel Carson Center for Environment and Society.

Shopov, A. 2020. Cities of rice: risiculture and environmental change in the Early Modern Ottoman Balkans. *Levant* 51(2), 169-183, DOI: 10.1080/00758914.2020.1807127

Stoianovich, T. 1992. Between East and West: The Balkan and Mediterranean worlds. Studia Balcanica, Islamica et Turcica, New Rochelle, NY

Tabak, F. 2008. The Waning of the Mediterranean, 1550–1870; A Geohistorical Approach. Johns Hopkins University Press, Baltimore

Tezcan, B. 2010. The Second Ottoman Empire: Political and social transformation in the early modern world. Cambridge University Press, New York.

Touchan R., Xoplaki E., Funkhouser G., Luterbacher, J., Hughes, M.K., Erkan, N., Akkemik, Ü., Stephan, J. 2005. Reconstructions of spring/summer precipitation for the Eastern Mediterranean from tree-ring widths and its connection to large-scale atmospheric circulation. *Climate Dynamics* 25, 75–98. DOI: 10.1007/s00382-005-0016-5

Türkeş, M. 1996. Meteorological Drought in Turkey: A Historical Perspective, 1930–93 (1996). *Drought Network News (1994-2001)* 84.

Türkeş, M., Tatlı, M. 2011. Use of the spectral clustering to determine coherent precipitation regions in Turkey for the period 1929–2007. *International Journal of Climatology* 31, 2055–2067. DOI: 10.1002/joc.2212

Veinstein, G. 2001. Karadeniz'in Kuzeyinde Büyük 1560 Kuraklığı: Osmanlı Yetkililerinin Durumu Algılayışı ve Gösterdikleri Tepkiler. In: Zachariadou, E. (ed.) Osmanlı İmparatorluğu'nda Doğal Afetler. Tarih Vakfı Yurt Yayınları, İstanbul, 297–306.

Venzke, M. L. 1992. Rice Cultivation in the Plain of Antioch in the 16th Century: The Ottoman Fiscal Practice. *Archivum Ottomanicum* 12, 175–276.

Warman, A. 2003. Corn and Capitalism: How a botanical bastard grew to global dominance. University of North Carolina Press, Chapel Hill

Watson, A.M. 1981. A Medieval Green Revolution: New Crops and Farming Techniques in the Early Islamic World. In: Udovitch, A.L. (ed.) The Islamic Middle East, 700-1900: Studies in economic and social history (Princeton studies on the Near East). Darwin Press, Princeton, NJ, 29–58.

Wessel, P., Luis, J.F., Uieda, L., Scharroo, R., Wobbe, F., Smith, W.H.F., Tian, D. 2019. The Generic Mapping Tools Version 6. *Geochemistry, Geophysics, Geosystems* 20, 5556–5564. DOI: 10.1029/2019GC008515

White, S., Pfister, C., Mauelshagen, F. 2018. The Palgrave Handbook of Climate History. Palgrave Macmillan UK, London

White, S. 2011. The Climate of Rebellion in the Early Modern Ottoman Empire. Cambridge University Press, Cambridge

Wiesner, M. 2013. Early modern Europe, 1450–1789. Cambridge University Press, Cambridge

sciendo

Journal of Environmental Geography 14 (1–2), 15–23.

DOI: 10.2478/jengeo-2021-0002
ISSN 2060-467X

MODELLING THE IMPACT OF TILLAGE ON WATER QUALITY FOR SUSTAINABLE AGRICULTURAL DEVELOPMENT IN A SAVANNA ECOLOGICAL ZONE, KWARA STATE, NIGERIA

Toluwalope Mubo Agaja[1]*, Lanre Tajudeen Ajibade[1], Micheal Olufemi Agaja[2]

[1]Department of Geography and Environmental Management, Faculty of Social Sciences,
University of Ilorin, P.M.B. 1515, Ilorin, Kwara State Nigeria.
[2]National Centre For Agricultural Mechanization (NCAM),
Km-20, Ilorin-Lokoja Highway, Idofian, Ilorin, Kwara State Nigeria.
*Corresponding author, email: specialgel@yahoo.com, agaja.tm@unilorin.edu.ng

Research article, received 6 November 2020, accepted 5 April 2021

Abstract

The aim of the study was to examine the effects of tillage methods on surface runoff and model the pattern and processes of surface water pollution associated with tillage methods using Soil Water Assessment Tool (SWAT). This model was designed to predict the impact of land management practices on water, sediment, and varying tillage types in watersheds over two planting seasons. Traditional heap (T), Plough/Harrow (PH), Plough/Harrow/Ridge (PHR) and No-tillage (NT) methods commonly used in the study area were applied to experimental plots at Unilorin Teaching and Research Farm and National Center for Agricultural Mechanization, Idofian (Nigeria). Using Randomized Complete Block Design (RCBD), each treatment had three replicates making 12 experimental plots at each location for the 2015 and 2016 planting season. Nine biophysical parameters were purposively selected, examined and modelled. The study revealed that four of nine biophysical factors (sediment yield: 10.54 t/ha; groundwater discharge: 174.45 mm; organic nitrogen: 62.62 kg/ha, and nitrogen in surface runoff: 5.15 kg/ha) were higher for traditional heaps, while three parameters (surface runoff: 374.42 mm; evapotranspiration: 752.78 mm, and soil loss: 1.05 kg/ha) were higher under plough/harrow and plough/harrow/ridge cultivation practices. The study concluded that tillage methods have impact on water quality. However, plough/harrow has comparatively more favorable effect on the contribution to surface runoff. It is therefore recommended that this type of tillage should be adopted to reduce water pollution and for sustainable environment.

Keywords: tillage, environment, sustainability, water quality, pollution

INTRODUCTION

Agriculture is an essential human activity that facilitates food production. For a long time, the increasing demand for food was met by the extension of cultivated area under cultivation. One of the consequences of crop production is the clearing of natural vegetal cover which in turn exposes the cleared land to weathering processes and degradation. Such weathering processes include soil erosion, leaching of nutrients and change in nutrient profile of the soil, which increase the pollution of fresh water sources. Tillage is the agricultural preparation of the soil by mechanical, draught-animal or human-powered agitation involving activities such as ploughing, digging, overturning, shoveling, hoeing and raking (Aina, 2011) while conservation tillage is an option for maintaining soil health and the surrounding environment for intensive agriculture, especially in the tropical climate (Sayed et al., 2020).

The soil tillage systems influence the soil structure and can have considerable impact on the environment. This substantially affect water quality, nutrient availability, crop yield, sediment transport, pesticide distribution, air quality and greenhouse processes. The effects of soil structure on agricultural production range on scales from soil productivity and sustainability at a local scale, to water quality and landscape at a regional scale, and water and energy balance and greenhouse effect at a global scale (Derpsch, 2007; Hobbs, 2007). Agricultural practices have been a major contributor to water pollution more than any other single source (Gliessman, 1998). Overland flow from farms can contain lots of sediment, pesticides, and fertilizers as well as animal waste products. The leading cause of decreased water quality in lakes and estuaries is agricultural nutrient pollution, whereas agricultural fertilizers are the dominant source of nutrient pollution in any watershed (Mateo-Sagasta et al., 2017). Most crops remove more nitrogen from the soil than any other nutrient, so more nitrogen is applied as fertilizer. About 50% of the nitrogen fertilizers applied to crops is not taken up by the plant and remains as residue in the fields. These residues are carried by runoff and easily leach into groundwater especially when fields are irrigated (Hallberg, 1987). Also, 75% of the sediment in watercourses is estimated to have come from agricultural lands (Anthony and Collins, 2006).

Typically, runoff water contains sediment, dissolved nutrients, and possibly some chemicals from conventional tillage methods. Water runoff could be

reduced by conservation tillage, thereby increasing infiltration of water into the soil. One immediate and obvious result of conservation tillage is improved surface water quality. Stimulation and excessive growth of algae and other aquatic vegetation may occur as a result of agricultural runoff, causing severe water quality problems. Overgrowth of algae, in particular, causes oxygen depletion that may kill fish, and also leads to taste and odor problems for drinking water supplies. Sediments from cropland erosion may also increase the turbidity (cloudiness) of water, impairing fisheries (Devlin and Barnes, 2009). Li and Guo (2020) reported that the total nitrogen loads are much higher than the total phosphorus loads from agricultural lands. The land use types showed great pollution loads resulting from various significant spatial differences: agricultural lands have the greatest total nitrate and phosphorus load per unit area, followed by grasslands. Forested lands have the least pollution load per unit area.

Water-borne diseases like diarrhoea has killed more than 100,000 children under five years of age in Nigeria as reported by the United Nations Children's Fund, and 90 % of those deaths were directly attributed to unsafe water and sanitation (Onwuzoo, 2020). Also, Galadima et al. (2011) reported that the most common causes of illness and death are water related diseases affecting mainly poor inhabitants in the local communities. Several cases of death due to water related diseases have been reported: in October 2010, 1191 deaths of cholera from 29115 cases was reported in 15 of the 36 states in Nigeria, including the Federal Capital Territory, Abuja (Galadima et al., 2011). It was observed that the outbreak is still in existence in new areas due to continuous water pollution.

Agricultural diffuse water pollution remains a notable global pressure on water quality, posing risks to aquatic ecosystems, human health and water resources and as a result legislation has been introduced in many parts of the world to protect water bodies. Due to this, water quality models such as Soil Water Assessment Tool (SWAT) have been increasingly applied to catchments to better understand the pattern and process of water pollution from water sheds in different regions which will help identify and provide mitigation options that can be introduced to reduce agricultural diffuse water pollution and improve water quality (Taylor et al., 2016).

According to Gassman et al., (2014), one of the most widely used water quality watershed- and river basin-scale models worldwide is the SWAT model. It can be useful extensively for a broad variety of hydrologic and/or environmental problems. Some of the major advantages of the use of SWAT and its wide acceptance internationally can be attributed to its flexibility in addressing water resource problems comprehensive online documentation and supporting software can be adapted for use for specific application needs.

Shen et al. (2013) applied the SWAT in the Three Gorges Reservoir basin (China) to estimate nitrogen and phosphorus loads and identify causal factors. They found the paddy (rice) fields and non-irrigated cultivated areas to be the most important sources of both nutrients. Einheuser et al. (2012) simulated nutrient concentrations in the Saginaw River (USA) with SWAT, and linked them to indicators of stream health. The results of the study suggest that nutrient concentrations have the highest influence on stream health. This combined modelling system was used to predict the effect of various conservation practices on stream health.

Tillage is the agricultural preparation of the soil by mechanical, draught-animal or human-powered agitation, such as ploughing, digging, overturning, shoveling, hoeing and raking. The term tillage used broadly, embraces all operations of seedbed preparations that optimize soil and environmental conditions for seed germination, seedling establishment and crop growth. Tillage includes mechanical methods based on conventional technologies of ploughing and harrowing, weed control using herbicides and fallowing with cover crops controlled by direct seeding through its residue mulch according to Ohu (2011). There are two main types of tillage systems which are conventional tillage and conservation tillage. Conventional tillage is any tillage and planting system that leaves less than 15% residue cover after planting or less than 560 kg/ha of small grain residue equivalent throughout the critical wind erosion period as proposed by CTIC (2004). Firstly, it includes systems such as mechanized tillage involving the mechanical soil manipulation of an entire field, by ploughing followed by one or more harrowing. The degree of soil disturbance depends on the type of implement used, soil and intended crop type. Secondly, traditional tillage is practiced mostly by manual labor in the humid and sub-humid regions of West Africa, and in some parts of South America. It uses native tools which are generally few and simple, the most important are the cutlass and hoe which come in many designs depending on function as observed by Aina (1993).

The second type of tillage is Conservation tillage which is any tillage and planting system that covers 30% or more of the soil surface with crop residue after planting, to reduce soil erosion by water is conservative tillage (CTIC, 2004). There are many variations of conservation tillage systems covering abroad spectrum of farming methods primarily aimed at reducing soil disturbance, conserving and managing crop residue to reduce erosion. Ohu (2011) divided conservation tillage practices into no-tillage, ridge tillage, strip tillage and the mulch tillage having varying practices and application but with the focus of conserving the resources on the soil.

Alternative land management practices such as conservation or no-tillage, contour farming, terraces, and buffer strips are increasingly used to reduce nonpoint source and water pollution resulting from agricultural activities. Models are useful tools to investigate effects of such management practice alternatives on the watershed level. However, there is a lack of knowledge about the sensitivity of such models to parameters used to represent these conservation practices (European Environment Agency, 2005, as cited by Taylor et al., 2016). Consequently, the effort at reducing pollution has not been too successful since a

little understanding exists on sources and processes of pollution especially in watershed areas.

Though there is a lot of information on tillage studies, the aspects that characterize the complexity of tillage systems and its impact on water quality is yet to be fully researched. Therefore, the aim of the study was to examine the effects of various tillage methods on surface runoff and to model the pattern and processes of surface water pollution associated with tillage methods using Soil Water Assessment Tool (SWAT).

STUDY AREA

The study was carried out at the University of Ilorin Teaching and Research Farm, Ilorin (UTRF) and National Centre for Agricultural Mechanization (NCAM), Idofian Kwara State (Nigeria) respectively (Fig. 1).

The climate of the study area falls within the tropical hinterland climatic zone, having a dry season occurring between November to April while the rainy season is between May and October. Occasionally, there could be an earlier beginning of the rainy and the dry season (Mustapha, 2008). The dry season is characterized by low amount of rainfall, high temperature and mean monthly rainfall total of about 360 mm. The mean annual evaporation is in the range of 1000-1200 mm, the humidity ranges between 30-80%. Relative humidity is high during the rainy season and low in dry season. The temperature ranges between 20-30 oC (Adelana and Olasehinde, 2004). The type of rainfall experienced is convectional storms, sometimes very windy. The heaviest rainfall is usually recorded between June and early August. There is a short spell of drought between August and early September (Oyegun, 1983; Olaniran, 2002).

The experimental sites are located in the Guinea Savannah grassland and characterized by the presence of fire tolerant woody shrubs and trees which are biologically suited to withstand dry conditions. The plants are about 12 m high with grass of about 1.5-2.5 m in height while some parts of the study area have some rainforest trees (such as acacia trees, locust bean etc; Jimoh and Ajao, 2009).

The type of soil is ferruginous tropical soil and the parent material consists of Micaceousschists and genesis of basement complex origin which are rich in ferro-magnesian minerals. The soil formation is characteristic of the geology of the study area exhibiting Jurassic, pan African and Precambrian geological structure (Ahaneku, 1997).

The UTRF and NCAM experimental sites are drained mainly by Oyun River (Fig. 2), which takes springs at Ita-Oregun (in Osun State) and flows through Otan-Aiyegbaju (in Osun State) to Offa and finally to Ilorin where it is dammed at the University of Ilorin main campus. The catchment of Oyun River is located between latitudes 9º50' and 8º24' North and Longitudes 4°38' and 4°03' East. Its total catchment area is 800 km^2 with a length of 71.4 km and it lies within Kwara State. The first experimental site (NCAM) is located at the upper catchment area of the river, while the second experimental site (UTRF) is located at the lower catchment area of River Oyun that bounds it to the west (Fig. 2).

The drainage pattern is dendritic with the tributaries joining Oyun and Asa River obliquely. This defines the form of the topography of the study area. The Oyun and Asa Rivers are located on topographical low lands, while the higher elevations are located to the east and south-east. (Fig. 2). The main river that drains the

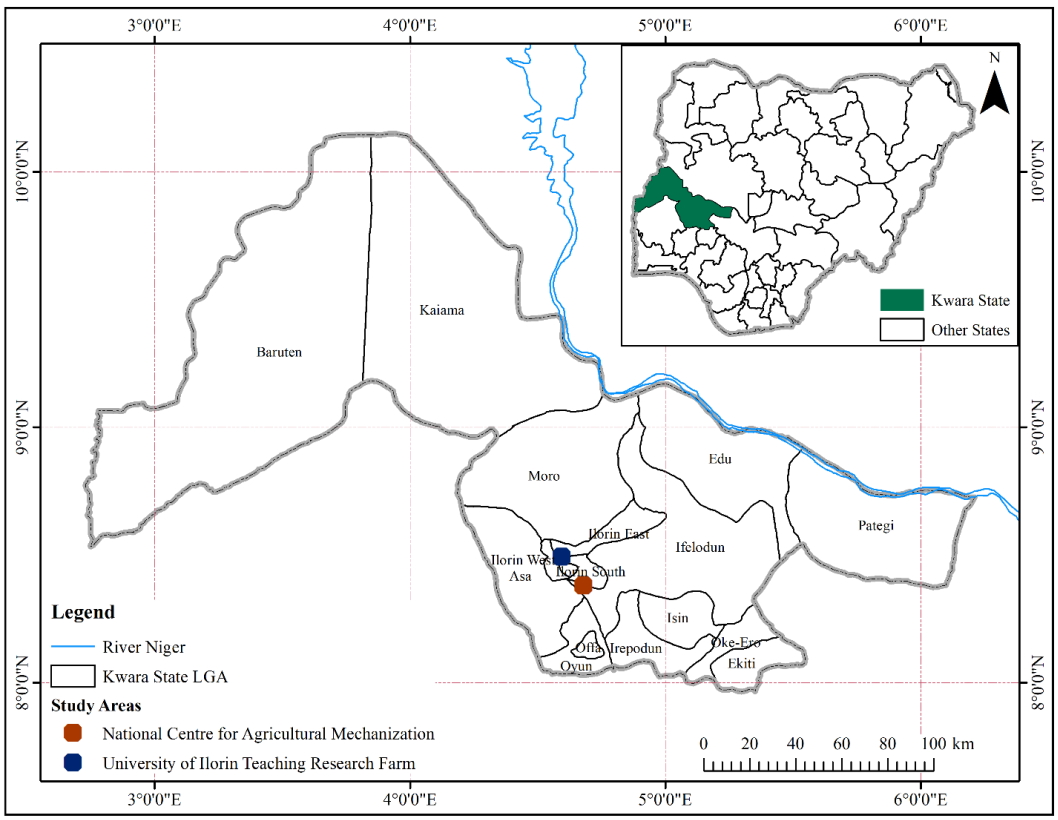

Fig. 1 The location of study areas in Kwara State, Nigeria
(Source: Kwara State Bureau of Lands and Survey 2002)

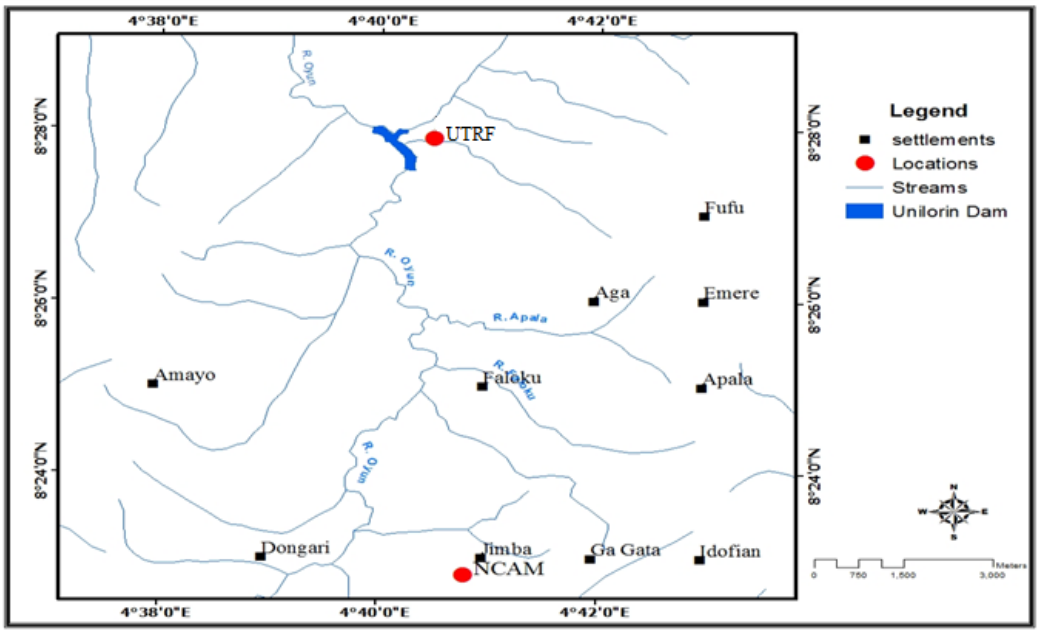

Fig. 2 Drainage pattern and settlements in the study area
(Source: Nigerian National Space Research and Development Agency 2017)

study area joins the Asa River which finally empties its water into the Niger River at Jebba in Niger state (KWSMI, 2002). The major land use type characterizing the Oyun drainage basin is agricultural land use though some other people engage in activities like trading, commerce, administration among others (KWSMI, 2002; Ahmed, 2009). The crops commonly grown include cassava, yam, melon, groundnut, sorghum, millet, pepper, tomato, and tree crops such as cocoa, kola, oil palm, mango, guava and citrus.

METHODS

Randomized Complete Block Design (RCBD) was applied with four different treatments replicated thrice. They were treatment NT (zero or no-tillage), treatment PH (plough and harrow), treatment PHR (plough, harrow and ridge), and treatment T (traditional heap farming). In the study area, these are the conservative and conventional tillage types used. Simulation of the tillage methods was made from the experimental plot for the entire Oyun drainage basin. Maize (Zea mays. L. SWAM 1 variety) was planted for 2015 and 2016 farming years on a 5m x 5m plot size at spacing of 75 cm between rows and 50 cm within row. Nitrogen, Phosphorus and Potassium i.e NPK (15:15:15) fertilizer was applied at 4 weeks and 8 weeks after planting while a normal agronomic practice such as pre-emergence and post emergence herbicide for weed control were administered on the sets of the experimental plot (Fig. 3).

Soil Water Assessment Tool (SWAT) was used to model the pattern and process of pollution from the tillage types through an ARCSWAT 2012.10.19 for ARCGIS software 10.2, 10.3 and 10.4. SWAT is a hydrologic model using the following components: weather, soil, land use as well as other variables to generate data on Hydrologic Response Unit (HRU). Some of the features modeled in the SWAT environment are described in Table 1. The SWAT was chosen because it can simulate the model with limited data and helps to describe the relationship of activities on land with the watershed hydrology.

SWAT model involved various kinds input data for simulation of the watershed. The Flow chart of the steps in the SWAT model application for the study area are shown in Figure 4. The input data included Digital Elevation Model (DEM), and maps of land use/land cover, soil cover, and precipitation. All these data were collected, processed and converted into the SWAT input format. The software was run by giving these data as inputs. The various steps involved in the software are watershed delineation, HRU analysis, and write input tables, edit input data and SWAT simulation. Afterwards, the software executed the command and the output file was printed. This output file was used to plot the graphs and maps. These graphs and maps show the characteristics of watershed.

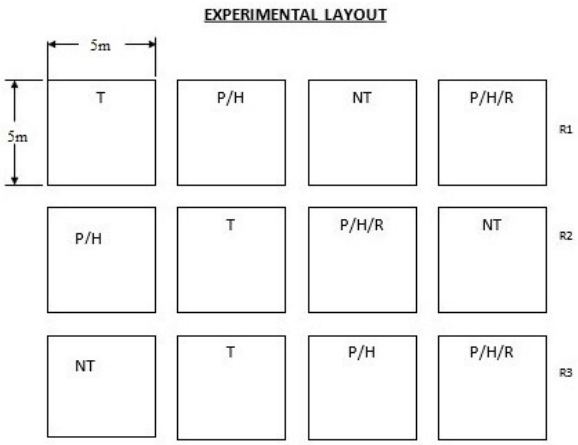

Fig. 3 Experimental layout at UTRF and NCAM Site to evaluate the effects of various tillage methods on soil erosion. Tillage methods: T: traditional heap; P/H: plough and harrow; P/H/R: plough, harrow and ridge; NT: No tillage; R1-R3: replications

Table 1 Features modelled in SWAT

PARAMETERS	DESCRIPTIONS
Hydrologic Response Unit (HRU)	The hydrologic response unit (HRU) is the smallest spatial unit of the model, and the standard HRU definition approach lumps all similar land uses, soils, and slopes within a subbasin based upon user-defined thresholds.
Sub-basin	A sub-basin (SUB) is a structural geologic feature where a larger basin is divided into a series of smaller basins with intervening intra-basin highs.
Precipitation (PREC)	Precipitation (mm) is any liquid or frozen water that forms in the atmosphere and falls back to the Earth. It comes in many forms, like rain, sleet, and snow.
SURQGEN	Amount of surface runoff (mm) contribution from streamflow from HRU during simulation. (Amount generated before transmission pothole, wetland and pond losses.)
Sediment yield (SED)	Sediment yield can be defined as the amount of sediment reaching or passing a point of interest in a given period of time, and sediment yield estimates are normally given as t/year or kg/year.
SURQ	Surface runoff (mm) generated in watershed for the day, month or year
Soil loss	Soil loss (kg/ha) during the time step calculated with the USLE equation (USLE_LS)
GWQ	Amount of lateral flow and ground water flow contribution (mm) to main channel from HRU during simulation
ET	Actual evapotranspiration (mm) in HRU during simulation
NO_3	Nitrate in surface runoff and lateral flow in HRU during simulation (kg N/ha)
ORGN	Organic Nitrogen in surface runoff in the HRU during simulation (kg N/ha)

RESULTS AND DISCUSSION

The hydrological cycle of the study area depicts the way and manner water and nutrients interact with the environment of the study area. The incoming amount of rainfall across the study area was 1230.9 mm and this number is distributed across runoff, infiltration and flow. The rate of surface runoff in this model shows a higher infiltration (distributed among the return flow, lateral flow as well as the percolation to the aquifer). The evapotranspiration rate shows a high rate of return which indicates that a deficit in precipitation would almost be certain to impact on the health of vegetation considering the rate of water loss through evapotranspiration (Fig. 5).

The model simulation is daily time step based. The values in Table 2 are real figures for the UTRF and NCAM watersheds according to the input data used in the SWAT model. Plough, harrow and ridge (PHR) tillage contributed the most to the amount of surface runoff to stream flow in the main channel, surface runoff generated in HRU during time step

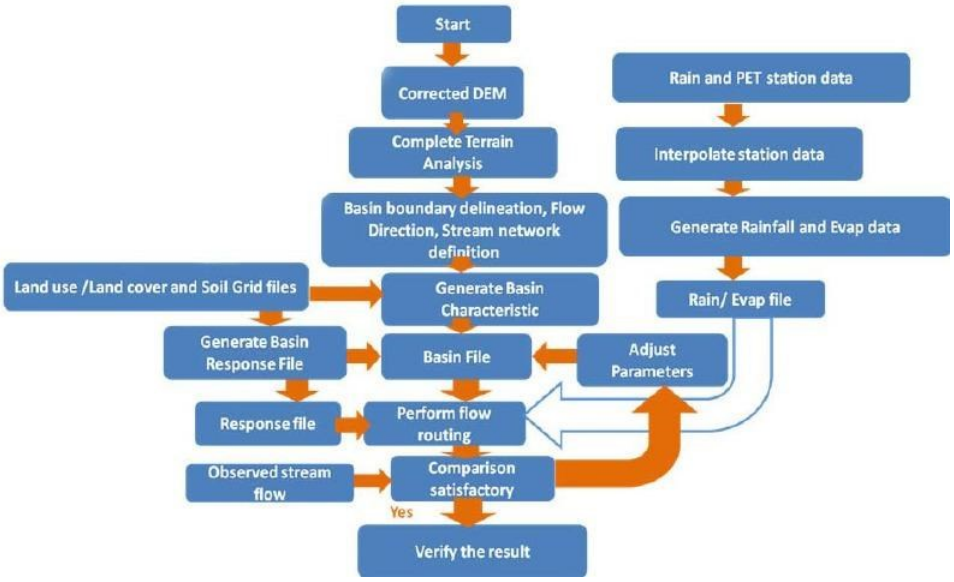

Fig. 4 Flow chart of the steps in the SWAT model to evaluate the soil erosion for the study area (adopted from Akpoti 2015)

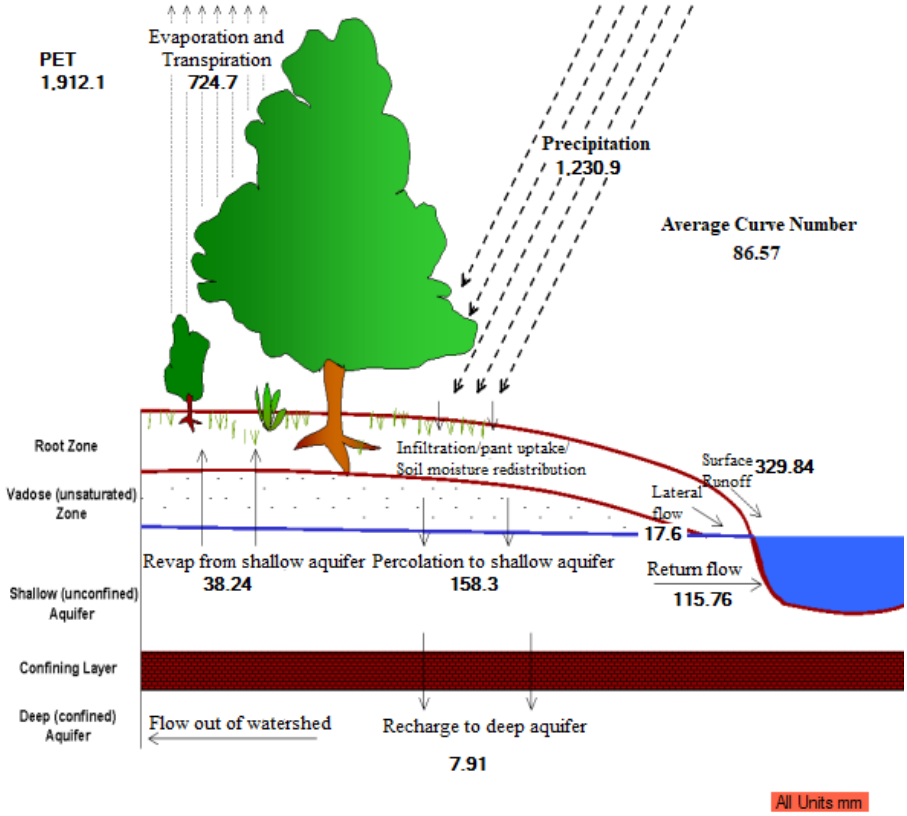

Fig. 5 Flow chart of the steps in the SWAT model to evaluate the soil erosion for the study area (adopted from Akpoti 2015)

and actual evapotranspiration generated from the UTRF site with 374.42 mm, 374.42 mm and 725.78 mm respectively; while highest in plough and harrow (PH) tillage on NCAM site with 284.86 mm, 284.87 mm and 698.1 mm respectively. No-till (NT) and traditional heap (T) generated the highest nitrate (5.15 and 4.42 kg/ha), organic nitrate (62.62 and 60.79 kg/ha), sediment yield (10.54 and 10.46 t/ha), soil loss (2.24 and 2.31kg/ha) and groundwater amount (174.45 and 96.32 mm) on UTRF and NCAM site respectively as shown in Table 2 and Figure 6, 7 and 8. The representation of the hydrological cycle reveals the mean values of some of features modelled for the entire study area.

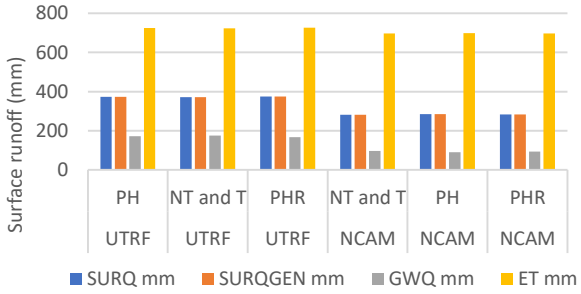

Fig. 6 Amount of surface runoff contribution from streamflow. Surface runoff generated in the watershed, lateral flow and ground water flow contribution to main channel from HRU during simulation, evapotranspiration in UTRF and NCAM sites.

Table 2 Distribution of the Hydrological Response Unit (HRU) and the SWAT modelled Parameters in UTRF and NCAM sub catchments

Tillage method	Name	HRU	SUB	SURQ [mm]	NO_3 [kg/h]	ORGN [kg/h]	PREC [mm]	SURQGEN [mm]	SED [t/ha]	Soil loss [kg/ha]	GWQ [mm]	ET [mm]
PH	UTRF	44	18	372.91	4.41	50.94	1314.21	372.91	5.31	1.05	171.19	724.79
NT and T	UTRF	45	18	371.53	5.15	62.62	1314.21	371.53	10.54	2.24	174.45	723.6
PHR	UTRF	46	18	374.42	3.68	29.83	1314.21	374.42	1.81	0.44	167.86	725.78
NT and T	NCAM	103	42	281.94	4.42	60.79	1113.86	281.94	10.46	2.31	96.32	696.6
PH	NCAM	104	42	284.86	3.04	27.41	1113.86	284.87	1.57	0.38	90.41	698.1
PHR	NCAM	105	42	283.39	3.89	48.38	1113.86	283.39	4.79	1	93.29	697.47

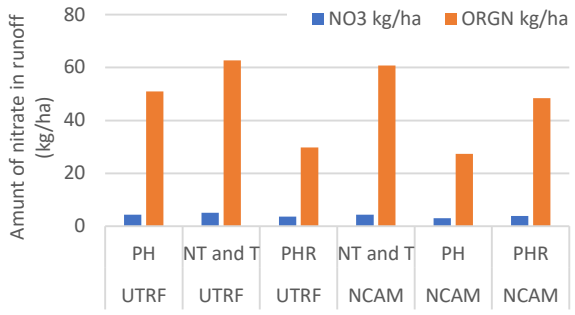

Fig. 7 Amount of nitrate and organic nitrate in surface runoff in the HRU during simulation in UTRF and NCAM sites

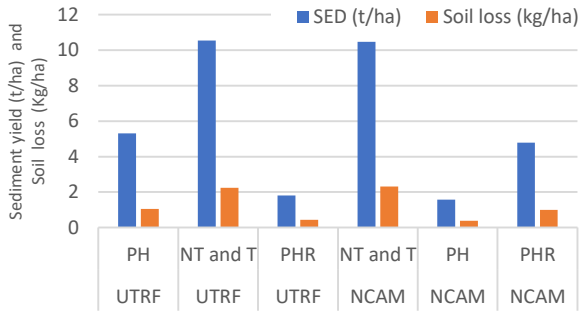

Fig. 8 Sediment yield and soil loss in surface runoff in the HRU during simulation

Effect of tillage methods on runoff

Non-point or diffused pollutants can enter into a river or lake through various points or locations whereas contamination from point source pollutant can be linked to specific discharge points of waste water treatment plants, sewers and factories. Drainage water from agricultural farm land is a major example of contamination from non-point source. The major pollutant from agricultural non-point solution (NPS) that is a product of these activities are sediment, pesticides, nutrients, salts and pathogens. The National Water Quality Inventory according to EPA (2012) reported that the leading source of impairment of water quality to surveyed lakes and rivers is agricultural nonpoint source (NPS) pollution, the third largest source of impairments to estuaries, and also a major contributor to the contamination of ground water as well as degradation of wetlands. Physical, chemical, and biological properties of soil are influenced by tillage systems and have a major impact on the productivity of soil and water quality at a wider scope.

Typically, runoff water contains nutrients that are dissolved, sediment and possibly some chemicals from conventional tillage methods whereas conservation tillage decreases runoff of water, thereby increasing penetration of water into the soil. Surface water quality improvement is one obvious and immediate result of conservation tillage. Runoff from Agricultural land may result in encouragement and excessive growth of algae and other aquatic plants, causing severe problem in water quality. Algae overgrowth in particular, causes odor and taste problems for drinking water supplies and the depletion of oxygen may kill aquatic animals. Sediment from cropland erosion may also increase the turbidity (cloudiness) of water, impairing fisheries (Devlin and Barnes (2009). This is because according to Cheikh et al., (2020), suspended sediments can influence light penetration into the column of water and will likely carry nutrients and pollutants which will affect the smooth functioning of the river ecosystems. Also, Abebe (2019) reported that Intensive agricultural practice such as tillage practices in Ethiopian highlands can results in increased soil erosion rates and sedimentation in the reservoir.

The result findings in this study revealed that No-till (NT) and Traditional heap (T) generated the highest nitrate loss (5.15 and 4.42 kg/ha) which is in line with Alam et al. (2014) reporting that the highest total N, P, K, and S in their available forms were recorded in zero tillage as compared to minimum tillage, conventional tillage, and deep tillage. Drainage water from watershed having conventional tillage is usually brown in color and carry a lot of sediments. However, in a Brazilian watershed area researcher adopted no-tillage, and found out that clear water is drained from the farmland even in times of heavy rainfall (Phillips et al., 1980). Turbidity and siltation levels are amplified in areas where conventional tillage practices still occur during various sampling of water quality and events of habitat assessment. The implication is that implementation of conservation tillage practices is likely to reduce fine clay particulates loading and materials from surface erosion that are delivered to adjacent waterways. Therefore, perhaps the greatest water quality benefit from conservation production systems is the resulting reduction sediment loss through soil erosion and runoff (Phillips et al., 1980).

In this study, Plough, harrow and ridge (conventional tillage) contributed more to the amount of surface runoff contribution to stream flow in the main channel, surface runoff generated in HRU during time step and Actual evapotranspiration generated from the UTRF site with 374.42 mm, 374.42 mm and 725.78 mm respectively; while No-till and Traditional heap generated the highest soil loss (2.24 and 2.31kg/ha). This is in contrast to the findings of Chowaniak et al. (2020) reporting that runoff was 4.3 ± 0.6% higher under No-till than under Conventional tillage, while soil loss was 66.8 ± 2.7% lower under No-till than under Conventional tillage.

In addition, Bertol et al. (2005) reported that Cu, Fe, Mn and Ni concentrations were higher under conventional tillage than under zero tillage on topsoil and runoff. Therefore, the application of tillage method can be used to achieve production, environmental and sustainable objective due to the fact that it can determine how much nutrient is available in the soil for plant growth as well as how these nutrients disintegrate into runoff and contaminate surface water.

Surface runoff is one of the diffused sources of the export of elements and chemical substances in water bodies. The findings of this study showed that No-till and Traditional heap generated the highest organic nitrate (62.62 and 60.79 kg/ha), soil loss

(2.24 and 2.31 kg/ha) and groundwater amount (174.45 and 96.32 mm) which is in line with Klimaszyk and Rzymski (2011), who stated that significant loads of nitrogen, phosphorus, organic matter among others can be transported in overland flow from the catchment area to freshwater. They also reported that the quality and quantity of surface runoff depends on many factors but some of the most important factors are tillage practices and the morphology of the catchment area. As a result, surface runoff from agricultural lands is a major contributor to the eutrophication in lakes and rivers. Therefore, the concentration of these parameters in overland flow can eventually contaminate fresh water sources around the catchment area. As a result, there is a need for appropriate tillage method that will contribute less to the concentration of the parameters to surface runoff. Thus, conservative tillage contributed more to the features as against the opinion of it been the most suitable tillage type for attaining the best environmental conditions for sustained land resources as highlighted by several references (Anthony and Collins, 2006; Derpsch, 2007; Aina, 2011; Onwuzoo, 2020). Therefore, farmers must be conscious of the agricultural land management activities such that the best tillage method that is suitable for such an environment is applied to have optimum crop yield yet conserving the water quality.

CONCLUSION

In conclusion, the different tillage methods had impact on water quality. The traditional heap and no-tillage methods contributed more to the surface runoff parameters than plough / harrow and plough / harrow / ridge, plough / harrow and plough / harrow / ridge contributes more to soil loss and surface runoff amount flowing to the nearest river/drainage than traditional heap and no-tillage. Therefore, the study recommends that plough/harrow should be adopted for a sustainable environment due to its comparatively favorable effect on its contribution to surface runoff in this ecological zone.

References

Abebe, T. A. 2019. Calibration, Validation and Performance Evaluation of Swat Model for Sediment Yield Modelling in Megech Reservoir Catchment, Ethiopia. *Journal of Environmental Geography* 12 (3–4), 21–31. DOI: 10.2478/jengeo-2019-0009

Adelana, S. M. A., Olasehinde, P. I. 2004. Assessment of aquifer system in parts of South-Western Nigeria using isotope techniques. *Proc. International Workshop on the Application of Isotope Techniques in Hydrological and Environmental Studies, Paris,* September 6-8.

Ahaneku, I. E. 1997. Comparative Evaluation of Some Tillage Systems for Effective Moisture Conservation. In: Oni, K. C. (Ed.) Proceedings of ISTRO - Nigeria: Tillage Research and Agricultural Development in Sub-Saharan Africa. 233–243.

Ahmed, Y. A. 2009. Settlements pattern and functional distribution in emerging communities: A case of a local government Area of Kwara State, Nigeria. *The Social Sciences*.4 (3), 256–263.

Aina, P. O. 2011. Conservation tillage for sustainable agricultural productivity, 'Tillage for Agricultural Productivity and Environmental Sustainability' Lead Paper. *International Soil Tillage Research Organization (ISTRO)-Nigerian Symposium Conference*, Ilorin, Nigeria, February 21-23 2011.

Aina, P. O. 1993. Rainfall runoff management techniques for erosion control and soil moisture conservation. In: FAO Information Division (Ed.) *Soil Tillage in Africa: Needs and Challenges. FAO Soils Bulletin, 69*. Food and Agricultural Organization of the United Nations, Rome, Italy.

Akpoti, K., Antwi, E., Kabo-bah, A. 2016. Impact of rainfall variability, land use and land cover change on stream flow of Black Volta Basin, West Africa. *Hydrology* 3 (3), 26. DOI: 10.3390/hydrology3030026

Alam, K., Islam, M., Salahin, N., Hasanuzzaman, M. 2014. Effect of tillage practices on soil properties and crop productivity in wheat-mungbean-rice cropping system under subtropical climatic conditions. *The Scientific World Journal* 2014, 437283, DOI: 10.1155/2014/437283

Anthony, S., Collins, A. 2006. Sediment gap analysis to support water framework directive, *Defra project WQ0106, Final report, 136 pp*

Bertol, I., Guadagnin, J. C., González, A. P., Amaral, A. J., Brignoni, L. F. 2005. Soil tillage, water erosion, calcium, magnesium and organic carbon losses. *Scientia Agricola (Piracicaba, Braz.),* 62 (6), 578–584. DOI: 10.1590/S0103-90162005000600011

Cheikh, F., Manuela G., Laurent, K., Elodie, R. 2020. Investigating the drivers of total suspended sediment regime in the senegal river basin using landsat 8 satellite images. *Journal of Environmental Geography* 13 (1–2), 31–42. DOI: 10.2478/jengeo-2020-0004

Chowaniak, M., Głąb, T., Klima, K., Niemiec, M., Zaleski, T., Zuzek, D. 2020. Effect of tillage and crop management on runoff, soil erosion and organic carbon loss. *Soil Use and Management* 36 (4), 581–593. DOI: 10.1111/sum.12606

CTIC 2004. National Survey of Conservation Tillage Practices. Conservation Technology Information Center, West Lafayette, IN.

Derpsch, R., 2008. No-tillage and Conservation Agriculture: A Progress Report. In: Goddard, T., Zoebisch, M. A., Gan, Y. T., Ellis, W., Watson, A. and Sombatpanit, S. (eds) No-Till Farming Systems. Special Publication Nº3, World Association of Soil and Water Conservation, Bangkok, ISBN:978-974-8391-60-1, 7–9

Devlin, D., Barnes, P. 2009. Impacts of no-till on water quality. *No Till Series,* Kansas State University, Online available at https://bookstore.ksre.ksu.edu/pubs/MF2907.pdf

Einheuser, M. D., Nejadhashemi, A. P., Sowa, S. P., Wang, L., Hamaamin, Y. A., Woznicki, S. A. 2012. Modeling the effects of conservation practices on stream health. *The Science of the Total Environment* 435-436, 380–391. doi:10.1016/j.scitotenv.2012.07.033

Galadima, A., Garba, Z. N., Leke, L., Almustapha, M. N., Adam, I. K. 2011. Domestic water pollution among local communities in Nigeria: causes and consequences. *European Journal of Scientific Research* 52 (4), 592–603. Online available at: https://nairametrics.com/wp-content/uploads/2013/03/2012-08-30-124334_5321.pdf

Gassman, P. W., Sadeghi, A. M., Srinivasan, R. 2014. Applications of the SWAT model special section: Overview and insights. *Journal of Environmental Quality* 43, 1–8, DOI: 10.2134/jeq2013.11.0466.

Gliessman, S. R. 1998. Agroecology: Ecological processes in sustainable agriculture. Ann Arbor Press, Chelsea, MI.

Hallberg, G. R. 1987. The impacts of agricultural chemicals on groundwater quality. *Geojournal* 15 (3), 283–295. DOI: 10.1007/BF00213456

Hobbs, P. R. 2007. Conservation agriculture: what is it and why is it important for future sustainable food production? *Journal of Agriculture Sciences* 145, 127–137. DOI: 10.1017/S0021859607006892

Jimoh, H. I., Ajao, L. I. 2009. Problems of suspended sediments loads in Asa River catchment, Ilorin, Nigeria. *Pakistan Journal Of Social Science*. 6, 19–25.

Klimaszyk, P., Rzymski, P. 2011. Surface runoff as a factor determining trophic state of Midforest Lake. *Polish Journal of Environmental Studies* 20 (5), 1203–1210.

KWSMI 2002. Kwara State Diary, Kwara State Ministry of Information, 1–10.

Li, M., Guo, Q. 2020. SWAT model simulation of non-point source pollution in the Miyun Reservoir Watershed. *IOP Conference*

Series: Earth and Environmental Science 428, 012075, DOI:10.1088/1755-1315/428/1/012075.

Mateo-Sagasta, J., Zadeh, S. M., Turral, H. 2017. Water pollution from agriculture: A global review. *Executive Summary*, 35. Online available at: http://www.fao.org/3/a-i7754e.pdf

Mustapha, K. M. 2008. Assessment of Water Quality of Oyun Reservoir, Offa, Nigeria, using Selected Physic-Chemical Parameters. *Turkish Journal of Fisheries and Aquatic Sciences* 8, 309–319.

Ohu, J. O. 2011. Tillage for Environmental Sustainability. In: Tillage for Agricultural Productivity and Environmental. *Proceedings of the Nigerian Branch of International Soil Tillage Research Organization (ISTRO)*, University of Ilorin, Ilorin, (2011), 1–10.

Olaniran, J. O. 2002. Rainfall anomalies in Nigeria: The contemporary understanding. 55th Inaugural Lecture, University Press, Ilorin. 66 p. Online available at: https://citeseerx.ist.psu.edu/viewdoc/download?doi=10.1.1.734.1395&rep=rep1&type=pdf

Onwuzoo, A. 2020. Over 100,000 under-five Nigerian children die from water-borne diseases annually-UNICEF. *The Punch Health Wise*, Online available at: https://healthwise.punchng.com/over-100000-under-five-nigerian-children-die-from-water-borne-diseases-annually-unicef/

Oyegun, R. 1983. Water Resources in Kwara State Nigeria. Matanmi and Sons Printing and Publishers, Ilorin, Nigeria

Phillips, R. E., Blevins, R. L., Thomas, G. W., Frye, W. W., Phillips, S. H. 1980. No-tillage agriculture. *Science* 208, 1108–1113. DOI: 10.1126/science.208.4448.1108

Sayed, A, Sarker, A, Kim, J, Rahman, M., Mahmud, G. A. 2020. Environmental sustainability and water productivity on conservation tillage of irrigated maize in red brown terrace soil of Bangladesh. *Journal of the Saudi Society of Agricultural Sciences* 19 (4), 276–284. DOI: 10.1016/j.jssas.2019.03.002

Shen Z, Chen, L., Hong, Q., Qiu, J., Xie, H., Liu, R. 2013. Assessment of nitrogen and phosphorus loads and causal factors from different land use and soil types in the Three Gorges Reservoir Area. *Science of The Total Environment* 454-455, 383–392, DOI: 10.1016/j.scitotenv.2013.03.036

Taylor, S. D., He, Y., Hiscock, K.M. 2016. Modelling the impacts of agricultural management practices on river water quality in Eastern England. *Journal of Environmental Management* 180, 147–163. DOI: 10.1016/j.jenvman.2016.05.002

sciendo

Journal of Environmental Geography 14 (1–2), 24–37.

DOI: 10.2478/jengeo-2021-0003
ISSN 2060-467X

ENVIRONMENTAL FACTORS THAT INFLUENCE THE GEOGRAPHY OF YEMEN LEADING TO DUST AND SAND STORMS - A CASE STUDY

Wadie Ahmed Mokbel Ghalib[1], Almoliki Mohammed Mansoor[2], Sajan Chimmikuttanda Ponnappa[3]*

[1]Taiz University, Faculty of Medical and Health Sciences, Laboratories department, Taiz, Yemen
[2]Taiz University, Faculty of Art, Geography Department, Taiz, Yemen
[3]R and D, Chemistry, VerdeEn Chemicals Pvt. Ltd,
D-11, UPSIDC Industrial Area, Masoorie-Gulawati Road, Hapur District, Uttar Pradesh, India-201015
Tel.: +90 (542) 3032275 ORCiD ID: 0000-0002-5759-1089
*Corresponding author, e-mail: sajan.saj@rediff.com

Research article, received 11 November 2020, accepted 5 April 2021

Abstract

In Yemen, the dust storm is a common phenomenon severely affecting the economy and health. Yemen is located in a semi-desert desert area, where dust and sand storms occur all year round, however they are the most common at summer (from June until the end of September). Coastal areas (Hajjah, Hoddeidah, Taiz, Lahg, Aden, Abyan, Shabwah and Hadramout) and desert areas (Marib and Al Jowf) are affected by dust and sandstorms almost all year round. The western and central governorates of Yemen are mountainous regions, but influenced by dust too. Dust storms in Yemen have an impact on humans, animals, plants and all environmental ecosystems. In this article, we attempted to understand the possible relationship between environmental parameters such as wind temperature, and precipitation, which influence the development of dust and sand storms in and around Yemen. Statistical analysis such as descriptive statistics, T-test, ANOVA one-way test, Tukey test, Levene test, and Correlation test were performed. The statistical analysis confirms that there is a significant correlation between wind, temperature and precipitation at 0.01 and 0.05 levels. The results further depict that environmental factors play a vital role in the formation of dust and sand storm. The results obtained are encouraging and further research will be conducted based on technological evidence.

Keywords: dust storms, desert, wind, temperature, atmospheric pressure, Yemen

INTRODUCTION

Sandstorms and dust storms are caused by strong high winds, which erode sand and sandy soils from arid and semi-arid environments and release them into the atmosphere (Goudie, 1988). The atmospheric dust is an integral part of the earth's atmosphere that has a direct impact on air quality and climate (Yin et al., 2002). Dust storms are frequent natural phenomenon in desert areas (Goudie & Middleton, 2001; Rezazadeh et al., 2013). Strong winds move dust and sand from the deserts and surrounding areas over long distances, triggering these incidents (Pye, 1987; Knippertz et al., 2007). The Northern Hemisphere is home to the world's largest dust source regions. They are found in North Africa, the Middle East, East Asia, and North America and are known as the "dust belt." In contrast, the Southern Hemisphere has less land; dust sources are found in Australia, South America, and South Africa and they are smaller in scale (Miguel, 2017). Dust storms have been widespread in the Favonian (west wind), Saharan, and Arabian regions. Dust storms that originate in the Gobi and Taklimakan deserts are only found in East Asia (Southern Mongolia and Northern China). However, prevailing winds bring the aerosols eastward, passing through China, Korea, Japan, and the North Pacific on their way to the Hawaiian Islands and the Western United States (Orlovsky et al., 2013). Rarely, significant concentrations of dust can be carried as far as the Western United States. Dust storm, originating in the Sahara region, travel through Western Sahara, Tunisia, Algeria, Morocco, West Africa, Sudan, Somalia, Ethiopia, the Canary Islands, the Mediterranean coast of Malaga-Alicante, etc. In case of Arabian dust storms, dust is blown from the deserts of Egypt, Saudi Arabia, Iran, Iraq, and Pakistan and from the surrounding areas into the Arabian Sea, the Red Sea and the Arabian Gulf (Pease et al., 1988). Dust storms affect the majority of the Middle East, in addition to the African Sahara region (Barnum et al., 2004; Rezazadeh et al., 2013; Furman, 2016).

The Arabian Peninsula is well-known for being one of the world's most prolific sources of dust storms (Fig. 1; Luo et al., 2004; Prospero et al., 2012). The Arabian Peninsula's large dunes, the deserts, the geologically diverse terrain with little rainfall, and sparse vegetation cover are the main sources that evoke dust in the air (A1-Sanad et al., 1993; Shepherd et al., 2016). On average, in every year Yemen has one to five dust storms with a visibility of less than 1 km (Middleton, 1986). Location, topography and climatic conditions are the key factors that caused sand and dust storms in Yemen. Dust storms have a serious impact on health, infrastructure, economy, agriculture, etc. As the

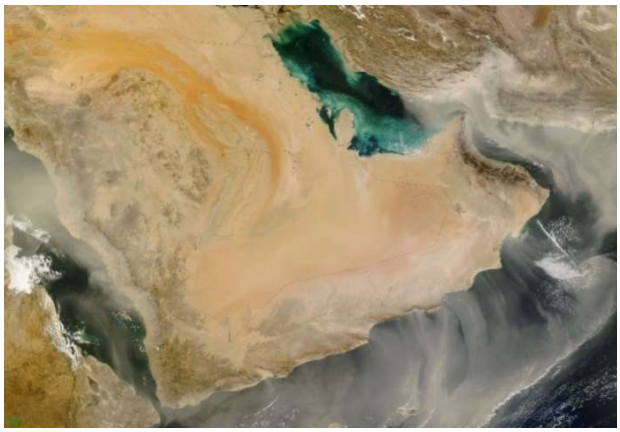

Fig. 1 Satellite image showing the dust storms over the Republic of Yemen and the Middle East (MODIS image taken by Tera/Aqua satellite, 2008)

dust storm is a meteorological phenomenon, it is impossible to eliminate it (Middleton, 2001). However, by understanding the environmental factors that lead to duststorms, we can minimise their environmental impact.

In this study, we have aimed (1) to understand the interaction of environmental factors that play key role in the development of dust and sandstorms; and (2) to highlight their impact on human health and the Yemeni environment including merits and demerits. In addition, (3) we are proposing possible measures to be taken by the authorities to mitigate the impact of the dust and sand storms on the region of Yemen.

STUDY AREA

The geography of Yemen

The Republic of Yemen between 12ºN and 19ºN is located in a tropical region and has all the general characteristics of the tropical region concerning the climate and its geographical determinants, except for local differences. Within a tropical climate zone Yemen is situated in a desert to the semi-desert region (Country Profile: Yemen, 2008). It is within the orbital zone of deserts extending from the east coast of the Atlantic Ocean to Morocco and, Mauritania, and further to the east of the Arabian Peninsula and continues to Iran. This expansion of deserts has a serious impact on the dust and dust storms in large parts of the Republic of Yemen. Yemen is located in the southwestern part of the Asian continent and the south of the Arabian Peninsula (Cullen, 2005). This geographical location is close to the continent of Africa. Saudi Arabia borders Yemen in the north, and the two countries share Rub' Al Khali, one of the world's driest deserts, and a major source of dust in the Arabian Peninsula. The south of the country is surrounded by water bodies. The impact of the Arabian Sea and the Indian Ocean on the territory of Yemen differs from the impact of the northern and eastern continents. Based on the geography of Yemen, there are variations in environmental factors, such as atmospheric pressure, wind and temperature, which cause dust or sandstorms in the territory of the Republic of Yemen.

The topography

The territory of Yemen is divided into two distinct topographical regions from the point of the dust and sand storms (Fig. 2). The first region is the hotspot for dust and sand storms, while the second represents the environment where dust and sand storms occur. The first region includes the west, south, and south-east coastal plains, as well as the Rub' Al Khali desert, and this large area is a source of dust and sand storms. Meanwhile, dust and sandstorms are coming in from the outside of Yemen's geographical borders too. The second region includes the Western highlands, Hadramout plateau, and interior basins. Due to the wide distance between the source and the receiving location, this region is mostly affected by dust rather than sand storms.

The climate

Yemen's climate can be characterized as a subtropical dry, hot desert climate with little annual precipitation. Yemen's summer lasts from June to September. In the summer, the temperature is high (40°C), and the amount of rainfall is very limited. The winter is colder, while the spring and autumn are mild. Rain usually appears in the spring, but only on rare occasions. In the dry periods the hot winds known as Shamal carry dust, and blow in the spring and summer (i.e. between March and August). The most important factor in the occurrence, transfer, and spread of dust and sand storms is the climate. The formation of dust and dust storms is directly related to various climate elements such as heat, rain, wind conditions, pressure, humidity, and solar radiation. It spreads as the drought worsens, causing temperature changes, changes in wind speed, and changes in wind direction (Climate Change Profile: Yemen, 2018). The driving force behind all aspects of climate is atmospheric pressure. Winds are created by differences in atmospheric pressure in different areas or layers of the upper atmosphere. The wind is one of the most important outputs for determining atmospheric pressure differences on the ground or in the upper atmosphere layers. It is also one of the most powerful factors in the movement of dust and sand storms. During the study of dust, it is necessary to analyze the wind moment because the wind is the energy that carries and spreads the dust by its direction (Rafferty, 2011). Seasonal variations in atmospheric pressure and winds result in the formation of various types of wind and breeze, such as:

Local wind is produced by a change in local air pressure. Atmospheric depressions are formed as a result of these winds. West and south of Yemen there are water bodies while highlands and lowlands of different natural terrain areas characterize the land of the country. The land surface is more exposed to sunlight triggering a frequent local and seasonal breeze known as land and sea breeze (Allaby & Garratt, 2007; Winter et al., 2020). The key factors

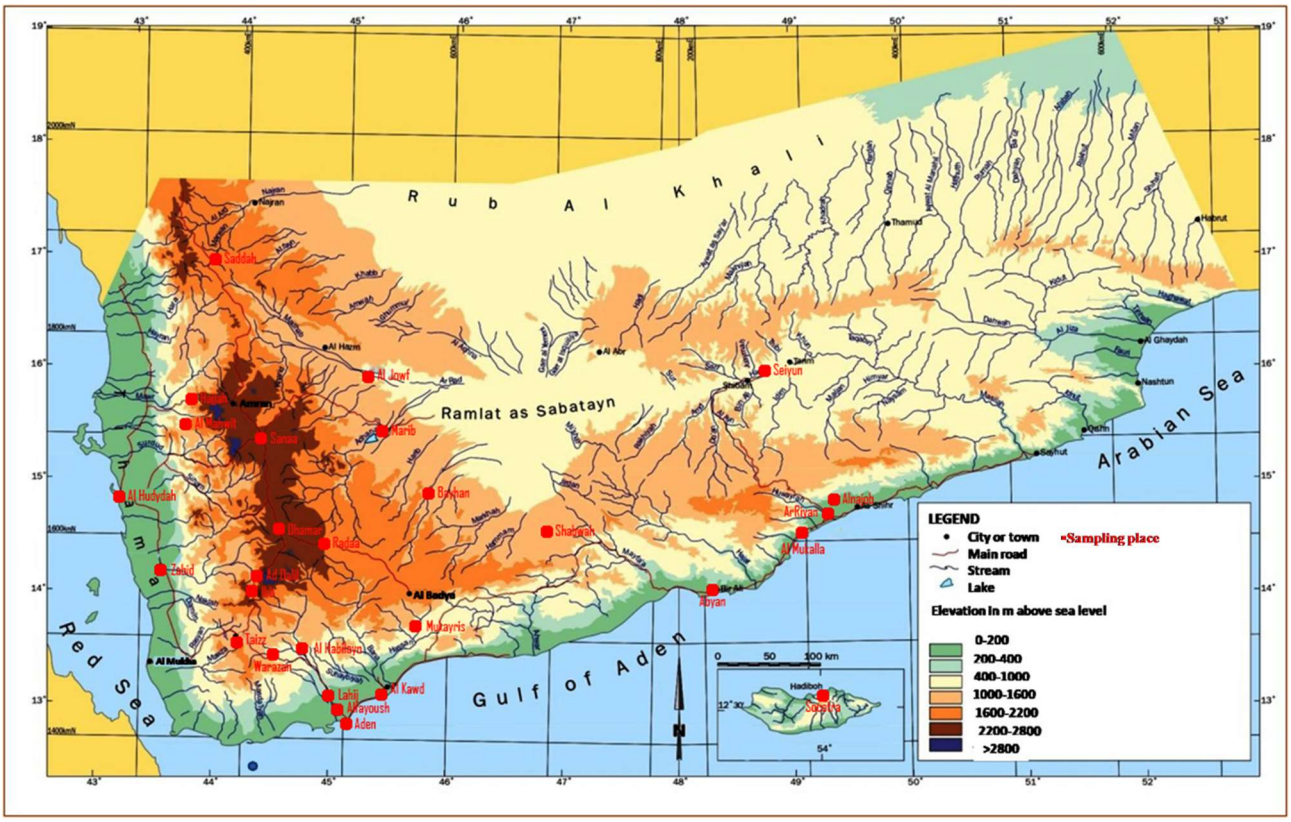

Fig. 2 Topographical map of the Republic of Yemen

driving the land and sea breeze are variations in temperature and air pressure between dry land and the adjacent water bodies. In case of land breeze the land cools faster than the sea, allowing the air in contact with it to cool. This causes air to sink over the land, allowing sea air to replace it at a high level. The land breeze is a low-level flow of cool air from the land to the sea (Allaby & Garratt, 2007; Davis et al., 2019).

Sea breeze forms when the wind blows from the sea to the land throughout the day. The frequency of the sea breeze is determined by a variety of factors. This involves the area and level of the water, the temperature difference between land and water, the prevailing winds, the coastal topography up to 15-50 km from the coastline areas, and the prevailing wind direction of more than 100 km, all of which contribute to high relative humidity and supporting temperatures in coastal areas. The temperature of the coastal areas directly affects human comfort in the summer by altering the effect of the sea breeze on the Yemeni coast, resulting in temperature variations influencing air pressure and wind direction (Allaby & Garratt, 2007; Crowther et al., 2019; Davis et al., 2019). The blowing wind, the extension of the coastal area, and the natural mountain barriers all influence the sea breeze reaching the west and southern coasts. In the summer, the sea breeze has the greatest effect on the west coast, reaching up to 80 kilometres with a maximum wind speed of 7 m/s. The effect of the sea breeze on the southern coast approaches 80-100 km/h. This is due to the regressive strength of the pressure, the lack of a winding coast, and the lack of mountain barriers to alleviate the high summer heat. In winter, the sea breeze is weak compared to summer due to high pressure, which replaces the low pressure that blocked the flow of sea breeze to long-distance inside the coast, where its impact on the west coast between 40-60 km/h with a maximum speed of 3.5 m/s.

The *valley* and *mountain breeze* blows in places with a lot of topographical contrast. During the day, temperatures rise at the bottom of valleys, causing depressions and the air rises, causing its density to drop and the air to rise upwards the mountain peaks in the form of upwards foot winds known as valley breezes. These valley breezes are the persistent winds that bring warm air upwards, assisting in the growth of numerous trees. The self-cooling mechanism happens as air travels upwards, allowing water vapor to condense and form fog. Furthermore, some cumulus clouds form over the high mountain peaks when the air humidity is higher and the altitude is higher. The interaction of the air with the foot of the mountain in low-lying areas or restricted areas between mountainous areas during the night induces rapid heat loss by radiation, resulting in cold air in the surrounding. If the temperature decreases, the density of the air rises, causing cold air to slide down in the form of soot winds, which pass down into the depressions and are known as mountain breezes (Baumbach & Vogt, 1999; Allaby & Garratt, 2007). This decreases the temperature and, on rare occasions, causes frosts in the winter, resulting in crop losses in Kaa al Hakl, Jahran, Ma'abar, and Ka'a Amran. As a result, farmers cover certain fields to shield them from frost.

Fohen winds are warm and dry. By compressing when they land on the mountain slopes, these winds gain heat on their own (Gaffin, 2007). Because of the mountains and depressions in Yemen, this is a natural air phenomenon. The central depression arises in the valley of Al Jowf. It's also caused by a difference in air pressure at the foot of the mountains that developed as a result of temperature variations (Gaffin, 2007). The temperature difference in the mountains is determined by the level of the area exposed to sunlight. The high-pressure winds result in travel into the hills, leaving the depressions, and the air above the depressions increases, allowing the temperature to rise. Another reason in its development is that when humid winds hit the mountains, they rise on the mountain slopes, forming clouds and precipitation. They land on the other side of the slopes (the rain-shadowed foothills), where their temperature rises spontaneously due to compression during their landing beneath the feet of mountain slopes. Plants and crops benefit from these winds because they speed up the start of the growing season. (Sweeney et al., 2010; Iizumi & Ramankutty, 2015).

The *Al Ghawbah* is a local name for wind in Aden, Lahg, and their surrounding areas. In the summer, these winds, along with the southwestern winds, are caused by thermal depressions and dust-laden winds. The geography of an area surrounded by sand is the primary cause of dust-laden wind, which causes obstructed vision, and blocked sunlight. With a speed of 40-60 km/h and a frequency of 18-21 per day, they cause environmental and human disasters. Summer and autumn are the seasons when these winds blow, and they usually come from the north and west.

The warm (*Al-Kawi*) winds blow from the interior desert areas of the Rub' Al Khali (the Empty Quarter) desert in the summer and spring. To reach the coastal areas, the thermal depressions move south to the Aden Gulf and the Arabian Sea. These are hot winds that cause an increase in air temperatures or a dusty drying of agricultural land. They are common in Aden, Lahg, Shabwah, Bayhan, and in other northern governorates.

MATERIALS AND METHODS

Wind, temperature, and precipitation data were gathered from 28 stations located throughout the county (Fig. 2). For each parameter, 84 samples were taken for each season, totaling 336 samples per year. As a consequence, the total number of samples for all three parameters is 1008. An anemometer model Windtronix 2 was used to measure wind speed, a HORIBA thermometer and thermography was used to measure temperature, and a rain gauge was used to collect precipitation data. These data were then statistically analysed using the Origin 8 and SPSS 19 versions of the software. These data will assist in the understanding of the interactions between environmental factors that affect dust and sand storms. During the overall research period, data were collected for seven years, from 2010 to 2016, for all seasons. Statistical analysis such as descriptive statistics, T-test, ANOVA one-way test, Tukey test, Levene test, and Correlation test were performed.

Descriptive statistics

Descriptive statistics is a technique for calculating the central tendency and spread of a set of data. The central tendency for wind speed, temperature, and precipitation was calculated in this study. T-test was performed based on the results of the descriptive statistics. A T-test is a useful tool for determining whether there is a significant difference between the means of two groups that are related in some way.

Correlation Test

The correlation test is a statistical method for evaluating the degree of a linear relationship between two variables. The range of correlation analysis is between 1 and 1. If the values obtained are closer to 1 or -1, there is a clear positive linear relationship between the variables being correlated; however, if the values obtained are closer to 0, there is no linear relationship between the variables being correlated.

RESULTS

Seasonal changes in atmospheric pressure and wind

In Yemen, the annual atmospheric pressure and wind data can be divided into four periods based on the seasons mentioned below.

Atmospheric pressure and wind during winter

During the winter season the superheat center travels towards the southern hemisphere therefore the northern hemisphere would be colder. In the meantime, the water bodies hold the temperature and become warmer than the land. Over Siberia, a high Asian atmospheric pressure (Siberian) is formed (mid- Asia, Arabian Gulf, Eastern, and Central of Arabian Peninsula). The high atmospheric pressure is generated in the Atlantic Ocean's north, spreading eastward which include North Africa. The high atmospheric pressure is developed between the height of the Arabian Peninsula and the height of the Sahara Desert. The atmospheric pressure values range between 1018-1020 mbars (Allaby & Garratt, 2007). The Mediterranean Sea's water bodies are dominated by low atmospheric pressure, caused by the thermal variations between the warm water and the surrounding landmasses. The Arabian Sea, the Gulf of Aden, the Red Sea, the Abyssinia plateau, Sudan, the equator zone, and southern Africa are all affected by the low atmospheric pressure. The dry and cold wind is produced in Central North Asia and the Arabian Peninsula, and it travels towards the low atmospheric pressure centers in the Indian Ocean's north. This is due to variations in atmospheric pressure and heat distribution across the world; triggering northern and northeast winds (Collier and Corporation, 1957; Yiannopoulos, 2018). Yemen and the rest of the Arabian Peninsula are affected by these winds, which keep the temperature steady and bring winter rain. In

general, the temperature of these winds is near 0°C, but in the highland areas of Yemen, it can drop below 0°C, retaining the temperature of the surrounding area. The collision of cold and warm air masses caused by the wind moving through water bodies causes rain in Yemen's south and east. Rainfall is often in the form of sudden rains, which has a detrimental effect on agricultural land. The Mediterranean Sea also has an effect on Yemen's climatic conditions, as some meteorological fronts, depressions, and air masses cross the northern Arabian Peninsula from the Mediterranean Sea. The cold northern air fronts have been left behind; creating an unstable frontal depression that is causing rainfall in Yemen's west region and to a lesser degree in the coastal plains.

Wind speed during winter

During the winter, the prevailing winds are the north trade winds and north-eastern winds. The wind speed varies from region to region due to topographical variations, direction, and the constant movement of pressure areas (Allaby & Garratt, 2007). Based on our data (Fig. 3) during the summer, the recorded minimum wind speed was 0.4 m/s. During the winter, while raining, a mean wind speed of 0.5 m/s was recorded. During the autumn season, a maximum speed of 7 m/s was recorded. During the winter and spring seasons, the mean wind speed was 2.01 m/s. Similarly, during the summer and autumn seasons, the mean wind speeds was within 2.0 m/s and 2.1 m/s, respectively. In the coastal areas, winds were stronger (Al Hudaydah: 4.9 m/s; Al Mukalla: 3.8 m/s; and Aden: 4.09 m/s). The equability of the surface, the heat disparity between the surface water, and the relatively low atmospheric pressure with land adjacent to it all contribute to this. The winds were strong in Sa'dah, Al Jowf, Taiz, and Al Mahwit, with gusts ranging from 2.1 to 2.9 m/s, medium in Dhamar, Al Kawd, Marib, Ar Riyan, Abyan, and Al Habilayn, (1.5-2 m/s) and weak in the rest of the stations, with gusts ranging from 1.1 to 1.3 m/s. The wind speed with the lowest rate was recorded in Alnajob, Rad, Zabid, Lahij, Ad Dali, and Shabwah, which was less than 1 m/s in Alfayoush and Seiyun. Figure 3 shows a graphical representation of wind speed in 28 stations during various seasons.

Atmospheric pressure and wind during spring

Between the winter and summer solstices, spring is a transmission season. The weather is influenced by the Arabian Peninsula's high atmospheric pressure centers, which begin to drop out to the far north, where atmospheric pressure values reach between 1010 and 1012 mbars (Allaby & Garratt, 2007). The seasonal air depression, which is located/centered on the plateau of the lakes on the African continent, moves towards stations above the eastern regions and north from Sudan's center. These changes cause air depressions due to the relatively high temperatures which replace

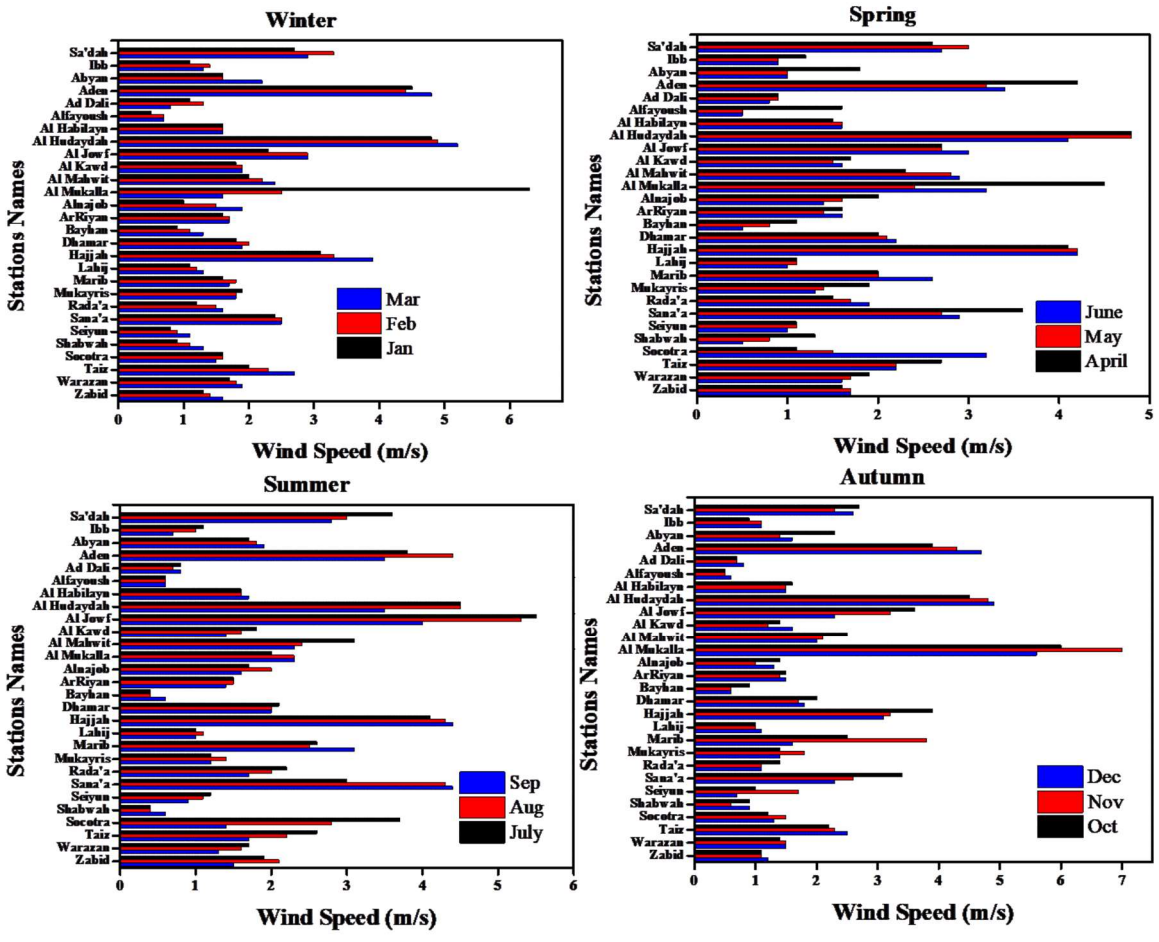

Fig. 3 Seasonal variations in wind speed in 28 stations at Yemen in 2010

the air heights above the center of the Arabian Peninsula and North Africa.

Yemen is subjected to different air blocks originating in the north and south while high atmospheric pressure increases in the southern hemisphere. This results in spring air turbulence and rainfall, particularly in Yemen's central and southern regions (Ibb, Al Mahwit, Hajjah, Aden, and Al Rayyan), which varies year to year. The predominant winds in the country's southern stations are mostly from the south to southeast. In late April and early May, southwest winds are the dominant winds in the north and western stations. In the spring, there is also an increase in rainfall, but only in small amounts for short periods (Elzz et al., 1991; Algifri, 1998).

Wind speed during spring

Several stations, such as Hodeidah, Al Rayyan, Mokiras, and Habelin, do not experience any changes in wind speed between winter and spring (Elzz et al., 1991; Algifri, 1998). In contrary, Sa'dah, Al Jowf, Ad Dali, Al Mukalla, Al Kawd, and Socotra are among those stations where the wind speed is lower in the spring than in the winter. Wind speed increases in the rest of the stations during the winter. During the spring, the highest fast rates are recorded at Hajjah and Aden Stations, ranging from 4.1 to 4.9 m/s, followed by 2.9 to 2.5 m/s at mountain high stations like Sanaa, Al Mahwit, and Taiz. The lowest wind speeds, 0.9 m/s, were recorded at the Ad Dali and Alfayoush stations.

Atmospheric pressure and wind during summer

The Yemeni seasons are similar to Indian seasons, with a low atmospheric pressure of 998 mbar on average and low eastern Sudanese atmospheric pressure that affects Yemen. South of the equator, there is a high level of atmospheric pressure. As a result, the Indian Ocean is dominated by hot, humid south-western monsoon winds. Summer rains in Yemen are caused by the monsoon wind colliding with the mountain slopes. Summer is the most popular season in Yemen for dust and sand storms, which occur from June to the end of September every year. The strength of the dust and sand storms decreases during the rainy season. Rainwater cleans the air by removing dust particles and allowing them to settle. Furthermore, rainy years, which are typical in most parts of Yemen, hold the soil moist, minimizing soil erosion, which would otherwise be transferred as dust. Meanwhile, areas with less rain, especially in the west and south, contribute to the spread of dust, which is then dispersed throughout the atmosphere.

Atmospheric pressure and wind during autumn

The autumn season is a transitional period between the summer and the winter seasons. The depressions above the Arabian Peninsula and North Africa start to deteriorate during this season and are replaced by air blowing in from Asia. The atmospheric pressure is between 1012 and 1016 mbar during autumn. Meanwhile, the Sudanese air depression has influenced the surrounding environment, causing them to settle over the Abyssinia plateau and eastern Sudan. Meanwhile, during the summer in India, the seasonal low atmospheric pressure is dominant. The atmospheric pressure begins to fall to the east and is replaced by high Siberian pressure, which begins to spread westward. The northeasterly wind moves to Yemen, carrying steady rain until mid-September. At the beginning of October, the northern cold winds approach Yemen. Yemen is subjected to a combination of northern and southern air currents, resulting in atmospheric pressure centres that are still in the transitional stage. During the autumn, the south air mass brings moisture and travels north, triggering rainfall in Yemen's southern regions.

Wind speed in autumn

In most stations, the wind speed is lower in the autumn than in the summer. Except for a few stations on the east, west, and southern coasts, it is relatively quiet (Elzz et al., 1991; Algifri, 1998). Al Mukalla Station has the greatest average speed of 6.2 m/s, followed by Hodeidah 4.7 m/s, Aden 4.3 m/s, Hajjah 3.1 m/s, and Al Jowf 3.03 m/s respectively. The slowest speed was registered at Alfayoush station, which was less than 0.5 m/s. The average wind speed in Bayhan, Shabwa, and Al-dale was 0.7 m/s (Fig. 3).

Seasonal change in temperature

Dust storms have indirect relationship with temperature. The change in temperature plays a major role in physical and chemical weathering, which aid in the fragmentation and breaking of rocks in their immediate surroundings. Rising temperatures and decreasing rainfall cause an increase in the evaporation rate, leading to desiccation in surrounding desert areas. As a long term result, in the Republic of Yemen's the desert and semi-desert regions are expanding. Mountain breezes, valley breezes, land and sea breezes are caused by temperature variations within Yemen's topography, during day and night, and between water bodies. These are the result of differences in atmospheric pressure, which cause local winds to form, which contribute to the formation of sand storms and the spread of dust. Throughout the year, the temperature in desert and semi-desert areas ranges from 20 to 32°C, with significant differences in monthly and seasonal temperatures between Yemen's various regions, reaching up to 40°C in some areas (Hoddeidah, Aden, Hajjah and Marib). Because of the altitude factor, it decreases slightly in highland areas. During the summer, the minimum temperature was 12.3°C, and during the winter, spring, and autumn seasons, it was 22.4°C, 29.7°C, and 24.2°C. Summer temperatures reached 55.2°C, while winter, spring, and autumn temperatures reached 48.2°C, 54.4°C, and 49.9°C, respectively. Figure 4 shows a graphical representation of the seasonal variation in temperature at the 28 meteorological stations.

Seasonal changes in precipitation

The seasons of spring and autumn are considered transitional periods between monsoon seasons. Since

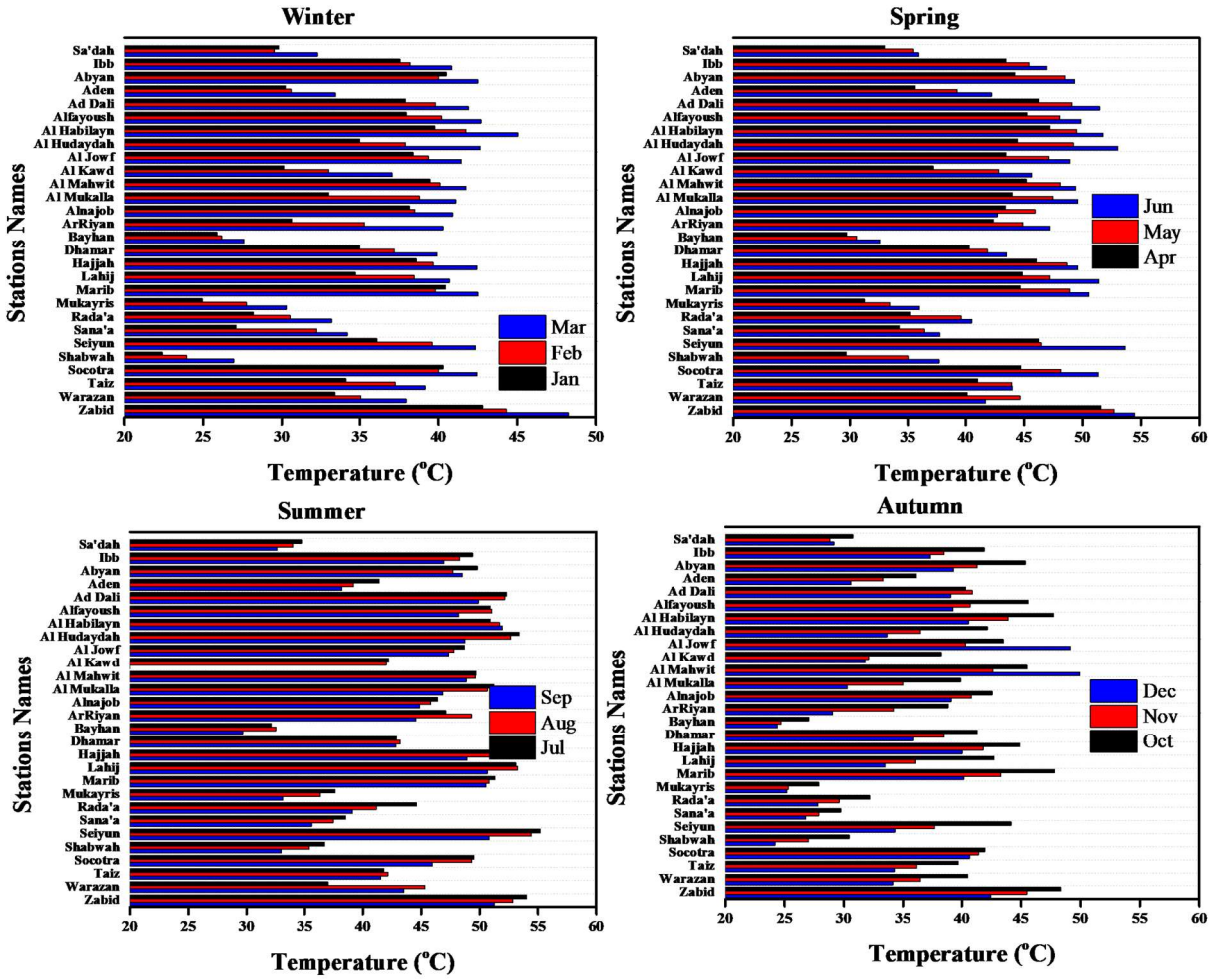

Fig. 4 Seasonal variations in the temperature in 28 stations at Yemen in 2010

1960, the precipitation has been decreasing at a rate of 1.2 mm/month/decade, and this trend is expected to continue (Sweeney et al., 2010). During the winter, the lowest amount of rainfall recorded was 0.0 mm, while the highest amount was 330.8 mm. The highest recorded value was 196.4 mm in the summer. Figure 5 shows the seasonal variation in monthly precipitation at 28 meteorological stations.

Statistical Analysis

Descriptive statistics

The descriptive statistical results obtained for the wind speed data and T-statistic values are listed in Table 1. Based on the above data, we can conclude that each season has a significant variation in all variables. Because the P-value of all the seasons is greater than 0.05, the T-test data reveals that the group means (wind speed) for all seasons are significantly different at the 0.05 level.

There is a significant variation in all variables during each season (Table 2). The T-test results show that the group means (temperature) for all seasons are significantly different at the 0.05 level (Table 2) because the P-value for all seasons is greater than 0.05.

In each season, there are significant variations in all variables (Table 3). The T-test results show that the group's means (precipitation) for all seasons differ significantly at the 0.05 level (Table 3). The mean value is greater than zero in all three cases, i.e., wind speed, temperature, and precipitation, so we reject the null hypothesis and conclude that the values obtained for all three parameters are significantly different at the 0.05 level, because the P-values for all three seasons are greater than 0.05.

Oneway ANOVA Test

The one-way analysis of variance (ANOVA) is used to determine whether the means of three or more independent (unrelated) groups differ statistically significantly. In this study, each of the three parameters/environmental factors is treated as a separate group. All three parameters were subjected to an ANOVA test in this study. Table 4 shows the descriptive statistical data obtained for the samples. Table 5 shows the results of the one-way ANOVA.

We can conclude from the results that the means of all parameters are significantly different at the 0.05 level, rejecting the null hypothesis. The ANOVA test revealed that F (2, 1005) = 301.683, P=0 for the three parameters of wind speed, temperature, and precipitation. The null hypothesis is rejected because the P-value is less than 0.05. Since we reject the null hypothesis, we must use/opt for another test, the Tukey test and Levene's Test.

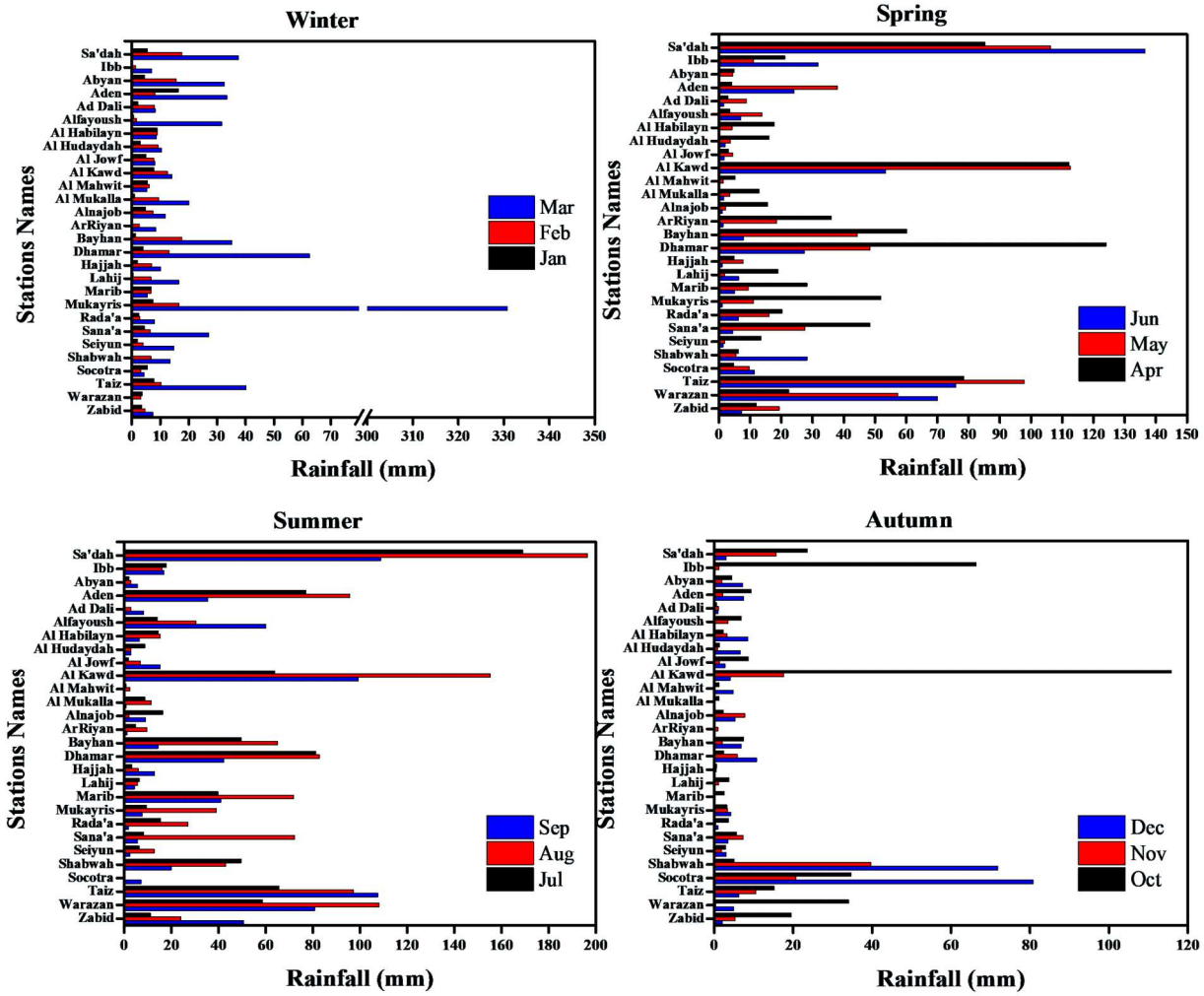

Fig. 5 Seasonal variations in monthly precipitation in 28 stations at Yemen in 2010

Table 1 The descriptive statistics and T-test results of wind speed

Seasons	# of samples	MEAN	STDEV	SUM	MIN	MED	MAX	t- Statistic	DF	Prob>|t| (P)
Winter	84	2.016	1.119	169.4	0.5	1.7	6.3	16.510	83	5.94563E-28
Spring	84	2.014	1.067	169.2	0.5	1.7	4.8	17.293	83	2.98687E-29
Summer	84	2.102	1.253	176.6	0.4	1.75	5.5	15.372	83	5.25922E-26
Autumn	84	2	1.354	168	0.5	1.5	7	13.529	83	1.06277E-22

Null Hypothesis, Mean=0; Alternative Hypothesis, Mean <>0; Winter - At 0.05 levels, the population mean is significantly different from the test mean; Spring - At 0.05 levels, the population mean is significantly different from the test mean; Summer - At 0.05 levels, the population mean is significantly different from the test mean; Autumn - At 0.05 levels, the population mean is significantly different from the test mean

Table 2 The descriptive statistics and T-test results of temperature

Seasons	# of samples	MEAN	STDEV	SUM	MIN	MED	MAX	t- Statistic	DF	Prob>|t| (P)
Winter	84	36.541	5.518	3069.45	22.4	38.175	48.25	60.692	83	1.53413E-70
Spring	84	43.829	6.096	3681.7	29.7	44.775	54.45	65.888	83	1.92414E-73
Summer	84	45.168	7.236	4697.55	12.35	47.525	55.2	63.651	103	1.61097E-84
Autumn	84	37.138	6.559	3119.6	24.2	38.675	49.95	51.888	83	4.90731E-65

Null Hypothesis, Mean=0; Alternative Hypothesis, Mean <>0; Winter - At 0.05 levels, the population mean is significantly different from the test mean; Spring - At 0.05 levels, the population mean is significantly different from the test mean; Summer - At 0.05 levels, the population mean is significantly different from the test mean; Autumn - At 0.05 levels, the population mean is significantly different from the test mean

Table 3 The descriptive statistics and T-test results of precipitation

Seasons	# of samples	MEAN	STDEV	SUM	MIN	MED	MAX	t- Statistic	DF	Prob>|t| (P)
Winter	84	13.728	36.572	1153.21	0	7.2	330.8	3.440	83	9.11391E-4
Spring	84	24.269	32.313	2038.62	0	10.35	136.5	6.883	83	1.02907E-9
Summer	84	33.046	41.469	2775.9	0	14.15	196.4	7.303	83	1.55517E-10
Autumn	84	9.345	18.869	784.98	0	3.25	115.8	4.538	83	1.89283E-5

Null Hypothesis, Mean=0; Alternative Hypothesis, Mean <>0; Winter - At 0.05 levels, the population mean is significantly different from the test mean; Spring - At 0.05 levels, the population mean is significantly different from the test mean; Summer - At 0.05 levels, the population mean is significantly different from the test mean; Autumn - At 0.05 levels, the population mean is significantly different from the test mean

Table 4 Overall descriptive statistics

Samples	# of samples	MEAN	STDEV	SE of Mean
Wind Speed	336	2.033	1.199	0.06543
Temperature	336	40.649	7.478	0.40801
Precipitation	336	20.097	34.495	1.8819

Table 5 One-way ANOVA/ Overall ANOVA

	Sum of Squares	Mean Square	DF	F Value	Prob>F (P)
Model	250866.449	125433.224	2	301.683	0
Error	417856.680	415.777	1005		
Total	668723.129		1007		

Null Hypothesis - The means of all level are equal; Alternative Hypothesis - The mean of one or more level are different; At the 0.05 level, the population means are significantly different

The quality of linear regression is given in Table 6. Here, the R- Square or coefficient of determination (COD) value is nearer to/lies between 0 and 1and hence we can say that there is a strong relationship between the parameters analyzed.

Tukey test and Homogeneity of Variance Test/ Levenes Test

The Tukey test compares the means of the three groups to determine which group's mean is different (Table 7). It was discovered that the Sig value in all three cases is 1. The mean difference is significant at the 0.05 level, as evidenced by this. The homogeneity of variance test was also carried out.

Table 6 Fit statistics

R-Square	CoeffVar	Root MSE	Data Mean
0.375	0.974	20.390	20.926

At the 0.05 level, it was discovered that there is a significant difference in variance (Table 8). Figure 6 shows a graphical representation of the data distribution.

Wind speed, temperature, and rainfall vary greatly from season to season and month to month (Table 9). The day-to-day fluctuations in the variability and differences in the climatic elements have a major impact on dust and sand storms, especially in Yemen's desert and semi-desert areas and surrounding areas (Akhtar, 2018).

Correlation Test

The correlations of climatic variables in all research samples are indicated in Table 9. To evaluate the linear relationship between seasonal variables, correlation analyses were conducted. The effects of the seasonal variation of all parameters, including wind speed, temperature, and precipitation, were analysed using correlation analysis. According to the overall statistical findings, there are fourteen positive and ten negative correlations that are significant at the 1 and 5% levels. By comparing the findings, we can see that the parameters have a greater positive correlation and are statistically relevant at the 1% stage. The power of the positive correlation, on the other hand, is weaker (Table 9).

Table 7 Means comparison / Tukey test

Comparison	MeanDiff	SEM	q-value	Prob	Alpha	Sig	LCL	UCL
Temperature / Wind Speed	38.615	1.573	34.714	0	0.05	1	34.923	42.308
Precipitation / Wind Speed	18.064	1.573	16.238	0	0.05	1	14.371	21.756
Precipitation / Temperature	-20.551	1.573	18.475	0	0.05	1	-24.244	-16.859

Sig equals 1, indicates that mean difference is significant at 0.05 level; Sig equals 0, indicates that the mean difference is not significant at the 0.05 level

Table 8 Homogeneity of variance Test/ Levenes test

	Sum of squares	Mean square	DF	F-value	Prob>F
Model	76810.833	38405.416	2	153.977	0
Error	250668.914	249.421	1005		

At the 0.05 level, the population variance is significantly different.

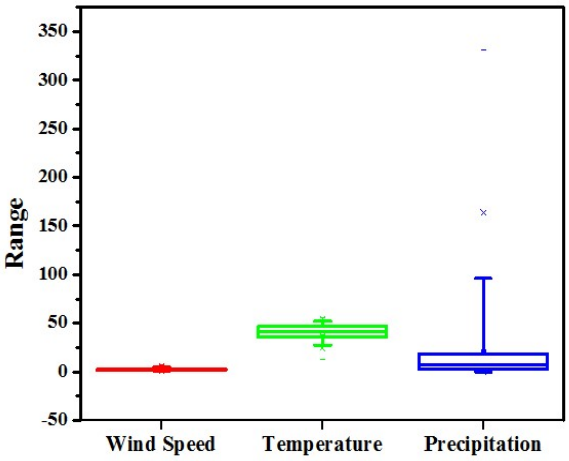

Fig. 6 Graphical representation of data distribution (wind speed, temperature, and precipitation)

There are fourteen positive correlations and ten negative correlations in all the studies analyzed since the majority of the correlations between the parameters are statistically insignificant. The most significant positive correlation between variables was found, while the others were all negative.

Impact of dust and sand storm

Dust storm and sand storm have both positive and negative effects on the environment.

Negative impact of dust and sand storms

Dust and sand storms have impact on the main roads, which are linked to an internal network between the highland, coastal regions and island region. Hoddeidah, Aden, and Hadramout are Yemen's most important cities and ports, and they serve as the country's key transportation hubs. Yemen and Saudi Arabia are linked by an international line in this area. Furthermore, desert areas are of similar significance in terms of transportation routes. Yemen is linked to Saudi Arabia via the Al Jowf and Marib international lines, while the country is linked to Oman via the governorates of Shabwah, Hadramout, and Al Mahrah. Sands and dust storms minimize the horizontal visibility on these highways, resulting in horrific traffic accidents (Notaro et al., 2013). Besides, the accumulation of sand on all major roads and sub-roads is a problem, as it triggers the closing of some of them, and drivers who are unaware of the sandstorm's occurrence have their vehicles crash, resulting in major material and human injuries.

Sandstorms transport sand and dust to agricultural lands, destroying crops, especially those that can't withstand the force of wind or the deposition of sand and dust. Meanwhile, farmers are trying to restore agricultural lands that have been buried by sand. Year after year, sand and dust storms intensify desertification in arid and semi-arid regions. The storms also transport certain plants and crop diseases from the blown-out areas to the target lands. There have been a few cases when fungi have been transported from the south of Saudi Arabia to Yemen by these storms and have directly affected plants (Stefanski & Sivakumar, 2009).

Sand and dust storms cause large-scale economic losses in the short term as well, such as livestock disease leading to death, crop destruction, building and infrastructure damage, and vehicle damage. Besides, to clean the accumulated sand and dust, costs a lot of money (Sufian et al., 2017). Sand storms are having a big effect on Yemeni tents. Due to war in some areas, such as the Aljafnah camp in the Marib governorate in August 2018, the majority of people took refuge in tents. These storms have raised their tents. Similarly, tents were raised in areas where African refugees fled their countries due to violence and found refuge in UN refugee shelters along the coast. Owing to the extreme dust storm that passed through those regions, many schools and educational institutions were forced to close. Aden city was recently subjected to violent dust storms on September 11, 2019, with winds exceeding 22 km/h and a temperature of 35°C (according to the National Center for Meteorology and in Aden).

Table 9 Correlation of all studied variables during the seasons

Variables		Wind				Temperature				Rainfall			
		Wi	Sp	Su	Au	Wi	Sp	Su	Au	Wi	Sp	Su	Au
Rainfall	Au	NS	NS	NS	NS	NS	NS	NS	NS	NS	.245*	NS	
	Su	NS	NS	NS	NS	-.328**	-.395**	-.509**	-.300**	NS	.778**		
	Sp	NS	NS	NS	NS	-.381**	-.438**	-.454**	-.266*	NS			
	Wi	NS	NS	NS	NS	NS	NS	-.263*	-.288**				
Temperature	Au	NS	NS	NS	NS	.683**	.657**	.733**					
	Su	NS	NS	NS	NS	.666**	.720**						
	Sp	NS	NS	NS	NS	.933**							
	Wi	NS	NS	NS	NS								
Wind	Au	.800**	.802**	.665**									
	Su	.697**	.785**										
	Sp	.858**											
	Wi												

Wi = winter, Sp = Spring, Su = Summer and Au = Autumn

** Correlation is significant at the 0.01 level (2-tailed). * Correlation is significant at the 0.05 level (2-tailed) and NS = Non Significant

In the long run, it involves soil degradation, habitat pollution, and desertification, as well as the costs of health care and wasted labor. According to a UN (United Nations) survey published in 2016, dust storms and the sediments resulting from sand and dust storms cost the Arab region's total local production about 13 billion dollars per year. It obstructs irrigation canals and covers drainage routes, causing contamination of river water and streams (Prakash et al., 2015; Karagulian et al., 2019). Dense dust is highly dangerous during aircraft landings and takeoffs, causing landing positions to be changed and takeoff times to be postponed. The engines are damaged by the effect of dust on the aircraft's surface (Notaro et al., 2013). Solar power plants, particularly those that depend on direct solar radiation, are also influenced by dust. Keeping solar collectors clean of dust so that dust particles do not obstruct the incoming radiation which takes time and effort, and is a major source of concern for station operators.

Positive impact of dust and sand storm

The renewal of the soil is a beneficial result of sand and dust storms. During dust storms, loads of dust is transported to the troposphere, from where it is deposited during a calm weather or rain, and falls on the ground in areas hundreds of kilometers away from the dust storm's origin. This dust becomes mixed with the soil and can transfer to sedimentation areas. Thousands of tons of new soil are applied annually for agricultural terraces in the bottom and above the surface layer of Yemeni land, which are affected by sand storms and dust. Dust storms and dust contribute in plant pollination, as well as the movement of certain plant seeds from the source to the destination areas. An investigation found that new plants, which were previously unknown in many areas of Yemen, originated in desert and semi-desert areas and were carried by storms. (Karagulian et al., 2019).

The dust serves as a soil fertilizer and assists in the ripening of fruits. The dust layer that forms above the fruits in Yemen aids in their rapid ripening. The dust in the wet ripening of palm products in the Tihamah plain helps farmers in that area. Instead of using pesticides and industrial fertilizers, farmers in many areas use dust to regenerate fresh leaves and speed up their development. Nutrient minerals (e.g. iron) and other elements in the dust are beneficial to land and water ecosystems. Hawaii's rain forests get their nutrients from dust brought by the wind from Central Asia. Phytoplankton in the Mediterranean Sea benefit from metals and nutrients brought by desert winds coming from the north of Libya and the Sahara dust provides phospholipids additives that offset the loss of the Amazon rainforest as a result of river flow. The Mediterranean Sea's habitats, which form the plankton at the base of its food pyramid, are being threatened by rising drought in the upper soils (Forner et al., 2018).

The effects of dust on human health

The dust storm and dust in air can cause allergy of the eye, of the nose and ear, asthma attacks, dermatitis, and it can negatively influence the condition of people with cardio-vascular diseases. Fine dust enters the eye and causes conjunctivitis in the eyelids region, causing redness and itching, as well as tears (World Health Organization, 2013; Aili & Oanh, 2015).

The small dust particles brought by dust storms (Fig. 7) can get into the respiratory system, causing inflammation of the mucous membranes, clogged noses, and respiratory irritation when inhaled. It also induces shortness of breath when exerting physical activity, as well as an itchy nose that can spread to the eyes and ears. They can even make the nose run, in case of increased sensitivity, nosebleeds can appear (Ghio et al., 2014; Gross et al., 2018). The ear's sensitivity to dust causes inflammation, which causes extreme itching (World Health Organization, 2013; Ghio et al., 2014; Aili & Oanh, 2015). Dust asthma attacks are also common, particularly if the person is exposed to dust because dust can carry bacteria and pollen that cause asthma (World Health Organization, 2013; Ghio et al., 2014; Aili & Oanh, 2015; Gross et al., 2018). When some people inhale dust, it causes skin inflammation, especially eczema, which causes itching (World Health World Health Organization, 2013; Ghio et al., 2014; Aili & Oanh, 2015). Chest diseases affect a large percentage of heart patients. Because of their susceptibility to dust particles, they suffer from heart muscle inflation and high pulmonary arterial pressure, which contributes to emphysema and capillary breakage (World Health Organization, 2013; Ghio et al., 2014; Aili & Oanh, 2015; Gross et al., 2018).

Problems faced by the Yemen Government relating to the dust and sand storms phenomenon

The Yemeni Government is grappling with a slew of issues related to dust and sand storms. The absence of advanced meteorological stations, for precisely monitoring and recording this phenomenon. The shortage of well- equipped laboratories. Scientific evidence related to this phenomenon is unavailable due to a lack of financial resources and hence financial support or sufficient funding is very essential. There is a lack of knowledge about environmental initiatives related to this phenomenon and how to deal with it both before and after it happens. There are no short or long-term plans or initiatives in place to mitigate or eliminate the risk associated with this phenomenon that exists across wide areas of Yemen. If the Yemeni government can update and fix all of the above-mentioned problems, we can at least reduce the potential impact of the dust storm and sand storm in Yemen.

Fig. 7 Heavy dust storms crossing some of the Yemeni cities (source: Yiannopoulos, 2018)

CONCLUSION

Yemen is affected by dust all over year, although it is less prevalent in the winter and more prevalent in the summer, although it is unpredictable in the spring and autumn due to the general weather condition. Coastal areas (Hajjah, Hoddeidah, Taiz, Lahg, Aden, Abyan, Shabwah, and Hadramout) and desert areas (Marib and Al Jowf) are the most affected by dust and sandstorms during the year, while the western and central governorates of Yemen in the mountainous region are predominantly affected by dust over the winter. Wind speeds in coastal areas such as Al Hudaydah (4.9 m/s), Al Mukalla (3.8 m/s), and Aden (4.09 m/s) rise in intensity. The equability of the surface, the contrast heat between the surface water, the relatively low air pressure, and land adjacent to it all contribute to the change in wind speed. Yemen is subjected to different air blocks, originating in the north and south, forming spring, air turbulence, and rainfall, particularly in the central and southern areas, as atmospheric pressure rises in the southern hemisphere. In between summer season, rain continues to fall until mid-September, as the result of the return of the northeast storms. Different atmospheric pressures generate different forms of wind, including sea and land breezes, mountain and valley breezes, Fohen, Al Ghawbah, and warm (Al-Kawi) winds. The presented research shows that environmental factors play an important role in the creation of dust and sand storms. According to the statistical analysis, environmental parameters are significantly correlated with one another, resulting in the development of dust and sand storms. Dust storms in Yemen have several effects on humans, animals, plants, and all-natural habitats, and they can be categorized as both positive and negative based on their impact on environmental components.

ACKNOWLEDGEMENT

The authors of this article wish to acknowledge NASA for the satellite image, and everyone has directly or indirectly contributed during this entire work.

References

A1-Sanad, H. A., Ismael, N. F., Nayfeh, A. J. 1993. Geotechnical properties of dune sands in Kuwait. *Engineering Geology* 34, 45–52. DOI: 10.1016/0013-7952(93)90042-B

Aili, A., Oanh, N. T. K. 2015. Effects of dust storm on public health in desert fringe area: Case study of northeast edge of Taklimakan Desert, China. *Atmospheric Pollution Research* 6 (5), 805–814, DOI: 10.5094/apr.2015.089.

Akhtar, S. 2018. Sand and Dust Storms in Asia and the Pacific: Opportunities for Regional Cooperation and Action. The Economic and Social Commission for Asia and the Pacific (ESCAP), Bangkok, Thailand. 1–76 p.

Algifri, A. H. 1998. Wind energy potential in Aden-Yemen. *Renewable Energy* 13, 255–260. DOI: 10.1016/S0960-1481(97)00069-4

Allaby, M., Garratt, R. 2007. Encyclopedia of Weather and Climate (Science Encyclopedia). Facts On File, Inc. An Imprint of Infobase Publishing, New York, 709 p.

Barnum, B., Winstead, N., Wesely, J., Hakola, A., Colarco, P., Toon, O., Ginoux, P., Brooks, G., Hasselbarth, L., Toth, B. 2004. Forecasting dust storms using the CARMA-dust model and MM5 weather data. *Environmental Modelling & Software* 19 (2), 129–140, DOI: 10.1016/s1364-8152(03)00115-4.

Baumbach, G., Vogt, U. 1999. Experimental determination of the effect of mountain-valley breeze circulation on air pollution in the vicinity of Freiburg. *Atmospheric Environment* 33, 4019–4027. DOI: 10.1016/S1352-2310(99)00143-0

Climate Change Profile: Yemen. 2018. Ministry of Foreign Affairs of the Netherlands. Netherland, 16 p.

Country Profile: Yemen. 2008. Library of Congress – Federal Research Division, Yemen, 26 p.

Crowther, J. M., Walker, D. J., Masouleh, Z. P. 2019. A Long-Term Study of Sea-Breeze Characteristics: A Case Study of the Coastal City of Adelaide. *Journal of Applied Meteorology and Climatology* 58 (2), 385–400, DOI: 10.1175/jamc-d-17-0251.1.

Cullen, H. M. 2005. Asia, Climate of Southwest. In J. E. Oliver (Ed.), Encyclopedia of World Climatology Dordrecht: Springer Netherlands, 125 p.

Davis, S. R., Farrar, J. T., Weller, R. A., Jiang, H., Pratt, L. J. 2019. The Land-Sea Breeze of the Red Sea: Observations, Simulations, and Relationships to Regional Moisture Transport. *Journal of Geophysical Research: Atmospheres* 124 (24), 13803–13825, DOI: 10.1029/2019JD031007

Elzz, H. M. A. E., Motawakel, M. K. A., El-Etzz, Z. A. A. 1991. Wind Characteristicand Energy Potentialities of some selected sites in the Yemen Arab Republic and the Republic of Egypt. *Renewable Energy* 1, 675–681. DOI: 10.1016/0960-1481(91)90013-F

Forner, A., Valladares, F., Bonal, D., Granier, A., Grossiord, C., Aranda, I. 2018. Extreme droughts affecting Mediterranean tree species' growth and water-use efficiency: the importance of timing. *Tree Physiology* 38 (8), 1127–1137, DOI: 10.1093/treephys/tpy022

Furman, H. K. H. 2016. Dust Storms in the Middle East: Sources of Origin and Their Temporal Characteristics. *Indoor and Built Environment* 12 (6), 419–426, DOI: 10.1177/1420326x03037110

Ghio, A. J., Kummarapurugu, S. T., Tong, H., Soukup, J. M., Dailey, L. A., Boykin, E., Gilmour, M. Ian., Ingram, P., Roggli, V. L., Goldstein,H. L., Reynolds, R. L. 2014. Biological effects of desert dust in respiratory epithelial cells and a murine model. *Inhalation toxicology* 26 (5), 299–309, DOI: 10.3109/08958378.2014.888109

Goudie, A. S. 1988. Aeolian Dust and Dust Deposits. *Journal of Arid Environments* 14 (1), 103–104, DOI: 10.1016/s0140-1963(18)31104-2

Goudie, A. S., Middleton, N. J. 2001. Saharan dust storms: nature and consequences. *Earth-Science Reviews, 56*, 179–204. DOI: 10.1016/S0012-8252(01)00067-8

Gaffin, D. M., 2007. Foehn Winds That Produced Large Temperature Differences near the Southern Appalachian Mountains. *Weather and Forecasting* 22 (1), 145–159, DOI: 10.1175/waf970.1

Gross, J. E., Carlos, W. G., Cruz, C. S. D., Harber, P., MD, S. J. 2018. Sand and Dust Storms: Acute Exposure and Threats to Respiratory Health. *American Thoracic Society* 198, 13–14, DOI: 10.26616/nioshpub2018129.

Iizumi, T., Ramankutty, N. 2015. How do weather and climate influence cropping area and intensity? *Global Food Security* 4, 46–50, DOI:10.1016/j.gfs.2014.11.003

Karagulian, F., Temimi, M., Ghebreyesus, D., Weston, M., Kondapalli, N.K., Valappil, V.K., Aldababesh, A., Lyapustin, A., Chaouch, N., Hammadi, F.A., Abdooli, A. A. 2019. Analysis of a severe dust storm and its impact on air quality conditions using WRF-Chem modeling, satellite imagery, and ground observations. *Air Quality, Atmosphere & Health* 12 (4), 453–470, DOI: 10.1007/s11869-019-00674-z

Knippertz, P., Deutscher, C., Kandler, K., ller, T. M., Schulz, O., & Schütz, L. 2007. Dust mobilization due to density currents in the Atlas region: Observations from the Saharan Mineral Dust Experiment 2006 field campaign. *Journal of Geophysical Research, 112* (D21), 1–14, doi:10.1029/2007jd008774

Luo, C., Mahowald, N., Jones, C. 2004. Temporal variability of dust mobilization and concentration in source regions. *Journal of Geophysical Research* 109 (D20), 1–13, DOI: 10.1029/2004jd004861

Middleton, N. J. 1986. A Geography of Dust strome in South-West Asia. *Journal of Climatology* 6, 183–196. DOI: 10.1002/joc.3370060207

Miguel, L. V. 2017. *Modeling the dust life cycle and its associated meteorological processes from global to regional scales*. Doctoral program in Environmental Engineering, Universitat Politècnica de Catalunya, 123p.

Notaro, M., Alkolibi, F., Fadda, E., Bakhrjy, F. 2013. Trajectory analysis of Saudi Arabian dust storms. *Journal of Geophysical Research: Atmospheres* 118 (12), 6028–6043, DOI: 10.1002/jgrd.50346

Orlovsky, N. S., Orlovsky, L., Indoitu, R. 2013. Severe dust storms in Central Asia. *Arid Ecosystems* 3 (4), 227–234, DOI: 10.1134/s2079096113040082

Pease, P. P., Tchakerian, V. P., indale, N. W. 1988. Aerosols over the Arabian Sea: geochemistry and source areas for aeolian desert dust. *Journal of Arid Environments* 39, 477–496. DOI: 10.1006/jare.1997.0368

Prakash, P. J., Stenchikov, G., Kalenderski, S., Osipov, S., Bangalath, H. 2015. The impact of dust storms on the Arabian Peninsula and the Red Sea. *Atmospheric Chemistry and Physics* 15 (1), 199–222, DOI: 10.5194/acp-15-199-2015

Prospero, J. M., Bullard, J. E., Hodgkins, R. 2012. High-Latitude Dust Over the North Atlantic: Inputs from Icelandic Proglacial Dust Storms. *Science* 335, 1078–1082. DOI: 10.1126/science.1217447

Pye, K. 1987. Aeolian Dust and Dust Deposits. Academic Press, Elsevier, London, 334 p.

Rafferty, J. P. 2011. Storms, Violent Winds, and Earth's Atmosphere (Dynamic Earth). In Levy, M.I. (ed.), Britannica Educational Publishing, New York, 251 pp.

Rezazadeh, M., Irannejad, P., Shao, Y. 2013. Climatology of the Middle East dust events. *Aeolian Research* 10, 103–109, DOI: 10.1016/j.aeolia.2013.04.001

Shepherd, G., Terradellas, E., Baklanov, A., Kang, U., Sprigg, W. A., Nickovic, S., Boloorani, A. D., Dousari, A. A., Basart, S., Benedetti, A., Sealy, A., Tong, D., Zhang, X., Guillemot, J.S., Zhang, K., Knippertz, P., Mohammed, A. A. A., Dabbas, M. A., Cheng, L., Otani, S., Wang, F., Zhang, C., Ryoo, S. B., Cha, J. 2016. Global Assessment of Sand and Dust Storms. United Nations Environment Programme (UNEP), Nairobi, 123 p.

Stefanski, R., Sivakumar, M. V. K. 2009. Impacts of sand and dust storms on agriculture and potential agricultural applications of a SDSWS. *IOP Conference Series: Earth and*

Environmental Science 7, 012016, DOI: 10.1088/1755-1307/7/1/012016

Sufian, T., Ögutcu, C., Barra, M. 2017. Energy Investment and Business Climate report for Observed Countries *The Republic of Yemen*. Energy Charter Secretariat, Brussels, Belgium, 53 p.

Sweeney, C. M., New, M., Lizcano, G., Lu, X. 2010. The UNDP Climate Change Country Profiles. *Bulletin of the American Meteorological Society* 91 (2), 157–166, DOI: 10.1175/2009bams2826.1

Winter, W. d., Donker, J., Sterk, G., Beem, J. v., Ruessink, G. 2020. Regional versus local wind speed and direction at a narrow beach with a high and steep foredune. *PLoS One* 15 (1), 1–19, DOI: 10.1371/journal.pone.0226983

World Health Organization, 2013. Review of evidence on health aspects of air pollution – REVIHAAP Project. The WHO European Centre for Environment and Health, Bonn, WHO Regional Office for Europe. Denmark, 300 p.

Yiannopoulos, A. 2018. Yemen: civilians are not a target. Online available at https://views-voices.oxfam.org.uk/2018/08/yemen-civilians-are-not-a-target/

Yin, Y., Wurzler, S., Levin, Z., & Reisin, T. G. 2002. Interactions of mineral dust particles and clouds: Effects on precipitation and cloud optical properties. *Journal of Geophysical Research: Atmospheres* 107 (D23), AAC 19-11-AAC 19–14, DOI: 10.1029/2001jd001544

sciendo

Journal of Environmental Geography 14 (1–2), 38–46.

DOI: 10.2478/jengeo-2021-0004
ISSN 2060-467X

DETECTION OF PLASTIC GREENHOUSES USING HIGH RESOLUTION RGB REMOTE SENSING DATA AND CONVOLUTIONAL NEURAL NETWORK

Balázs Jakab[1]*, Boudewijn van Leeuwen[1], Zalán Tobak[1]

[1]Department of Geoinformatics, Physical and Environmental Geography, University of Szeged,
Egyetem u. 2-6, 6722 Szeged, Hungary
*Corresponding author, email: jakabbalazs501@gmail.com

Research article, received 5 February 2021, accepted 13 April 2021

Abstract

Agricultural production in greenhouses shows a rapid growth in many parts of the world. This form of intensive farming requires a large amount of water and fertilizers, and can have a severe impact on the environment. The number of greenhouses and their location is important for applications like spatial planning, environmental protection, agricultural statistics and taxation. Therefore, with this study we aim to develop a methodology to detect plastic greenhouses in remote sensing data using machine learning algorithms.
This research presents the results of the use of a convolutional neural network for automatic object detection of plastic greenhouses in high resolution remotely sensed data within a GIS environment with a graphical interface to advanced algorithms. The convolutional neural network is trained with manually digitized greenhouses and RGB images downloaded from Google Earth. The ArcGIS Pro geographic information system provides access to many of the most advanced python-based machine learning environments like Keras – TensorFlow, PyTorch, fastai and Scikit-learn. These libraries can be accessed via a graphical interface within the GIS environment.
Our research evaluated the results of training and inference of three different convolutional neural networks. Experiments were executed with many settings for the backbone models and hyperparameters. The performance of the three models in terms of detection accuracy and time required for training was compared. The model based on the VGG_11 backbone model (with dropout) resulted in an average accuracy of 79.2% with a relatively short training time of 90 minutes, the much more complex DenseNet121 model was trained in 16.5 hours and showed a result of 79.1%, while the ResNet18 based model showed an average accuracy of 83.1% with a training time of 3.5 hours.

Keywords: plastic greenhouse, deep learning, convolutional neural network, satellite image, Google Earth

INTRODUCTION

In recent years, agricultural production in greenhouses showed a rapid growth (Agüera and Liu, 2009; Wu et al., 2016; Nemmaoui et al., 2019). In many arid and semi-arid countries, plastic greenhouses form a large share in the total number of greenhouses, since they are more affordable and can be used temporary as well. Plastic greenhouses are made of a partly transparent plastic cover to be able to control the environmental and growing conditions inside the greenhouse. It is important to monitor their spatial distribution, since this form of intensive farming requires large amounts of water and fertilizers and can have a severe impact on the environment. Estimation of the share of plastic greenhouses in the total agricultural activities can be performed by directly counting the number of greenhouses. This is slow, labor intensive and consequently expensive, therefore, it makes sense to apply remote sensing data-based algorithms to detect them. Apart from spatial planning and environmental protection, another reason to acquire knowledge of the number and location of greenhouses is that their registration is obligatory for taxation purposes.

Research on the classification of plastic or glass greenhouses using very high to medium resolution (multi-spectral) remote sensing data and methodologies has been published earlier. Wu et al. (2016) applied random forest (RF) and support vector machine (SVM) on medium resolution multispectral data. Also, Yang et al. (2017) used medium resolution data, but they presented an index-based approach resulting in an overall accuracy of 91%. Koc-San (2013) reported high accuracies of classification of glass and plastic greenhouses using maximum likelihood (ML), RF and SVM methods based on Worldview-2 very high-resolution data. Agüera et al. (2008) received promising results when applying texture analysis combined with ML on very high-resolution satellite imagery. Agüera and Liu (2009) used ML classification to automatically delineate greenhouses. They report results with medium accuracy. Supervised classification based on a combination of orthophotos and Landsat data was proposed by González-Yebra et al. (2018). Novelli et al. (2016) used a combination of Landsat and Sentinel-2. They classified medium resolution data using Object Based Image Analysis (OBIA) and RF. Accuracies ranged between 89 and 93%. Very high-resolution satellite imagery was used by Nemmaoui et al. (2019) to derive surface and terrain models to extract plastic greenhouses. They report very high accuracies of up to 98%. Most recently, Yang et al. (2021) published a

manual approach to identify greenhouses to study urban fringe based on imagery downloaded from Google Earth.

The term artificial intelligence (AI) was first used in 1955 (McCarthy et al., 1955). Given that intelligence is difficult to define, this term is not easy to define either. It can be formulated as a process that mimics human abilities and behavior according to pre-programmed rules (Nilsson, 1980; Simon, 1995). Machine learning (ML) is a part of artificial intelligence that, based on collected data, can learn and develop itself in an iterative way using pre-programmed rules (Michie, 1968). Artificial Neural Networks (ANN) are a type of ML algorithms loosely based on the biological functioning of the brain. Artificial neurons process and transmit many input signals to a large number of neighboring neurons. The neurons are stored in layers, the final layer collects the signals and processes them to an output signal, with is the result of the network. The network learns from input and output data pairs and stores their combined relationship as weights (Müller et al., 1995). Deep learning is a group of ML algorithms that uses ANNs with many hidden layers. The more hidden layers, the deeper and more complex the neural network and the more complicated tasks it can potentially solve. In the present age, deep learning has become widespread and makes it possible to process large data sets that are otherwise often too big to manage. Examples of applications of deep learning include face recognition, image recognition, or self-driving vehicles (Goodfellow et al., 2016).

The current revolution in deep learning algorithms for computer vision also provides opportunities to improve analysis of remote sensing data. Numerous studies have been published on the classification of medium (e.g., Watanabe et al., 2018; Gallwey et al., 2020; Rai et al., 2020; Virnodkar et al. 2020) and high resolution (e.g. Flood et al., 2019; Schiefer et al., 2020; Zhang et al., 2020) satellite images using deep learning methods (Kattenborn et al., 2021). Detection of individual objects in the imagery is not as common as classification but has been published as well (Ding et al., 2018; Jiang et al., 2019; Guo et al., 2020; Pi et al., 2020). The difference between the two results is important; classification provides a label for every pixel, specifying the class it belongs to. This is the most common approach when converting remote sensing data to thematic maps. On the contrary, object detection provides an output layer on top of the original remote sensing image where the objects of interest are shown with a square bounding box around them indicating their precise location and accuracy estimation.

The aim of our research is to evaluate if the current innovations in machine learning based technologies can be applied to detect plastic greenhouses. The presented methodology is based on object detection using a convolutional neural network (CNN). A CNN is an ANN that is designed to learn the spatial features, e.g. edges, corners, textures, or more abstract shapes, that best describes the target class or quantity. Like other ANNs, CNNs are based on neurons that are organized in layers and are connected through weights and biases. The initial layer is the input layer, e.g. remote sensing data, and the last layer is the predicted output (Kattenborn et al., 2021).

In recent years, accessibility to machine learning algorithms and deep learning models in particular has been improved by implementations in user-friendly environments under Python or R. A next step in the development towards easier excess to the algorithms is the implementation of graphical user interfaces on top of the functionality. One implementation is the Deep learning toolset in ArcGIS Pro (ESRI, 2021) which implements third-party deep learning frameworks – such as Keras – TensorFlow (Abadi et al., 2015; Chollet, 2015), PyTorch (Paszke et al., 2019), fastai (Howard and Gugger, 2020) and Scikit-learn (Pedregosa et al., 2011).

In this study, we present a methodology based on freely available images and a convolutional network to detect plastic greenhouses in an area in the south of Hungary. The area is mainly agricultural with a large amount of tunnel shaped plastic greenhouses. The earlier mentioned studies applied deep learning techniques for classification of high resolution remote sensing data, but none of them used CNN for object detection based on data from Google Earth.

STUDY AREA

A 230 km^2 area in the south east of the Great Hungarian Plain, near the town of Szeged (Fig. 1) has been selected to test the CNN algorithm. The area is mainly agricultural and has a large number of greenhouses. Other main land use/land cover classes in the area are forest, urban/build up and some water bodies. Most of the area has chernozem and sandy soils, but in some areas arenosol can be found. The sandy soils absorb water quickly causing the soil to dry out and reduce its fertility. The area suffers from high air pollution and dust content. In the 1750s, locust tree (Robinia pseudoacacia) was introduced in the region as an ornamental plant. The invasive species spread quickly through the region, and helps to reduce wind erosion, but it also reduces the nutrients in the soil. With 400-450 mm, the annual rainfall is low compared to the mean precipitation (600-700 mm) of the country (Mezősi, 2011).

DATA AND METHODS

The imagery used as input data for the presented detection algorithm was extracted from Google Earth. The high-resolution data is a georeferenced red-green-blue (RGB) image collected by CNES/Airbus in August 2020. The image was downloaded using the Tile+ extension in QGIS.

The concept of convolutional neural networks was introduced in the 1980s by Yann LeCun (LeCun et al., 1990). CNNs differ from fully connected ANNs by having each neuron being connected to only a limited number of neurons in the previous layer. CNNs assume that the input is an image and look for features through a kernel. The detection is performed through convolution between the input and the kernel thus the term convolutional neural networks. The kernels form a

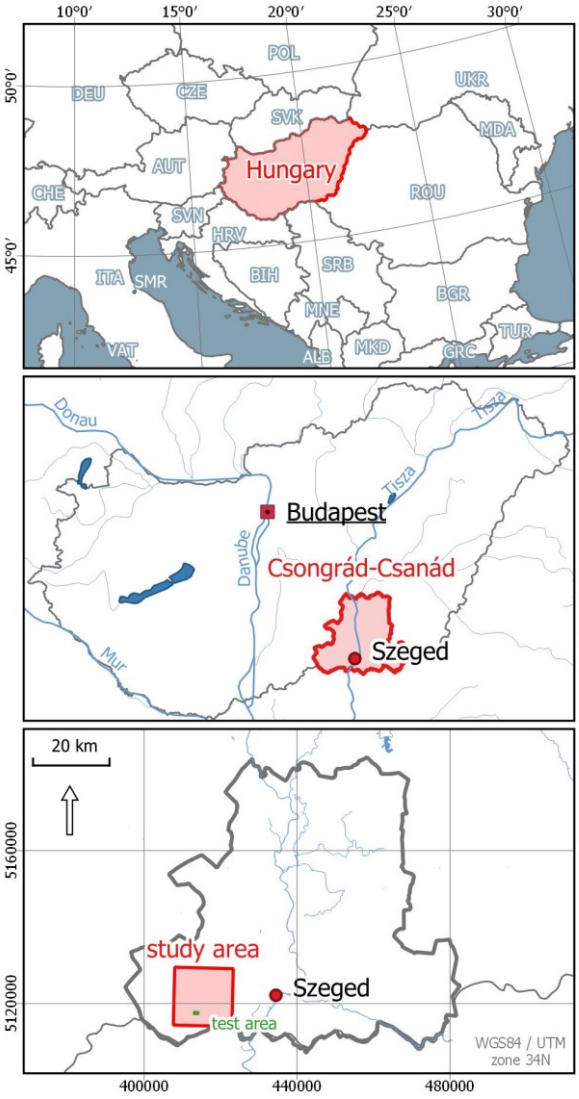

Fig. 1 Location of the study area

convolutional filter, and a set of stacked convolutional filters makes a convolutional layer (Fig. 2). Convolutional layers are followed by activation functions which introduce nonlinear behavior to the model. Each convolutional layer extracts features with increasing complexity from the input layer. After each convolutional layer, a pooling layer extracts the most prominent features and reduces the resolution of the previous input. A CNN thus contains a stack of convolutional layers followed by activation functions and pooling layers, and finally an addition of one or more Fully Connected (FC) layers. FC layers form an ANN head on top of the CNN that is used to classify the CNN output into a set of finite classes (Davies, 2018). In case of object detection, objects are not only classified, but their locations are indicated with bounding boxes as well (Liu et al., 2016).

The methodology to detect plastic greenhouses can be separated in 6 sequential steps. The first step is to download of the input image. The second is the generation of training and validation samples and the creation of image chips, and the third is the creation of the model architecture. The next step is the training of the model based on the training data. Then, the model parameters are fine-tuned based on the validation data set. The sixth and final step is the inference of the trained model with the total image.

The detection of greenhouses requires very high resolution data with at least 3 layers. This type of data can be provided by drones, aerial photographs or very high resolution satellite images. Since it is the aim of our research to apply the methodology on a large area, images collected by drones are not an option. Google Earth provides a source of high-resolution aerial photographs and satellite images that can be downloaded for free for non-commercial use. Therefore, an RGB image was downloaded from Google Earth with a resolution of 2000 dpi. This resulted in a 1 gigabyte three layer TIF file with an approximate spatial resolution of 50 cm. Selection criteria for the image were cloud cover percentage, spatial resolution and number of greenhouses. The extracted image covers an area of 230 km^2.

During the second step, samples of plastic greenhouses were identified in multiple subsets of the image. In each subset, all greenhouses were digitized manually to make sure that the model would not be trained with pixels that belong to greenhouses, but that were labeled as non-greenhouse pixels. In total, 2352 greenhouse samples were created. The higher the spatial resolution of the image, the easier is the identification of individual greenhouses; the downloaded image was of sufficient spatial resolution. The selection of the samples is of decisive important for the result of the detection of greenhouses. Using rotation, it is possible to perform data augmentation, with is the artificial creation of more training samples by capturing the sample created by the user at multiple angles.

The samples were used to generate training data in the PASCAL visual object classes meta data format (Everingham et al., 2010) and serve as input for the process of sub-setting the total image into individual chips. Only chips with (a part of) at least one sample in it were stored. With each chip an .xml file is produced that stores the location of the sample within the chip.

The training data was used as input for the training phase, where the algorithm aims to detect the

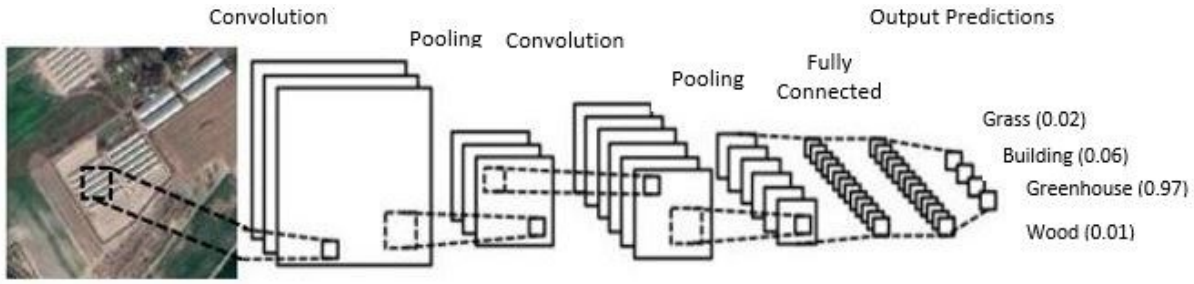

Fig. 2 Classification using a convolution neural network

greenhouses. During object detection, the algorithm uses bounding boxes to delimit the objects' location. The purpose of the training is to minimize the difference between the real and the modeled bounding boxes. In case there are several different objects in the image, all possible positions and box sizes need to be evaluated, which is calculation intensive. For this reason, originally, the R-CNN method was developed, which provides region suggestions. Single-shot detectors are an improved detection algorithm and are designed to skip making region suggestions and solve classification and regression tasks in one step, making them more efficient and faster. The two best known algorithms are YOLO (You Look Only Once) and SSD (Single Shot Detector) (Liu et al., 2016). The latter is used this research, because it is the most accurate and fastest (Poirson et al., 2016). Training performance can be increased considerably by applying transfer training based on a model with many parameters that was pre-trained for a different task (Howard and Gugger, 2020). A large number of pre-trained models can be downloaded via the internet. Each model has its specific architecture, among others they differ in number of layers and filter sizes. They can also vary in the type of data that was used to train them. The selection of the backbone model determines the architecture of the model used for the training. Many experiments were carried out to determine the best backbone model. In the presented research, we evaluated the ResNet18, DensNet121 and VVG_11 models for training and inference. The learning rate is an important parameter during this phase. It determines the size of the adaptation of the weights during one pass of the training data through the network. If the learning rate is too low, the optimal solution for the model may not be found, if it is too high the model may take too long to converge, and training will never end. The best learning rate can be found manually, but in ArcGIS Pro, it is possible to use fast.ai's learning rate finder, which suggests an optimal learning rate. The maximum number of epochs is used to specify the maximum number of times the training data is used to adapt the weights of the network and therefore limits the training time. The batch size is a hyperparameter that defines the number of samples to work through before updating the model parameters. Other parameters are the number of grids cell in which the image is divided, and the size and ratio parameters for the detection boxes.

Once the model and hyperparameters were determined, they were stored and used for inference on the image of the complete area. During the inference, parameters for the confidence threshold and non maximum suppression (nms) need to be determined. The confidence threshold is the minimum confidence that is required for an object to be stored. For example, in our research a setting of 0.5 was used, which means that the algorithm must be at least 50% confidence that it has found a plastic greenhouse. Objects with a lower confidence are ignored for further processing. The output of the inference gives many overlapping boxes with different confidences. The nms parameters is used to remove overlapping boxes of the same objects and to determine how much overlap is allowed between adjacent boxes. The plastic greenhouses in the study area are located close to each other, therefore a 40% overlap setting was used in this research.

Each step of the workflow to detect plastic greenhouses was performed using the Deep learning toolset of ArcGIS Pro 2.7. The separate tools for the creation of samples, export of image chips, and the training and inference of the model provide a user-friendly interface to the complex algorithms that are used to detect the objects (ESRI, 2021). To be able to use the toolset, an ArcGIS Pro license is required, and an open-source deep learning environment based on python implementations of well-known machine learning libraries like Keras – TensorFlow, PyTorch, fastai and Scikit-learn needs to be installed. Although, it is possible to train the models using a CPU, it is highly recommended to use a GPU.

RESULTS AND DISCUSSION

For the training in total 2352 plastic greenhouses were digitized with an average size of 200 m^2. These were used to create 6228 partly overlapping image chips. Each image chip had a size of 256 x 256 pixels and the average number of greenhouses per chip was 5. Examples of image chips are shown in Figure 3.

Many settings of the hyperparameters for the training were tested, and the optimum combination was reached with 50 iterations, a batch size of 8, grid values of 4, 2, and 1, zoom values of 0.7, 1.0, 1.3 and [1,1], [1, 0.5], [0.5, 1] for the ratio values. The learning rate was set to automatic, and 20% of the data was used for model validation. During the training phase, numerous experiments have been executed to determine the architecture of the model and the values of the hyperparameters. All training and inference tests were executed on a PC with and Intel Core I5, 8th generation processor, 8 GB RAM and a Geforce GTX 1050 graphics card. First, backbone models ResNet18, ResNet34, ResNet50 and DenseNet121 were tested as architectures for the training.

A subset of the result of the training with the ResNet18 backbone model is shown in Figure 4.

Obviously, the larger the model, the longer the time required for training. In our case, it took 16h 31m to train the large DenseNet121 model, while the ResNet18 model with the same parameters took only 3h 24m.

Fig. 3 Image chips with multiple samples of plastic greenhouses

Fig. 4 Training results of model with Resnet18 backbone, at the left the input sample is shown, while the right image shows the detected result

The main problem with the larger backbone models was overfitting, therefore more samples were added to the training set by data augmentation, where the original training samples were rotated with 45° and 180° angles. DenseNet121, with 121 layers was finally trained with 6228 chips but did not provide better detection. This model gave the highest training accuracy of 79.1%. Also, the ResNet18 model was trained with the same sample set, acquired by data augmentation. The ResNet18 training with 50 iterations and a batch size of 8 and resulted in an average accuracy of 80.1%. Figure 5 shows the training and validation loss and clearly proves that the model is converging to an optimal solution.

In the first test, the VGG_11 backbone model was evaluated for the training. This model has only 11 layers and is therefore much faster to train. The training and validation loss plot is shown in Figure 6. The training took 90 minutes and the maximum number of epochs was set to 25, the number of samples was 5168.

To prevent overfitting of the VGG_11 model, different settings for dropout were tested. Dropout is a regularization method where randomly a part of the output of a layer is ignored and not read into the next layer. A value of 0.3 (30% of the data is ignored) gave the best result (Fig. 7).

The results of inference shown here are all executed on the same smaller test area. The main consideration for the selection of the area was that there are many plastic greenhouses that were not included in the training data set, so that it is possible to assess the quality of the inference. Additionally, it was important to select as many different types of greenhouses as possible (different in size, color and damage) to be able to evaluate the capabilities of the models to detect all plastic greenhouses. Figure 8 shows the inference results of the VGG_11 model.

The model successfully found the large majority of objects of interest. The red symbols indicate the 222 greenhouses that the model detected. Some objects were detected by this model, that are not a plastic greenhouse. These are indicated in black in Figure 8. For example, the model also recognized large tents that are very similar in shape to greenhouses. The average accuracy of the bounding boxes detected during the inference using VGG_11 in the test area is 79.2%.

The next backbone model used for inference was DenseNet121 (Fig. 9). The model showed a slight over fitting in the initial trials, but adaptation of the hyper parameters and enlarging the training set showed that the model can detect greenhouses successfully. As a result of the inference using the DenseNet121 model, 230 plastic greenhouses were found in the test area. Comparing with the results of the VGG_11 model, it can be observed that the inference made with the DenseNet121 model is more accurate. DenseNet121 did not erroneously detected the large tents as plastic greenhouse unlike VGG_11 model (yellow circles in Fig. 9). The DenseNet121 model yielded an average of 79.1% for the accuracy value.

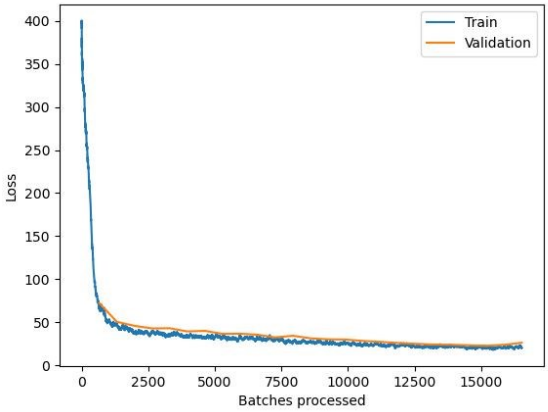

Fig. 5 Training and validation loss using the ResNet18 backbone and 2352 samples

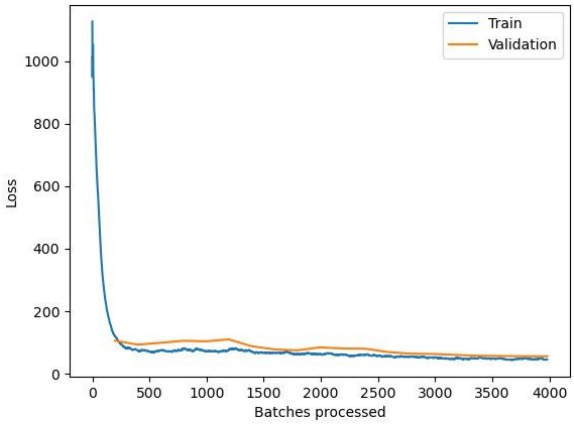

Fig. 6 Training and validation loss using the VGG_11 backbone

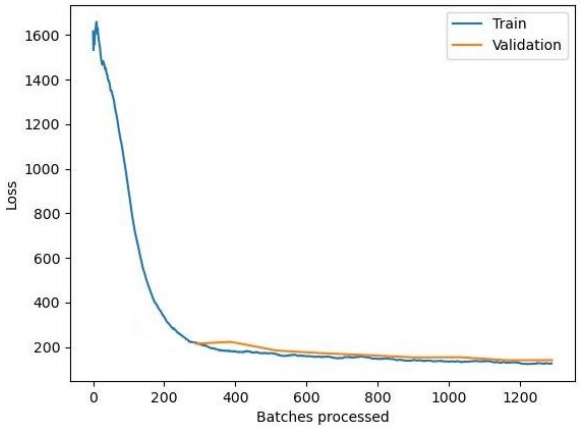

Fig. 7 Training and validation loss using the VGG_11 with dropout 0.3

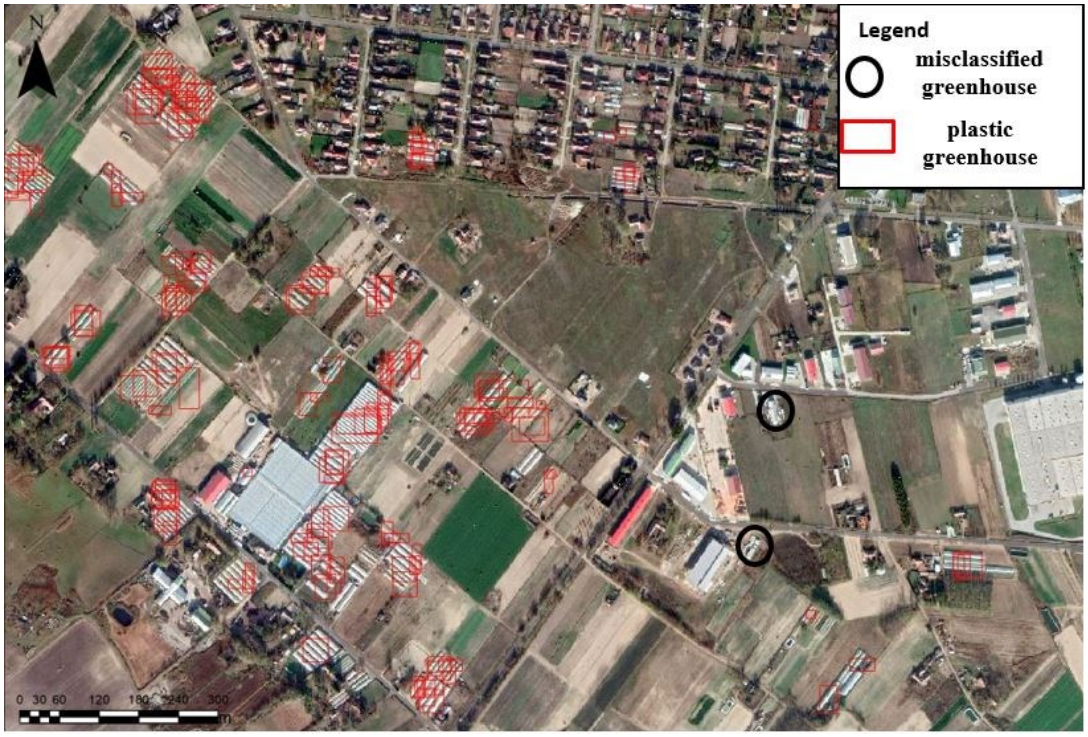

Fig. 8 Detection of plastic greenhouses on the test area using VGG_11

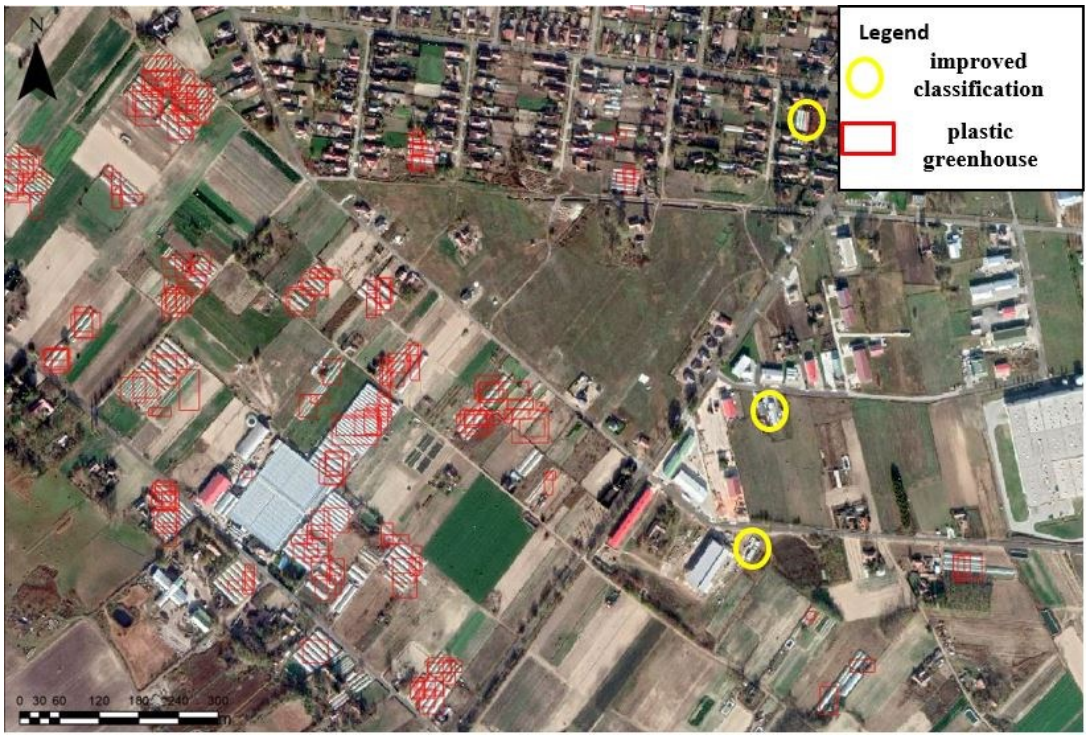

Fig. 9 Detection of plastic greenhouses on the test area using DenseNet121

Finally, the results of the ResNet18 model are presented in Figure 10. During the first training, a higher learning rate of 0.03 was used, but this did not give satisfying results. Then, the training was performed with the learning rate finder, suggesting far lower rates that provided a much better result. For the presented inference, the ResNet18 model trained with the suggested learning rates was used. The manual learning rate setting resulted in a worse result, giving an average accuracy value of 78.3% and the model placed 225 bounding boxes during detection. The most accurate result was achieved by the ResNet18, with the optimal learning rate. It gave an average accuracy of 83.1% for the detected 232 bounding boxes. Improvement over the DenseNet121 result is indicated in yellow.

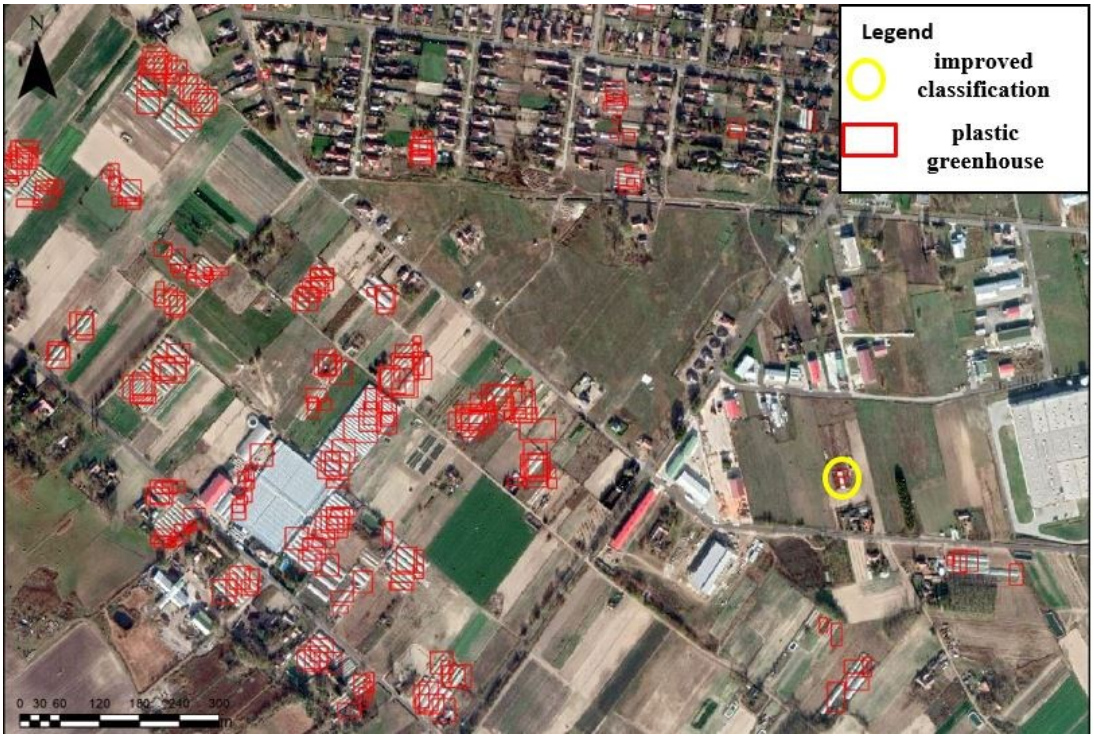

Fig. 10 Detection of plastic greenhouses on the test area using ResNet18

ArcGIS Pro provides a user-friendly environment to sophisticated deep learning algorithms. The dialogs hide the complexity of working with machine learning algorithms from the user, but to use the functionality optimally, it is required to have detailed knowledge of the hidden algorithms. This also helps to make efficient decisions on the many options that need to be specified during the creation of the training data, the training and the inference. Erroneous settings of the hyperparameters during training can easily result in models that never reach an optimal solution.

The selection of the backbone model is of decisive importance for the CNN processing. The complexity of the model, combined with setting for the learning rate, batch size and maximum number of epochs determine the accuracy of the results and the time required to train the model. Often, it might be more efficient to allow a slightly lower accuracy over much better performance.

The size and quality of the training data is another important condition for successful use of the deep learning functionality. Data augmentation is a powerful procedure to generate more training data without digitizing more examples. It also reduces the chance of overfitting, since more and different types of examples that may occur in other areas, are shown to the model.

Detection of objects in remotely sensed images provides a different result than the classification results that are common in remote sensing studies. For this reason, it is difficult to compare the results of traditional classifications and object detection as presented in our research. Traditional classifications provide one class label for each pixel in the image, while object detection aims to detect all objects of interest and their locations in the image. The metrics used for the estimation of the accuracy are also different since the location of an object is not an output of classification algorithms.

In the presented research, RGB channel images downloaded from Google Earth are used as input data. The limited number of channels is a disadvantage compared to other data sets, when the data would be used for traditional classification. The models used as backbone for the convolutional neural network model are trained with three channel data though and are therefore particularly suitable as input data.

CONCLUSION

The presented research explores the possibilities for detection of plastic greenhouses in an agricultural area in the south east of Hungary using freely available high resolution satellite imagery and a convolutional neural network. The aim was to use state of the art deep learning techniques without the need to go into the depths of writing code, therefore we used the recent ArcGIS Pro deep learning implementation. This user-friendly environment allows to experiment with many setting for creation of the training data, the backbone model, the training, and the inference. It also provides feedback to the user on the success of the training. The connection between the deep learning algorithms and the GIS functionality of the software makes it easy to perform all steps in the detection of greenhouses in a spatial environment and display the results as maps and images.

The results of the inference show that - with careful selection of the network architecture and hyper parameters - it is possible to achieve high accuracy output maps. The calculation intensive experimentation

requires a high-performance computer. The use of pre-trained backbone models is essential.

We successfully tested a possibility to determine the number of plastic greenhouses and their locations based on freely available, high resolution data and we are optimistic that the technology will be used in the future for applications like statistics on agriculture, environmental impact studies and taxation purposes.

References

Abadi, M., Agarwal, A., Barham, P., Brevdo, E., Chen, Z., Citro, C., Corrado, G.S., Davis, A., Dean, J., Devin, M., et al. 2015. TensorFlow: Large-scale machine learning on heterogeneous systems. Online available at: https://arxiv.org/pdf/1603.04467.pdf

Agüera, F., Aguilar, M.A., Aguilar, F.J. 2008. Using texture analysis to improve per-pixel classification of very high resolution images for mapping plastic greenhouses. *ISPRS Journal of Photogrammetry and Remote Sensing* 63 (6), 635–646. DOI: 10.1016/j.isprsjprs.2008.03.003

Agüera, F., Liu, G. G. 2009. Automatic greenhouse delineation from QuickBird and Ikonos satellite images. *Computers and Electronics in Agriculture* 66, 191–200. DOI: 10.1016/j.compag.2009.02.001

Chollet, F. 2015. Keras. Online available at: https://github.com/fchollet/keras

Davies, E.R. 2018. Computer Vision: Principles, Algorithms, Applications, Learning. Academic Press, 5th edition, 866 p. DOI: 10.1016/C2015-0-05563-0

Ding, P., Zheng, Y., Deng, J-W., Jia, P., Kuijper, A. 2018. A light and faster regional convolutional neural network for object detection in optical remote sensing images. *ISPRS Journal of Photogrammetry and Remote Sensing* 141, 208–218. DOI: 10.1016/j.isprsjprs.2018.05.005

ESRI 2021, ArcGIS Pro online help. Online available at: https://pro.arcgis.com/en/pro-app/latest/tool-reference/image-analyst/an-overview-of-the-deep-learning-toolset-in-image-analyst.htm

Everingham, M., Gool, V., L., Williams, I., K., C., Winn, J., Zisserman, A. 2010. The PASCAL Visual Object Classes (VOC) Challenge. *International Journal of Computer Vision* 88, 303–338. DOI: 10.1007/s11263-009-0275-4

Flood, N., Watson, F., Collett, L. 2019. Using a U-net convolutional neural network to map woody vegetation extent from high resolution satellite imagery across Queensland, Australia. *International Journal of Applied Earth Observation and Geoinformation* 82, 101897. DOI: 10.1016/j.jag.2019.101897

Gallwey, J., Robiati, C., Coggan, J., Vogt, D., Eyre, M. 2020. A Sentinel-2 based multispectral convolutional neural network for detecting artisanal small-scale mining in Ghana: Applying deep learning to shallow mining. *Remote Sensing of Environment* 248: 111970. DOI: 10.1016/j.rse.2020.111970

Goodfellow, I., Bengio, Y., Courville, A. 2016. Deep Learning. MIT Press, Online available at: http://www.deeplearningbook.org

González-Yebra, Ó., Aguilar, A. M., Nemmaoui, A., Aguilar, J., F. 2018. Methodological proposal to assess plastic greenhouses land cover change from the combination of archival aerial orthoimages and Landsat data. *Biosystems Engineering* 175, 36–51. DOI: 10.1016/j.biosystemseng.2018.08.009

Guo, Y., Xu, Y., Li, S. 2020. Dense construction vehicle detection based on orientation-aware feature fusion convolutional neural network. *Automation in Construction* 112. 103124. DOI: 10.1016/j.autcon.2020.103124

Howard, J., Gugger, S. 2020. Fastai: A layered API for Deep Learning. *Information* 11 (2), 108. DOI: 10.3390/info11020108

Jiang, B., Ma, X., Lu, Y., Li, Y., Feng, L., Shi, Z. 2019. Ship detection in spaceborne infrared images based on Convolutional Neural Networks and synthetic targets. *Infrared Physics & Technology* 97, 229–234. DOI: 10.1016/j.infrared.2018.12.040

Kattenborn, T., Leitloff, J., Schiefer, F., Hinz, S. 2021. Review on Convolutional Neural Networks (CNN) in vegetation remote sensing. *ISPRS Journal of Photogrammetry and Remote Sensing* 173, 24–49. DOI: 10.1016/j.isprsjprs.2020.12.010

Koc-San D. 2013. Evaluation of different classification techniques for the detection of glass and plastic greenhouses from WorldView-2 satellite imagery. *Journal of Applied Remote Sensing* 7 (1): 073553. DOI: 10.1117/1.JRS.7.073553

LeCun y., Boser, B., Denker, S. J., Henderson, D., Howard, E. R., Hubbard, W., Jackel, D. L. 1990. Handwritten Digit Recognition with a Back-Propagation Network. pp. 396–403.

Liu, W., Anguelov, D., Erhan, D., Szegedy, C., Reed, S., Fu, Y. C., Berg, C. A. 2016. SSD: Singe Shot Multibox Detector. *European Conference on Computer Vision* 2016, 21–37. DOI: 10.1007/978-3-319-46448-0_2

McCarthy, J., Minsky, I. M., Rochester, N., Shannon, E., C. 1955. A proposal for the Dartmouth summer research project on artificial intelligence. *AI Magazine*, 27 (4), pp. 12–14. DOI: 10.1609/aimag.v27i4.1904

Mezősi, G. 2011. Magyarország természetföldrajza, (Physical geography of Hungary) Academic Press, Budapest, pp. 393.

Michie, D. 1968. „Memo" Functions and Machine Learning. *Nature* 218 (5136), 19–22. DOI: 10.1038/218019a0

Müller, B., Reinhardt, J., Strickland, M. T. 1995. Neural Networks: An Introduction. Springer, Berlin, pp. 307.

Nemmaoui, A., Aguilar, J. F., Aguilar, A. M., Qin, R. 2019. DSM and DTM generation from VHR satellite stereo imagery over plastic covered greenhouse areas. *Computer and Electronics in Agriculture* 164, 104903. DOI: 10.1016/j.compag.2019.104903

Nilsson, N., J. 1980. Principles of artificial intelligence. Morgan Kaufmann, California, pp. 475.

Novelli, A., Aguilar, A.M., Nemmaoui, A., Aguilar, J. F., Tarantino, E. 2016. Performance evaluation of object based greenhouse detection from Sentinel-2 MSI and LANDSAT 8 OLI data: A case study from Almería (Spain). *International Journal of Applied Earth Observation and Geoinformation* 52, 403–411. DOI: 10.1016/j.jag.2016.07.011

Paszke, A., Gross, S., Massa, F., Lerer, A., Bradbury, J., Chanan, G., Killeen, T., Lin, Z., Gimelshein, N., Antiga, L., Desmaison, A., Köpf, A., Yang, E., DeVito, Z., Raison, M., Tejani, A., Chilamakurthy, S., Steiner, B., Fang, L., Bai, J., Chintala, S. 2019. PyTorch: An Imperative Style, High-Performance Deep Learning Library. Cornell University. Online available at: https://arxiv.org/pdf/1912.01703v1.pdf

Pedregosa, F., Varoquaux, G., Gramfort, A., Michael, V., Thirion, B., Grisel, O., Blondel, M., Prettenhofer, P., Weiss, R., Dubourg, V., Vanderplas, J., Passos, A., Cournapeau, D., Brucher, M., Perrot, M., Duchesnay, É. 2011. Scikit-learn: Machine Learning in Python. *Journal of Machine Learning Research* 12, 2825–2830. Online available at: https://arxiv.org/pdf/1201.0490.pdf

Pi, Y., Nath, D. N., Behzadan, H. A. 2020. Convolutional neural networks for object detection in aerial imagery for disaster response and recovery. *Advanced Engineering Informatics* 43, 101009. DOI: 10.1016/j.aei.2019.101009

Poirson, P., Ammirato, P., Fu, C. Y., Liu, W., Košecká, J., Berg, C. A. 2016. Fast single shot detection and pose estimation. *Fourth International Conference on 3D Vision (3DV)*, Stanford, CA, USA, 2016, pp. 676–684, DOI: 10.1109/3DV.2016.78

Rai, K. A., Mandal, N., Singh, A., Singh, K. K. 2020. Landsat 8 OLI Satellite Image Classification using Convolutional Neural Network. *Procedia Computer Science* 167, 987–993. DOI: 10.1016/j.procs.2020.03.398

Schiefer, F., Kattenborn, T., Frick, A., Frey, J., Schall, P., Koch, B., Schmidtlein, S. 2020. Mapping forest tree species in high resolution UAV-based RGB-imagery by means of convolutional neural networks. *ISPRS Journal of Photogrammetry and Remote Sensing* 170, 205–215. DOI: 10.1016/j.isprsjprs.2020.10.015

Simon, A., H. 1995. Artificial intelligence: an empirical science. *Artificial Intelligence* 77 (1), 95–127. DOI: 10.1016/0004-3702(95)00039-H

Virnodkar, S.S., Pachghare, C.V., Jha, K.S. 2020. CaneSat dataset to leverage convolutional neural networks for sugarcane classification from Sentinel-2. *Journal of King Saud University – Computer and Information Sciences*. DOI: 10.1016/j.jksuci.2020.09.005 (in press)

Watanabe, S., Sumi, K., Ise, T. 2018. Using deep learning for bamboo forest detection from Google Earth images. *bioRxiv* 351643, DOI: 10.1101/351643

Wu, C., Deng, J. S., Wang, K., Ma, L. G., Tahmassebi, A. R. S. 2016. Object-based classification approach for greenhouse mapping

using Landsat-8 imagery. *International Journal of Agricultural and Biological Engineering* 9, 79–88. DOI: 10.3965/j.ijabe.20160901.1414

Yang, D., Chen, J., Zhou, Y., Chen, X., Chen, X., Cao, X. 2017. Mapping plastic greenhouse with medium spatial resolution satellite data: Development of a new spectral index. *ISPRS Journal of Photogrammetry and Remote Sensing* 128, 47–60. DOI: 10.1016/j.isprsjprs.2017.03.002

Yang, G., Xu, R., Chen, Yi., Wu, Z., Du, Y., Liu, S., Qu, Z., Guo, K., Peng, C., Chang, J., Ge., Y. 2021. Identifying the greenhouse by Google Earth Engine to promote the reuse of fragmented land in urban fringe. *Sustainable Cities and Society* 67, 102743 DOI: 10.1016/j.scs.2021.102743

Zhang, D., Pan, Y., Zhang, J., Hu, T., Z, J., Li, N., Chen, Q. 2020. A generalized approach based on convolutional neural networks for large area cropland mapping at very high resolution. *Remote Sensing of Environment* 247, 111912. DOI: /10.1016/j.rse.2020.111912

sciendo

Journal of Environmental Geography 14 (1–2), 47–57.

DOI: 10.2478/jengeo-2021-0005
ISSN 2060-467X

THE IMPACT OF SOIL EROSION ON THE SPATIAL DISTRIBUTION OF SOIL CHARACTERISTICS AND POTENTIALLY TOXIC ELEMENT CONTENTS IN A SLOPING VINEYARD IN TÁLLYA, NE HUNGARY

Samdandorj Manaljav[1,2], Andrea Farsang[2], Károly Barta[2], Zalán Tobak[2], Szabolcs Juhász[2], Péter Balling[3], Izabella Babcsányi[2]*

[1]Institute of Geography-Geoecology, Mongolian Academy of Science,Erkhuu str. 11th khoroolol, Sukhbaatar district, Ulaanbaatar, Mongolia
[2]Department of Geoinformatics, Physical and Environmental Geography, University of Szeged, Egyetem u. 2-6, 6722 Szeged, Hungary
[3]Research Institute for Viticulture and Oenology, Tokaj, Könyves Kálmán u. 54., Tarcal, Hungary, HU-3915

*Corresponding author, email: babcsani@geo.u-szeged.hu

Research article, received 25 February 2021, accepted 23 April 2021

Abstract

Soil erosion is a main problem in sloping vineyards, which can dramatically affect soil quality and fertility. The present study aimed to evaluate the spatial patterns of selected physico-chemical soil characteristics and the soil's potentially toxic element (PTE) contents in the context of erosion. The study was conducted in a 0.4 ha vineyard plot on a steep slope in Tállya, part of the wine-growing region of Tokaj-Hegyalja (Hungary). A total of 20 topsoil samples (0-10 cm) were collected and analysed for PTEs (B, Co, Ba, Sr, Mn, Ni, Cr, Pb, Zn, and Cu), soil pH (deionized water and KCl solution), particle-size distribution, soil organic matter (SOM), (nitrate+nitrite)-N, P_2O_5, and carbonate content. Among the selected PTEs, only Cu (125±27 mg/kg) exceeds the Hungarian standards set for soils and sediments (75 mg/kg) due to the long-term use of Cu-based pesticides in the vineyard. Examined PTEs are negatively correlated with the sand content of the topsoil, except for Mn, while the significant positive relationship with the clay content shows the role of clay in retaining PTEs in soil. SOM seems to play a minor role in binding PTEs, as Cu is the only element for which a significant correlation with the SOM content can be detected. The spatial distribution maps prepared by inverse distance weighting (IDW) and lognormal kriging (LK) methods show higher PTE contents at the summit and the shoulder of the hillslope and lower contents at the backslope and the footslope zones. The low slope gradients (0-5 degree) and the high contents of the coarse fraction (> 35%) likely protect the soil at the summit and the hillslope's shoulder from excessive erosion-induced losses. While the reraising PTE contents at the toeslope are likely due to the deposition of fine soil particles (silt and clay). The highest SOM contents at the summit and the toeslope areas, and increased contents of the coarse fraction at the backslope, confirm the effects of soil erosion on the spatial distribution patterns of main soil quality indicators. Overall, the LK outperformed the IDW method in predicting the soil parameters in unsampled areas.

Keywords: PTEs, soil organic matter, soil erosion, Tokaj, geostatistics, interpolation

INTRODUCTION

Viticulture is known to affect soil quality significantly, both its physical and chemical properties. Soil is one of the most important factors in viticulture, because its physico-chemical properties (e.g. pH, particle-size distribution, soil organic matter and N-, P- macronutrient contents) determine the nutrient supply for the growth of the vine. In general, vineyard soils tend to be poor in macronutrients and organic matter contents, and a general decrease in soil pH is often observed in older vineyards (Patinha et al., 2018). Past and present soil management in a vineyard, especially tillage in the vine inter-rows, is responsible for the degradation of the soil's physical characteristics that may have dramatic effects on its nutritional element contents (Biddoccu et al., 2016). Surface and subsoil hydraulic conductivity is highly affected by different soil management practices in vineyards (Bordoni et al., 2019). For example, tractor traffic has a considerable impact on the spatial distribution of the soil's water infiltration capacity and compaction, resulting in more surface runoff generation and enhanced soil erosion (Biddoccu et al., 2016; Capello et al., 2019). The rock fragment content and its spatial variability are also influenced by soil erosion and cultivation patterns in vineyard topsoils (Follain et al., 2012). Besides these fundamental characteristics of the soil, some specific soil components are also affected by viticultural practices and soil erosion dynamics.

Contamination of agricultural soils with potentially toxic elements (PTEs) may raise human health concerns due to their ability to integrate the human food chain. PTEs often show increased concentrations in agricultural soils due to the long-term use of chemical fertilizers and pesticides (Solgi et al., 2016). Biosolid applications may also increase PTE contents in agricultural soils, including Pb, Ni, Zn, Cu, Cd, Cr, and even contents of some rarely assessed PTEs, such as Ba (Ippolito and Barbarick, 2006,

Torri and Corrêa, 2012). However, PTE accumulation in the topsoil of biosolid-amended arable lands is not always detectable (Ladányi et al., 2020). Elevated contents of Cd, Cu and Zn have been observed in Chinese agricultural soils due to repeated treatments with chemical fertilizers and manure (Lu et al., 2012; Sun et al., 2013), additionally, Pb also accumulated in agricultural soils of the European Mediterranean region (Micó et al., 2006). In vineyard soils, Cu and Zn are often observed at elevated concentrations due to the repeated use of Cu- and Zn-based agrochemicals (Rodríguez Martín et al., 2006, Dos Santos et al., 2013). In Europe, Cu-based fungicides have been intensively used since the end of the 19th century to control fungal diseases. High Cu contents can accumulate in the topsoil of vineyards and surrounding areas, which may raise ecotoxicological concerns (Milićević et al., 2017, Ungureanu et al., 2017, Patinha et al., 2018). Additionally, the foliar applications of micronutrient fertilizers containing Fe, Mn, B, Cu, Zn and Mo are part of viticultural practices. Therefore, PTE concentrations in conventionally managed vineyard soils should be carefully assessed and the eventual PTE accumulation in the topsoil evidenced. On the other hand, soil erosion influenced by various agronomic practices can also considerably impact the spatial patterns of PTE soil contents.

Vineyards are often planted on steep slopes, thus they are prone to intensive soil erosion, enhancing the mobility of PTEs (Rodríguez Martín et al., 2007, Dos Santos et al., 2013). According to model forecasts, fewer but more intense rainfall events are likely to occur in Hungary during the 21st century (Mezősi and Bata, 2016). As rainfall intensity is a key triggering factor of soil erosion, its probable increase in the future can have dramatic effects on soil erosion rates, which will certainly impact soil quality. The spatial variability of topsoil PTEs may be affected by soil erosion processes and anthropogenic inputs. Given that some PTEs are also essential micronutrients for plants, their soil contents are an indicator of soil fertility too. Also, key soil properties, such as soil organic matter content, particle size distribution, and soil pH, are required to explain the distribution of PTEs. Overall, there is an increasing need to understand the impact of soil erosion on the spatial distribution of essential physico-chemical properties and PTE contents in cultivated soils (Rodríguez Martín et al., 2006; Solgi et al., 2016).

Predictive soil mapping has been efficient for assessing the spatial variability of soil properties at the field scale (Scull et al., 2003). However, few studies focused on mapping and explaining the spatial distribution of soil characteristics and PTEs in vineyards at a plot scale. Yet, this information is necessary to monitor soil quality changes as a consequence of soil erosion. The key objectives of this study are: (I) to identify relationships between soil properties and PTE contents, (II) to map the spatial distribution of essential soil characteristics and specific PTE contents in a vineyard's topsoil; and (III) to assess the accuracy of the applied interpolation models.

METHODS AND MATERIALS

Study area and soil sampling

The field survey was carried out in a 0.4 ha vineyard plot at the foothills of the Tokaj Mountains (North-eastern Hungary), in Tállya, part of the historical wine-growing region of Tokaj-Hegyalja (Fig. 1). The vineyard's elevation ranges from 269 m to 291 m above sea level. The plot has nine grapevine rows parallel to the main slope; vine stocks are spaced 1 m from one another, while

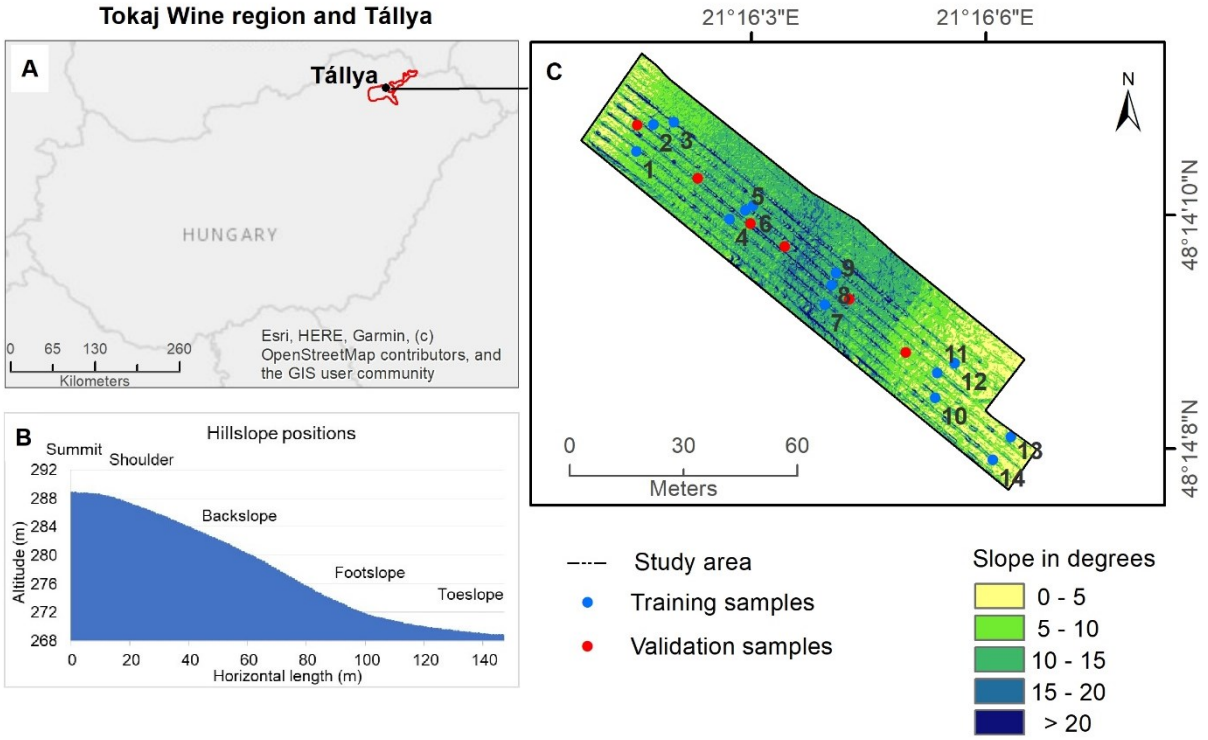

Fig. 1 A) The study area is a 0.4 ha vineyard plot near Tállya in the Tokaj wine region (NE Hungary). The slope profile (B) and slope map (C) were prepared based on the digital elevation model of the area. Sampling points are marked in blue for the training samples and red for the validation samples.

the inter-rows are 3.8 m wide. The total slope length is 130 m, and the mean slope is 18°. The soil type slightly varies along the transect. At the top of the hillslope, it belongs to the Skeletic Regosol (Loamic, Ochric) type, while at the backslope it shows Skeletic Leptosol (Loamic, Ochric) patterns, at the footslope the soil is Skeletic Colluvic Regosol (Loamic, Ochric) according to the World Reference Base for Soil Resources (2014). The soils in the area developed on a fine-grained extrusive igneous rock, rhyolite, and rhyolite tuff. Therefore, the soil has a weakly acidic character.

The vineyard is managed conventionally with regular uses of synthetic and inorganic pesticides, primarily Cu fungicides. The current application doses of the Bordeaux mixture amount to 2-2.5 kg/ha/year (applied three times a year in May, June, and July). The Bordeaux mixture was complemented with a foliar micronutrient fertilizer pulverized in a dose of 4-5 l/ha, containing Fe (3.2 m/v%), Mn (0.32 m/v%), Cu (0.15 m/v%), B (0.31 m/v%) and Mo (0.003 m/v%). The soil is regularly ploughed, and no cover crops are sown in the vine inter-rows for soil protection.

In May 2020, 14 point samples of topsoil (0-10 cm) were taken in the middle of the vine inter-rows based on random sampling (USDA, 2014) (Fig. 1). Additionally, six topsoil samples were collected in November 2019, which were used to check the interpolation methods' performance.

Aerial photography campaign using a DJI Phantom 4 drone and geodetic field measurements were performed to collect true colour images and elevation information. The digital elevation model (DEM) of the vineyard plot was prepared by stereo-photogrammetry described elsewhere (Szatmári et al., 2011). The slope map of the study area was generated from the DEM as its first derivative.

Soil analyses

All soil samples were air-dried at room temperature and passed through a 2 mm stainless steel sieve. The non-negligible coarse fraction (>2 mm) was systematically weighed. Soil organic matter was determined by oxidation with $K_2Cr_2O_7$ in the presence of sulphuric acid and the subsequent analysis of the reduced Cr^{3+} ions with a spectrophotometer (UNICAM Helios Gamma UV-VIS, Thermo Scientific) according to the Walkley Black method based Hungarian standards (MSZ 21470–52:1983). The carbonate content was measured by the volumetric method with a Scheibler calcimeter. Soil pH was determined by a pH-meter (Mettler Toledo FiveEasy) in a 1:2.5 ratio of soil: deionized water ($pH_{d.w.}$) and soil: 1 mol/L KCl (pH_{KCl}) (MSZ-08-0206-2:1978). Differences greater than one between the two pH values measured in the deionized water and the KCl solution suggest a susceptibility of the soil to acidification (Rodrigo Comino et al., 2016). The pipette method was used to determine soil particle size distribution using pyrophosphate for dispersing soil aggregates (USDA, 2014). The plant-available macronutrient contents of P_2O_5 extracted using ammonium-lactate and (nitrate+nitrite)-N extracted with a KCl-solution according to standard procedures (MSZ20135:1999), were measured by a flow injection analysis (FIA) spectrometer (FIA STAR 5000, Foss).

Pseudototal PTE analyses

Digestion in aqua-regia allows for determining the so-called pseudototal element content because it does not dissolve the silicate matrix. Soil samples (<2 mm) were ground to a fine powder (<0.25 mm) in an agate ball mill and dried in an oven at 105°C for 24 h. Approximately 0.5 g of each ground soil sample was weighed into pre-cleaned PFA vessels using an analytical balance and digested in aqua regia (HCl: HNO_3 ratio of 3:1). All labware was acid-cleaned before use, and acids were for trace metal analysis (Normatom®, VWR Chemicals). The pseudototal digestion was performed in a laboratory microwave digestion system (Multiwave 3000, Anton Paar). After cooling, the digested samples were filtered into 50 ml volumetric flasks (acid-cleaned plastic flasks), and the volume was made up with ultrapure water (TKA MicroPure). The concentrations of selected PTEs (B, Co, Ba, Sr, Mn, Ni, Cr, Pb, Zn, and Cu) were then determined by an inductively coupled plasma optical emission spectrometer using yttrium as an internal standard (Optima 7000 DV, Perkin Elmer) (±5%). Calibration standards were freshly prepared in 2% HNO_3 by diluting ICP Multi-Element Standards (CPAchem). ERM®-CC141 certified reference material (a loam soil) was used for quality control for the pseudototal element analysis. The recoveries for the certified elements (based on two digested aliquots of the reference material and four ICP analyses) are presented in Table 1.

Data analyses

Descriptive statistical analyses (minimum, maximum, mean, median, standard deviation, skewness, and kurtosis) were used to describe the soil characteristics and PTEs. The coefficient of skewness is a measure of the symmetry of a distribution. For symmetric distributions, the coefficient of skewness should be close to zero and the kurtosis must be near 3. The mean is greater than the median for positively skewed distribution and vice versa for negatively skewed distribution. Pearson's correlation was used to define the relationships between soil characteristics and PTE contents. All statistical analyses were carried out using IBM SPSS Statistics 25.

Table 1 The recoveries of the pseudototal element (aqua regia extractable) contents in ERM®-CC141 certified reference material (n=4) and the PTE contents of the local forest topsoil used as a reference for calculating enrichment factors in the vineyard soil.

	Unit	B*	Mn	Ni	Cr	Cu	Pb	Zn	Co	Ba*	Sr*
Recovery	%	-	102±2	117±2	116±2	104±3	87±1	92±2	88±0.2	-	-
Local forest soil	mg/kg	2	424	8	11	7	27	35	2	48	9

*The ERM®-CC141 is not certified for B, Ba and Sr.

Enrichment factors (EFs) were calculated to compare PTE contents observed in the vineyard topsoil with PTE background levels measured in a local forest topsoil (average of pseudototal PTE contents measured in 0-10 cm and 10-20 cm) (Table 1).

$$EF = \frac{\text{PTE(vineyard topsoil)}}{\text{PTE(reference soil)}} \qquad (1)$$

The observed PTE contents were also compared with the median PTE concentration data collected in the framework of the Hungarian Soil Information and Monitoring System (SIMS) based on 842 topsoil sampling points (0-30 cm) on arable land nation-wide in Hungary (Csorba et al., 2014).

Geostatistical approaches

In geostatistics, variograms or semivariograms are applied to measure the spatial patterns of a known variable. Its main contribution in soil science has been predicting and mapping the spatial variability of soil attributes at unsampled locations (Goovaerts, 1999; Guo et al., 2001). Interpolation is a process of estimating the values at unsampled places based on known values at sampled locations. In this study, interpolation maps were created using ArcGIS 10.5 Geostatistical Analyst extension (ESRI, Redlands, CA). We set the nearest 2 to 8 neighbour values and a sector type of 4 for defining neighbourhood to interpolate a surface. The estimated standard errors of kriged values can be used to test the accuracy of the kriging results (Rodríguez Martín et al., 2006). Several geostatistical methods exist for modeling the spatial variability of data (Szatmári et al., 2015). However, ordinary kriging is a robust and one of the commonly used spatial interpolation methods to estimate the value of target variables at unsampled points using the weighted average of sampled neighbouring points in the area of interest. Ordinary kriging computes a weighted average of the data:

$$\hat{Z}(\boldsymbol{X}_0) = \sum_{i=1}^{n} \lambda_i(\boldsymbol{X}_0) Z(\boldsymbol{X}_i) \qquad (2)$$

where, $\hat{Z}(\boldsymbol{X}_0)$ is the estimated value of the variable Z at any location $\mathbf{x}_0$; $Z(\boldsymbol{X}_i)$ is the measured data; $\lambda_i(\boldsymbol{X}_0)$ refers to the weight associated with the measured values, and n is the number of observations in a neighborhood.

Lognormal kriging (LK) is the ordinary kriging of the measured values' logarithms (Webster and Oliver, 2007). It is used for strongly positively skewed data that approximate a lognormal distribution, commonly the case with environmental data. For lognormal kriging the data should be transformed by the following equation:

$$y = log_{10} Z \qquad (3)$$

Inverse distance weighting (IDW) is more popular and based on inverse functions of distance in which the weights are defined by:

$$\lambda_i = 1/|x_i - x_0|^{\beta} \quad \beta > 0 \qquad (4)$$

Data points near to the target point carry larger weights than those further away. The most popular choice of β is 2 so that the data are inversely weighted as the square of the distance. Its attractive feature is that the relative weights decrease rapidly as the distance increases, and so the interpolation is locally sensible. Furthermore, because the weights never become zero, there are no discontinuities. Its disadvantages are that the weighting function's choice is arbitrary, and there is no measure of error (Webster and Oliver, 2007).

Assessment of model performance

In this study, independent validation was used to evaluate and compare the performance of interpolation models. The root mean square error (RMSE) measures the difference between predicted values and observed values, while the mean absolute error (MAE) computes how far estimated values are away from measured values (Xie et al., 2011). The smaller MAE and RMSE values indicate the better-predicted values. The RMSE and the MAE were estimated using the predicted and observed values at each validation sampling location:

$$RMSE = \sqrt{\frac{1}{n}\sum_{i=1}^{n}(P_i - O_i)^2} \qquad (5)$$

$$MAE = \frac{1}{n}\sum_{i=1}^{n}|P_i - O_i| \qquad (6)$$

where P_i, O_i are predicted (interpolated) and observed soil parameter values at location i, and n is the sample number.

RESULTS AND DISCUSSION

Soil characteristics and PTE concentrations in the vineyard topsoil

The descriptive statistics of the examined soil characteristics and PTE contents in the vineyard topsoil in Tállya are summarised in Table 2. Most soil properties had positively skewed distributions except for $CaCO_3$, P_2O_5, and clay content. But most of the PTEs had negatively skewed distributions except for the concentration data of Co and Sr. The examined vineyard soil is slightly acidic ($pH_{d.w.}$(mean): 6.4). However, the soil has a potential acidity due to the greater than one difference between the two pH values (measured in d.w. and in the KCl solution). Mean concentration of the soil organic matter (SOM) content is 1.5±0.4%, indicating that the vineyard soil is poor in SOM. A poor SOM content is often observed in vineyards planted on steep slopes as a consequence of intense soil erosion and redeposition and/or off-site export of organic carbon with surface runoff (Novara et al., 2018). SOM can influence PTE (particularly cationic metals) sorption in soils, probably attributed to its high cation exchange capacity (Rodrigues et al., 2010). Hence it is essential to assess SOM variations in the vineyard topsoil. The topsoil has a low carbonate

Table 2 Descriptive statistics of selected soil parameters, macronutrient, and PTE contents in the topsoil of the vineyard in Tállya.

		Vineyard topsoil (0-10 cm)						
	Unit	Min	Max	Mean	Median	Std.D	Skewness	Kurtosis
SOM	%	0.9	2.3	1.5	1.4	0.4	0.98	0.22
$CaCO_3$	%	0.4	2.0	1.3	1.6	0.5	-0.96	-0.35
$pH_{d.w.}$		6.1	6.9	6.4	6.4	0.2	0.67	-0.48
pH_{KCl}		4.6	5.8	5.2	5.0	0.4	0.34	-1.65
(nitrate+nitrite)-N	mg/kg	<0.1	2.5	0.8	0.6	0.8	1.06	-0.07
P_2O_5 [mg/kg]	mg/kg	107.9	299.4	196.6	200.1	55.7	0.02	-0.64
Coarse fraction (> 2mm)	%	31	48	40	40	5	-0.11	-0.82
Sand (0.05 - 2 mm)	%	32	60	41	39	9	0.93	0.00
Silt (0.002 - 0.05 mm)	%	21	35	27	26	4	0.42	0.04
Clay (<0.002 mm)	%	19	40	31	34	7	-0.53	-1.36
B	mg/kg	6	13	10	10	2	-0.27	-1.32
Mn	mg/kg	199	607	351	355	102	0.84	2.19
Ni	mg/kg	10	23	17	19	4	-0.36	-1.19
Cr	mg/kg	14	35	25	26	7	-0.22	-1.49
Cu	mg/kg	88	184	125	127	27	0.44	0.25
Pb	mg/kg	10	17	14	14	2	-0.13	-0.98
Zn	mg/kg	32	64	44	45	8	0.68	1.53
Co	mg/kg	5	8	7	6	1	0.05	-1.84
Ba	mg/kg	63	136	101	102	25	-0.10	-1.65
Sr	mg/kg	19	42	30	28	7	0.34	-1.16

content ($CaCO_3$) ranging from 0.4 to 2.0%. The ammonium-lactate soluble P_2O_5 content ranges from 107.9 to 299.4 mg/kg, while the KCl- soluble (nitrate+nitrite)-N content is low in the soil, varying from undetectable to 2.5 mg/kg. The vineyard soil in Tállya is characterised by a high proportion of the coarse fraction (>2 mm): 31-48%. Such important proportions of the coarse fraction embedded in the topsoil greatly impact soil erosion losses (Gong et al., 2018). The soils belong to the clay loam, sandy clay loam, loam textural categories depending on the hillslope position. The mean sand (0.05-2 mm), silt (0.002-0.05 mm), and clay (<0.002 mm) fractions are respectively 41%, 27%, and 31%.

The high standard deviations for Mn (102 mg/kg), Cu (27 mg/kg), and Ba (25 mg/kg) indicate a marked heterogeneous spatial distribution in the topsoil of the vineyard plot. Compared to the local forest topsoil we can observe increased PTE concentration levels in the cultivated soil, except for Mn and Pb. The median EFs range from 1.3 (for Zn) to 17.9 (for Cu) (Table 3). The calculated EFs (with the forest soil as a reference) indicate low enrichment for Zn (1.3), Co (2.4), Ni (2.5), Ba (2.1), and Cr (2.3), more significant accumulation for B (3.8), Sr (3.1) and a marked Cu pollution of the vineyard soil (17.9). Copper contents also exceed the Hungarian environmental quality standards set for soils and sediments (Joint Decree No. 6/2009. (IV. 14) KvVM-EüM-FVM). The EFs calculated taking the Hungarian arable soils as a reference show lower or no PTE concentration increase in the vineyard soil. Only B (EF: 1.6) and Cu (EF: 8.5) are considerably enriched in the vineyard topsoil in Tállya compared with the Hungarian arable soils. Altogether, these observations suggest that grape growing and more precisely, the related use of agrochemicals in vineyards significantly enriches the soil in PTEs. Only Pb and Mn contents are higher in the local forest topsoil underlining their geogenic origin. Compared to arable soils, the elevated concentration levels of Cu and B are attributed to plant protection practices specific to vineyards (and orchards). Copper-based fungicides (such as the Bordeaux mixture) are frequently applied to combat the fungal infections of grapevine, and micronutrient-rich fertilizers (with high B contents) are also regularly used in vineyards. Boron accumulation in cultivated soils has rarely been evidenced so far. However, EFs clearly demonstrate a moderate B accumulation in the vineyard soil due to current grape fertilizing methods.

Relationships between the soil PTE contents and the soil characteristics

The Pearson's correlation coefficients (r) between soil properties and PTE concentrations in the vineyard topsoil samples are summarised in Table 4. According to correlation analysis, a strong positive relationship was

Table 3 Median enrichment factors (EFs) of target PTEs compared to the PTE levels of a local forest topsoil and the Hungarian Soil Information and Monitoring System (SIMS) dataset. Median PTE contents of arable land (based on 842 sampling points) (Csorba et al., 2014) are compared with the topsoil PTE contents of the studied vineyard

	B	Mn	Ni	Cr	Cu	Pb	Zn	Co	Ba	Sr
EF (local forest)	3.8	0.8	2.5	2.3	17.9	0.5	1.3	2.4	2.1	3.1
EF (SIMS)	1.6	-	0.9	1.0	8.5	0.8	0.8	0.7	-	-

Table 4 Pearson's correlation matrix between examined soil characteristics and PTEs. The bold numbers denote statistically significant correlation coefficients (with p-value<0.05).

	SOM	$CaCO_3$	$pH_{d.w.}$	pH_{KCl}	(nitrate+ nitrite)-N	P_2O_5	Coarse f.	Sand	Silt	Clay
SOM	1									
$CaCO_3$	-0.25	1								
$pH_{d.w.}$	-0.01	-0.14	1							
pH_{KCl}	0.30	-0.15	**0.89****	1						
(nitrate+nitrite)-N	-0.45	0.23	0.10	0.30	1					
P_2O_5	0.52	0.26	-0.24	0.05	0.19	1				
Coarse franction	-0.43	0.22	-0.44	**-0.64***	-0.22	-0.30	1			
Sand	-0.31	-0.07	**0.67****	**0.65***	0.40	-0.45	-0.08	1		
Silt	**0.84****	-0.05	-0.28	-0.03	-0.30	**0.61***	-0.32	**-0.60***	1	
Clay	-0.06	0.11	**-0.68****	**-0.79****	-0.33	0.23	0.27	**-0.91****	0.21	1

	B	Mn	Ni	Cu	Cr	Pb	Zn	Co	Ba	Sr
SOM	0.11	0.22	0.06	**0.56***	0.05	0.14	0.14	0.17	0.07	0.31
$CaCO_3$	0.2	0.40	0.17	0.09	0.21	0.34	0.10	0.39	0.27	0.32
$pH_{d.w.}$	**-0.71****	**-0.67****	**-0.76****	-0.48	**-0.78****	**-0.80****	**-0.59***	**-0.87****	**-0.82****	**-0.71****
pH_{KCl}	**-0.74****	-0.51	**-0.78****	-0.30	**-0.78****	**-0.75****	-0.51	**-0.74****	**-0.79****	**-0.54***
(nitrate+nitrite)-N	-0.22	0.05	-0.25	-0.16	-0.23	-0.13	-0.13	-0.08	-0.18	-0.06
P_2O_5	0.41	0.37	0.36	**0.80****	0.43	0.22	0.50	**0.58***	0.45	**0.74***
Coarse fraction	0.17	0.33	0.18	-0.13	0.22	0.46	-0.13	0.31	0.23	-0.00
Sand	**-0.92****	-0.46	**-0.93****	**-0.83****	**-0.93****	**-0.63***	**-0.82****	**-0.79****	**-0.91****	**-0.88****
Silt	0.29	0.38	0.33	**0.76****	0.33	0.34	0.32	0.47	0.37	0.61*
Clay	**0.97****	0.36	**0.97****	**0.62***	**0.96****	**0.60***	**0.83****	**0.71****	**0.93****	**0.76****

*Correlation is significant at the 0.05 level (2-tailed). **Correlation is significant at the 0.01 level (2-tailed).

detected between the SOM content and the silt content (r = 0.84) of the samples, suggesting that particulate organic matter is mainly associated with the silt size fraction. Similarly, Parat et al. (2002) recovered the highest proportions of the soil organic carbon content in the silt fraction of Burgundy vineyard loam soils. The ammonium-lactate soluble P_2O_5 concentration presented a positive relationship with SOM (r = 0.52) and clay (r = 0.61) contents, implying that available P pools are present at higher concentrations in organic- and clay-rich topsoil samples. On the contrary, a strong negative correlation was found between the clay and the sand (r = -0.91) contents indicating the size sorting effect of soil erosion that produces high sand and low clay and vice versa containing topsoils at distinct areas of the hillslope. Correlation of the soil clay content with both pH values (measured in d.w. (r = -0.68) and the KCl solution (r = -0.79)) infer the role of exchangeable H^+ and hydroxy-Al ions adsorbed on clay minerals in determining soil (potential) acidity.

Significant correlation between SOM and silt contents with Cu (r = 0.56 for SOM - Cu and r = 0.76 for silt - Cu) suggests that the silt-bound particulate organic matter and organo-mineral complexes govern Cu binding in the vineyard soil. Former studies performed in high-Cu vineyard soils also emphasised the importance of the particulate organic matter in the sorption of pesticide-derived Cu (Besnard et al., 2001, Parat et al., 2002, Duplay et al., 2014). The closest relationship apparently exists between Cu and ammonium-lactate soluble P_2O_5 contents (r =0.80). Previous findings proposed that phosphate played a role in enhancing the adsorption of Cu (and Pb) to soil mineral phases, such as iron (hydr)oxides through the formation of ternary complexes (Tiberg et al., 2013). Soil pH and sand content showed negative correlation with the examined PTEs (except for the pairs of pH and Cu, sand and Mn). The clay content that markedly affects the soil pH (as previously shown) is also anticorrelated to the sand content. This can explain the negative relationship between PTE concentrations and sand content. Indeed, the PTE contents (except Mn) are significantly and strongly correlated with the clay-sized fraction in the topsoil. Clay-sized fractions are known carriers of PTEs in soils owing to their important metal retaining capacities and specific (organo-)mineral composition (Micó et al., 2006). Therefore, clay minerals and clay mineral-organic matter complexes that primarily constitute the clay fractions (Babcsányi et al., 2016) are proposed to be the main binding phases for B (r = 0.97), Ni (r = 0.97), Cr (r = 0.96), Zn (r = 0.83), Co (r = 0.71), Ba (r = 0.93) and Sr (r = 0.76) (significance at p< 0.01). A less significant correlation (significance at p< 0.05) in the case of Cu (r = 0.62) and Pb (r =0.60) with the clay-sized fraction presumes that additional soil constituents intervene in their binding in the soil, such as the silt-bound SOM in the case of Cu.

In contrast, Mn lacks any statistically significant relationship with the clay-sized fraction and soil characteristics involved in the study (except for $pH_{d.w.}$). This dissimilarity of Mn from the other target PTEs

may stem from the predominantly natural (geogenic) origin of Mn in the studied soil supported by the low (<1) EF (Mn) compared to the local background (Table 3.). This means that Mn mainly enters the soil by weathering of the parent material rhyolite containing an average of 600 mg/kg Mn according to Gilkes and McKenzie (1988). Moreover, Mn's behaviour in soils is complex. Mn is likely to exist in the form of precipitated manganic (oxy)hydroxides in soils with a reaction above pH 6.0, an insoluble form of Mn (Bradl, 2004).

As shown in Table 5, most of the analysed PTEs are strongly correlated with each other. The Mn, Pb, and Cu contents show weaker relations with the other selected PTEs, which may be explained by diverse sources and/or geochemical behaviour in the studied soils, as discussed above.

Spatial distribution of the topsoil characteristics and PTE contents (B, Mn, Ni, Cr, Pb, Cu, Zn, Co, Ba, Sr) in the vineyard topsoil

In this study, root mean square error (RMSE) and mean absolute error (MAE) were used to evaluate inverse distance weighting (IDW) and lognormal kriging (LK) interpolations' performance (summarised in Table 6). IDW generates smoother surfaces than LK, which may decrease its performance. Meanwhile, the LK method tends to underestimate the higher values and overestimate the lower values. The results indicate that LK shows an overall better performance to predict most of the examined soil parameters, except for $pH_{d.w.}$, sand, and SOM contents. IDW tends to compute higher prediction errors as weighting values increase. The LK outperformed the IDW method for predictions made for P_2O_5, $CaCO_3$,

Table 5 Pearson's correlation matrix among PTEs. The bold numbers denote statistically significant correlation coefficients (with p-value<0.05).

	B	Mn	Ni	Cu	Cr	Pb	Zn	Co	Ba	Sr
B	1									
Mn	0.42	1								
Ni	**0.99****	0.46	1							
Cu	**0.72****	0.34	**0.69****	1						
Cr	**0.99****	0.50	**0.99****	**0.73****	1					
Pb	**0.62***	**0.74****	**0.69****	0.44	**0.71****	1				
Zn	**0.90****	0.28	**0.89****	**0.72****	**0.88****	0.43	1			
Co	**0.81****	**0.73****	**0.83****	**0.72****	**0.87****	**0.84****	**0.69****	1		
Ba	**0.97****	**0.60***	**0.98****	**0.71****	**0.99****	**0.76****	**0.85****	**0.91****	1	
Sr	**0.87****	**0.59***	**0.87****	**0.90****	**0.89****	**0.67****	**0.83****	**0.90****	**0.91****	1

*Correlation is significant at the 0.05 level (2-tailed). **Correlation is significant at the 0.01 level (2-tailed).

Table 6 Performance of inverse distance weighting (IDW) and lognormal kriging (LK) for predicting soil characteristics and PTE contents in the vineyard topsoil. The smallest prediction errors are highlighted in bold. RMSE stands for root mean square error. MAE stands for mean absolute error.

Soil properties	Unit	RMSE		MAE	
		IDW	LK	IDW	LK
$pH_{d.w.}$		**0.38**	0.39	**0.34**	0.36
pH_{KCl}		**0.56**	**0.56**	**0.34**	**0.34**
(nitrate+nitrite)-N	mg/kg	**0.64**	0.65	0.51	**0.46**
P_2O_5	%	59.97	**55.83**	52.30	**49.09**
SOM	%	**0.42**	0.44	**0.38**	0.42
$CaCO_3$	%	0.50	**0.47**	0.47	**0.42**
Clay	%	3.15	**3.03**	2.79	**2.42**
Silt	%	3.32	**3.30**	2.69	**2.67**
Sand	%	**4.31**	5.22	**3.58**	4.53
Coarse fraction	%	11.91	**11.86**	11.42	**11.20**
PTEs					
Zn	mg/kg	3.66	**3.63**	3.30	**3.17**
Pb	mg/kg	**1.47**	1.53	1.30	**1.20**
Ni	mg/kg	1.62	**1.44**	1.29	**1.16**
Cr	mg/kg	1.48	**1.13**	1.17	**0.85**
Cu	mg/kg	**23.51**	23.76	15.93	**15.88**
Co	mg/kg	0.60	**0.58**	0.58	**0.52**
B	mg/kg	1.76	**1.72**	1.55	**1.55**

clay, silt, and coarse fractions. Furthermore, LK also showed smaller prediction errors than IDW for mapping the PTE contents except for Cu and Pb. As previously observed, the local minimum and maximum values are likely to be respectively overestimated and underestimated by LK, while the predicted local minimum and maximum values by IDW are similar to the measured ones (Xie et al., 2011). In the following, some maps for the selected soil properties and the B, Cu and Zn contents prepared by LK are displayed (Fig. 2).

Our results confirmed that terrain significantly impact the spatial variability of soil characteristics at the plot scale. Contrasting spatial patterns of soil texture can be delineated along the hillslope. The upper slope sections display higher proportions of clay and, accordingly, lower sand contents. Meanwhile, at the lower half of the hillslope, high sand contents coincide with reduced clay contents. The silt and the concomitantly varying SOM contents are found in higher concentrations at the summit and the shoulder positions of upslope areas. At the same time, a reraising trend can be observed at the toeslope zone. By contrast, in Mediterranean hillslope vineyards, the highest silt and total organic carbon contents were detected at the middle of a hillslope (Rodrigo Comino et al., 2016). The differences of the landscape topography and the soil characteristics may explain the observed differences. Indeed, the vineyard soil in Tállya is characterised by high contents of the coarse fraction (>30%), which is supposed to impact soil erosion dynamics significantly. Indeed, the slope steepness and the proportions of the coarse fraction in soil are found to determine soil loss rates. At mild slope gradients (at 5°), the high contents of the coarse fraction in the form of embedded rock fragments increase water infiltration rates, thus reducing overland flow. By contrast, at higher than 10° gradients, the coarse fraction seemingly enhances runoff generation and sediment transport (Gong et al., 2018). We can reasonably suppose that the coarse fraction protects the soil from excessive soil loss at the summit and the hillslope's shoulder, displaying <10° gradients (Fig. 1). The main erosion-impacted zone is situated at the backslope, where high slope gradients prevail. The highest contents of the coarse fraction are observed at the backslope section, further confirming intense losses of the fine earth (< 2 mm). Similarly, Rodrigo Comino et al. (2017) reported that the highest rock fragment contents (77%) were found at the hillslope's shoulder in a Spanish vineyard. Soil erosion induces particle size sorting according to the dominating sediment transport processes. Sediments moved during interrill erosion, transport predominantly fine soil particles (<0.05 mm) suspended in runoff, while rill development during intense rainfall displaces coarser soil fractions (fine sand, sand) (Shi et al., 2012).

Similar observations have been made in another sloping vineyard (Nagy-Eged Hill, Hungary), where grape rows were oriented parallel to the main slope and bare areas between rows enabled the downhill transport and the accumulation of both the fine fraction and the gravel eroded from uphill areas (Nagy et al., 2012). The accumulation of sand in the footslope zone of the vineyard in Tállya, together with reraising silt contents further downhill in the toeslope area, suggest that sediment grain-sorting also occurs during its deposition. The displaced coarse (sand, fine sand) soil fractions are preferentially deposited right at the footslope. The fine fractions of silt and clay are transported farther downslope, increasing the silt content in the toeslope zone.

In general, the spatial distribution maps of Cu, Zn and B show that higher concentrations are found in upslope areas, while markedly lower concentrations prevail in the backslope and footslope areas. Spatial distribution of B, Pb, and Co present lower variability in the plot. Meanwhile, Zn, Sr, and Cr show moderate spatial variability, and Mn, Co, and Ba demonstrate high spatial variability. Their similar spatial distribution further supports the intimate association of PTEs with the clay-sized fraction. The spatial trends reveal that the higher concentrations of PTEs at the summit and the shoulder of the hillslope are associated with the low slope gradients (0-5 degree) and the high contents of the coarse fraction (that protects the soil from excessive erosion-induced losses). While the reraising PTE concentrations mostly at the toeslope are likely due to the deposition of fine soil particles, mainly silt and to a minor extent clay, the main vectors of PTEs during sediment transport.

CONCLUSION

We have demonstrated that grape growing and, more precisely, the related use of agrochemicals significantly enriches the potentially toxic element (PTE) content of soils, except for lead (Pb) and manganese (Mn). The slightly acidic vineyard soil in Tállya (Hungary) bears higher boron (B), nickel (Ni), chrome (Cr), copper (Cu), zinc (Zn), cobalt (Co), barium (Ba) and strontium (Sr) contents compared to the local forest soil. The vineyard soil accumulated Cu and – to a smaller extent – B in excess, considering median contents of these elements in Hungarian arable soils as a reference. The latter is attributed to plant protection practices specific to vineyards, including frequent applications of Cu-based fungicides (such as the Bordeaux mixture) and micronutrient-rich fertilizers (with high B contents). Anthropogenic B accumulation due to farming practices in vineyard soils within a low geochemical B area has rarely been evidenced so far.

The examined soil's clay content strongly correlated with the bulk pseudototal PTE contents of B, Ni, Cr, Zn, Co, Ba and Sr. Indeed, clay-sized fractions are known carriers of PTEs owing to their high metal(loid) sorbing capacities. Presumably, these PTEs are adsorbed primarily to clay minerals and clay mineral-organic matter complexes. A less significant correlation (significance at $p < 0.05$) in the case of Cu and Pb with the clay content presumes that additional constituents intervene in their retention in the vineyard soil in Tállya. In the case of Cu, the silt-bound soil organic matter (SOM) is also a plausible sorbing material. Manganese (Mn) has geogenic origin in the vineyard soil primarily. The lack of significant correlation with the soil characteristics (but $pH_{d.w.}$) underlines the contrasting behaviour of Mn in the vineyard soil compared with the other PTEs involved in the study.

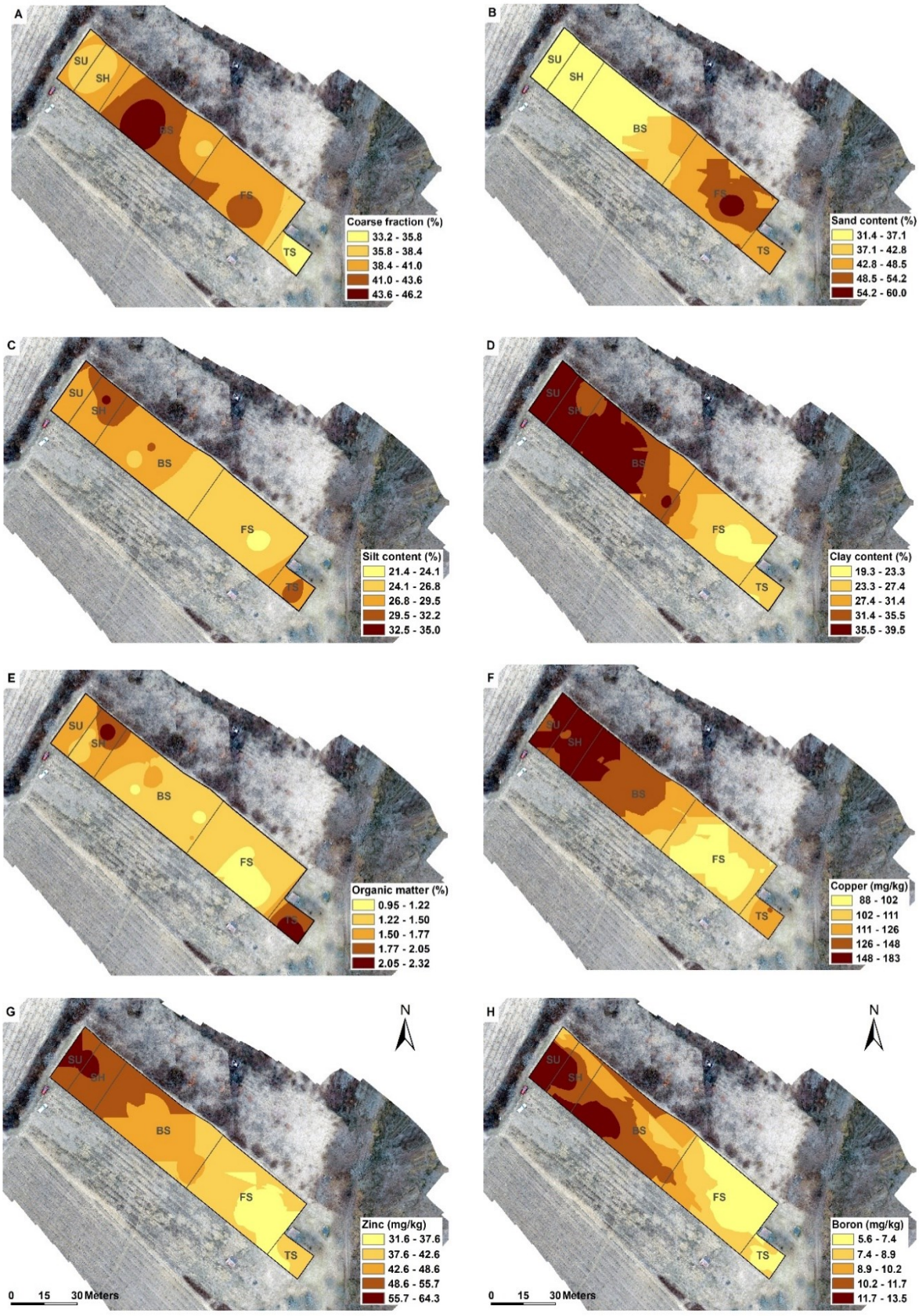

Fig. 2 Interpolated maps showing the spatial distribution of the topsoil contents of the (A) coarse fraction, (B) sand, (C) silt, (D) clay, (E) organic matter, (F) Cu, (G) Zn and (H) B predicted by lognormal kriging. Pixel values were reclassified using equal intervals, which divides the range of data values into equal-sized subranges. Hillslope positions are also displayed on the maps: SU (summit), SH (shoulder), BS (backslope), FS (footslope), TS (toeslope).

The LK outperformed the IDW method for predicting the majority of soil parameters. The spatial distribution maps show higher contents of PTEs at the summit and the hillslope's shoulder, while lower ranges prevail at the footslope zone. The soil samples from the summit and the toeslope zones have the highest contents of SOM, while increased contents of the coarse fraction are found at the backslope. These observations confirm that soil erosion and sediment transport processes govern the redistribution of different particle-size soil fractions, associated soil constituents and PTEs within the vineyard.

A better understanding of the impact of soil erosion on the spatial patterns of soil quality will advance our knowledge of erosion and sedimentation processes, which in turn will improve erosion modelling.

ACKNOWLEDGMENTS

I. Babcsányi is grateful for the financial support of the Premium Postdoctoral Research Program of the Hungarian Academy of Sciences. The authors wish to thank István Fekete and Amanda Kiss for assisting in sample treatment and laboratory analyses of samples. The authors are grateful to the local vine-growers of Tállya for allowing our field survey and sharing information on the agrichemicals' use and soil management.

References

Babcsányi, I., Chabaux, F., Granet, M., Meite, F., Payraudeau, S., Duplay, J., Imfeld, G. 2016. Copper in soil fractions and runoff in a vineyard catchment: Insights from copper stable isotopes. *Science of The Total Environment* 557-558, 154–162. DOI: 10.1016/j.scitotenv.2016.03.037

Besnard, E., Chenu, C., Robert, M. 2001. Influence of organic amendments on copper distribution among particle-size and density fractions in Champagne vineyard soils. *Environmental Pollution* 112 (3), 329–337. DOI: 10.1016/S0269-7491(00)00151-2

Biddoccu, M., Ferraris, S., Opsi, F., Cavallo, E. 2016. Long-term monitoring of soil management effects on runoff and soil erosion in sloping vineyards in Alto Monferrato (North-West Italy). *Soil and Tillage Research* 155, 176–189. DOI: 10.1016/j.still.2015.07.005

Bordoni, M., Vercesi, A., Maerker, M., Ganimede, C., Reguzzi, M.C., Capelli, E., Wei, X., Mazzoni, E., Simoni, S., Gagnarli, E., Meisina, C. 2019. Effects of vineyard soil management on the characteristics of soils and roots in the lower Oltrepò Apennines (Lombardy, Italy). *Science of The Total Environment* 693, 133390. DOI: 10.1016/j.scitotenv.2019.07.196

Bradl, H.K. 2004. Adsorption of heavy metal ions on soils and soils constituents. *Journal of Colloid and Interface Science* 277(1), 1-18. https://doi.org/10.1016/j.jcis.2004.04.005

Capello, G., Biddoccu, M., Ferraris, S., Cavallo, E. 2019. Effects of tractor passes on hydrological and soil erosion processes in tilled and grassed vineyards. *Water (Switzerland)* 11, 10352. DOI: 10.3390/w11102118

Csorba, S., Üveges, J., Makó, A. 2014. Relationship between soil properties and potentially toxic element content based on the dataset of the Soil Information and Monitoring System in Hungary. *Central European Geology* 57 (3), 253–263. DOI: 10.1556/ceugeol.57.2014.3.2

Dos Santos, G.C.G., Valladares, G.S., Abreu, C.A., De Camargo, O.A., Grego, C.R. 2013. Assessment of copper and zinc in soils of a vineyard region in the state of São Paulo, Brazil. *Applied and Environmental Soil Science* 2013, 790795. DOI: 10.1155/2013/790795

Duplay, J., Semhi, K., Errais, E., Imfeld, G., Babcsanyi, I., Perrone, T. 2014. Copper, zinc, lead and cadmium bioavailability and retention in vineyard soils (Rouffach, France): The impact of cultural practices. *Geoderma* 230-231, 318–328. DOI: 10.1016/j.geoderma.2014.04.022

Follain, S., Ciampalini, R., Crabit, A., Coulouma, G., Garnier, F. 2012. Effects of redistribution processes on rock fragment variability within a vineyard topsoil in Mediterranean France. *Geomorphology* 175-176, 45–53. DOI: 10.1016/j.geomorph.2012.06.017

Gilkes, R.J., McKenzie, R.M. 1988. Geochemistry and Mineralogy of Manganese in Soils. Manganese in Soils and Plants: Proceedings of the International Symposium on 'Manganese in Soils and Plants' held at the Waite Agricultural Research Institute, The University of Adelaide, Glen Osmond, South Australia, Dordrecht, Springer Netherlands: 23-35.

Gong, T., Zhu, Y., Shao, M. 2018. Effect of embedded-rock fragments on slope soil erosion during rainfall events under simulated laboratory conditions. *Journal of Hydrology* 563, 811–817. DOI: 10.1016/j.jhydrol.2018.06.054

Goovaerts, P. 1999. Geostatistics in soil science: State-of-the-art and perspectives. *Geoderma* 89, 1–45. DOI: 10.1016/S0016-7061(98)00078-0

Guo, X., Fu, B., Ma, K., Chen, L., Wang, J. 2001. Spatio-temporal variability of soil nutrients in the Zunhua plain, northern China. *Physical Geography* 22, 343–360. DOI: 10.1080/02723646.2001.10642748

Ippolito, J.A., Barbarick, K.A. 2006. Biosolids Affect Soil Barium in a Dryland Wheat Agroecosystem. *Journal of Environmental Quality* 35 (6), 2333–2341. DOI: 10.2134/jeq2006.0076

Joint Decree No. 6/2009. (IV. 14) KvVM-EüM-FVM of the Ministers of Environmental Protection and Water Management, Public Health, Agriculture and Regional Development on the Limit Values Necessary to Protect the Quality of Geological Medium and the Groundwater and on Measurement of Pollution.

Ladányi, Z., Csányi, K., Farsang, A., Perei, K., Bodor, A., Kézér, A., Barta, K., Babcsányi, I. 2020. Impact of Low-Dose Municipal Sewage Sludge Compost Treatments on the Nutrient and the Heavy Metal Contents in a Chernozem Topsoil Near Újkígyós, Hungary: A 5-Year Comparison. *Journal of Environmental Geography* 13 (1-2), 25–30. DOI: 10.2478/jengeo-2020-0003

Lu, A., Wang, J., Qin, X., Wang, K., Han, P., Zhang, S. 2012. Multivariate and geostatistical analyses of the spatial distribution and origin of heavy metals in the agricultural soils in Shunyi, Beijing, China. *Science of the Total Environment* 425, 66–74. DOI: 10.1016/j.scitotenv.2012.03.003

Mezősi, G., Bata, T. 2016. Estimation of the Changes in the Rainfall Erosivity in Hungary. *Journal of Environmental Geography* 9 (3-4), 43–48. DOI: 10.1515/jengeo-2016-0011

Micó, C., Recatalá, L., Peris, M., Sánchez, J. 2006. Assessing heavy metal sources in agricultural soils of a European Mediterranean area by multivariate analysis. *Chemosphere* 65, 863–872. DOI: 10.1016/j.chemosphere.2006.03.016

Milićević, T., Relić, D., Škrivanj, S., Tešić, Ž., Popović, A. 2017. Assessment of major and trace element bioavailability in vineyard soil applying different single extraction procedures and pseudo-total digestion. *Chemosphere* 171, 284–293. DOI: 10.1016/j.chemosphere.2016.12.090

MSZ-08-0206-2, 1978. Evaluation of Some Chemical Properties of the Soil. Laboratory Tests. (pH Value, Phenolphtaleine Alkalinity Expressed in Soda, All Water Soluble Salts, Hydrolite (y1-Value) and Exchanging Acidity (y2-Value)). Hungarian Standard Association, Budapest (in Hungarian).

MSZ 21470-52, 1983. Environmental Protection. Testing of Soils. Determination of Organic Matter. Hungarian Standard Association, Budapest (in Hungarian).

MSZ 20135:1999 Determination of the Soluble Nutrient Element Content of the Soil. Hungarian Standard Association, Budapest (in Hungarian).

Nagy, R., Zsófi, Z., Papp, I., Földvári, M., Kerényi, A., Szabó, S. 2012. Evaluation of the relationship between soil erosion and the mineral composition of the soil: A case study from a cool climate wine region of Hungary. *Carpathian Journal of Earth and Environmental Sciences* 7, 223–230.

Novara, A., Pisciotta, A., Minacapilli, M., Maltese, A., Capodici, F., Cerdà, A., Gristina, L. 2018. The impact of soil erosion on soil fertility and vine vigor. A multidisciplinary approach based on

field, laboratory and remote sensing approaches. *Science of The Total Environment* 622-623, 474–480. DOI: 10.1016/j.scitotenv.2017.11.272

Parat, C., Chaussod, R., Lévêque, J., Dousset, S., Andreux, F. 2002. The relationship between copper accumulated in vineyard calcareous soils and soil organic matter and iron. *European Journal of Soil Sciences* 53 (4), 663–670. DOI: 10.1046/j.1365-2389.2002.00478.x

Patinha, C., Durães, N., Dias, A.C., Pato, P., Fonseca, R., Janeiro, A., Barriga, F., Reis, A.P., Duarte, A., Ferreira da Silva, E., Sousa, A.J., Cachada, A. 2018. Long-term application of the organic and inorganic pesticides in vineyards: Environmental record of past use. *Applied Geochemistry* 88, 226–238. DOI: 10.1016/j.apgeochem.2017.05.014

Rodrigo Comino, J., Ruiz Sinoga, J.D., Senciales González, J.M., Guerra-Merchán, A., Seeger, M., Ries, J.B. 2016. High variability of soil erosion and hydrological processes in Mediterranean hillslope vineyards (Montes de Málaga, Spain). *Catena* 145, 274–284. DOI: 10.1016/j.catena.2016.06.012

Rodrigo Comino, J., Senciales, J.M., Ramos, M.C., Martínez-Casasnovas, J.A., Lasanta, T., Brevik, E.C., Ries, J.B., Ruiz Sinoga, J.D. 2017. Understanding soil erosion processes in Mediterranean sloping vineyards (Montes de Málaga, Spain). *Geoderma* 296, 47–59. DOI: 10.1016/j.geoderma.2017.02.021

Rodrigues, S.M., Henriques, B., da Silva, E.F., Pereira, M.E., Duarte, A.C., Römkens, P.F.A.M. 2010. Evaluation of an approach for the characterization of reactive and available pools of twenty potentially toxic elements in soils: Part I – The role of key soil properties in the variation of contaminants' reactivity. *Chemosphere* 81 (11), 1549–1559. DOI: 10.1016/j.chemosphere.2010.07.026

Rodríguez Martín, J.A., Arias, M.L., Grau Corbí, J.M. 2006. Heavy metals contents in agricultural topsoils in the Ebro basin (Spain). Application of the multivariate geoestatistical methods to study spatial variations. *Environmental Pollution* 144 (3), 1001–1012. DOI: 10.1016/j.envpol.2006.01.045

Rodríguez Martín, J.A., Vázquez De La Cueva, A., Grau Corbí, J.M., López Arias, M. 2007. Factors controlling the spatial variability of copper in topsoils of the northeastern region of the Iberian Peninsula, Spain. Water, Air, & Soil Pollution 186: 311–321. https://doi.org/10.1007/s11270-007-9487-9

Scull, P., Franklin, J., Chadwick, O.A., McArthur, D. 2003. Predictive soil mapping: A review. *Progress in Physical Geography: Earth and Environment* 27 (2), 171–197. DOI: 10.1191/0309133303pp366ra

Shi, Z.H., Fang, N.F., Wu, F.Z., Wang, L., Yue, B.J., Wu, G.L. 2012. Soil erosion processes and sediment sorting associated with transport mechanisms on steep slopes. *Journal of Hydrology* 454-455, 123–130. DOI: 10.1016/j.jhydrol.2012.06.004

Solgi, E., Solgi, M., Rodríguez Martín, J.A. 2016. Spatial variability of heavy metal concentrations in vineyard soils on Malayer Plains (Iran). *Environmental Forensics* 17 (1), 87–96. DOI: 10.1080/15275922.2015.1133728

Sun, C., Liu, J., Wang, Y., Sun, L., Yu, H. 2013. Multivariate and geostatistical analyses of the spatial distribution and sources of heavy metals in agricultural soil in Dehui, Northeast China. *Chemosphere* 92, 517–523. DOI: 10.1016/j.chemosphere.2013.02.063

Szatmári, G., Barta, K., Farsang, A., Pásztor, L. 2015. Testing a sequential stochastic simulation method based on regression kriging in a catchment area in Southern Hungary. *Geologia Croatica* 68 (3), 273–283. DOI: 10.4154/GC.2015.21

Szatmári, J., Tobak, Z., Van Leeuwen, B., Dolleschall, J. 2011. Data acquisition for inland excess water mapping and modelling using artificial neural networks. *Földrajzi Közlemények* 135 (4), 351–363.

Tiberg, C., Sjöstedt, C., Persson, I., Gustafsson, J.P. 2013. Phosphate effects on copper(II) and lead(II) sorption to ferrihydrite. *Geochimica et Cosmochimica Acta* 120, 140–157. DOI: 10.1016/j.gca.2013.06.012

Torri, S.I., Corrêa, R.S. 2012. Downward Movement of Potentially Toxic Elements in Biosolids Amended Soils. *Applied and Environmental Soil Science* 2012, 145724. DOI: 10.1155/2012/145724

Ungureanu, T., Iancu, G.O., Pintilei, M., Chicoş, M.M. 2017. Spatial distribution and geochemistry of heavy metals in soils: A case study from the NE area of Vaslui county, Romania. *Journal of Geochemical Exploration* 176, 20–32. DOI: 10.1016/j.gexplo.2016.08.012

Webster, R., Oliver, M.A. 2007. Geostatistics for Environmental Scientists. Second ed. John Wiley & Sons. DOI: 10.2136/vzj2002.3210

World Reference Base for Soil Resources 2014. International soil classification system for naming soils and creating legends for soil maps. World Soil Resources Reports No. 106. FAO, Rome.

USDA, 2014. Soil Survey Field and Laboratory Methods Manual. United States Dep. Agric. Nat. Resour. Conserv. Serv. 487. DOI: 10.13140/RG.2.1.3803.8889

Xie, Y., Chen, T. Bin, Lei, M., Yang, J., Guo, Q.J., Song, B., Zhou, X.Y. 2011. Spatial distribution of soil heavy metal pollution estimated by different interpolation methods: Accuracy and uncertainty analysis. *Chemosphere* 82, 468–476. DOI: 10.1016/j.chemosphere.2010.09.053

sciendo

Journal of Environmental Geography 14 (1–2), 58–67.

DOI: 10.2478/jengeo-2021-0006
ISSN 2060-467X

THE POTENTIAL USE OF OSL PROPERTIES OF QUARTZ IN INVESTIGATING FLUVIAL PROCESSES ON THE CATCHMENT OF RIVER MUREŞ, ROMANIA

Tamás Bartyik[1], Cristian Floca[2], Elemér Pál-Molnár[1,3], Petru Urdea[2], Diaa Elsayed Hamed[4], György Sipos[1]*

[1]Geomorphological and Geochronological Research Group, Department of Geoinformatics, Physical and Environmental Geography, University of Szeged, Egyetem u. 2-6, 6722 Szeged, Hungary
[2]Department of Geography, West University of Timişoara, B-dul. Vasile. Parvan Nr. 4, 300223, Timişoara, Romania
[3]Department of Mineralogy, Geochemistry and Petrology, University of Szeged, Egyetem u. 2-6, 6722 Szeged, Hungary
[4]National Research Institute of Astronomy and Geophysics, EL Marsad Street 1, Helwan, Cairo 11421, Egypt

*Corresponding author, email: gysipos@geo.u-szeged.hu

Research article, received 15 March 2021, accepted 23 April 2021

Abstract

To understand the functioning of fluvial systems it is important to investigate dynamics of sediment transport and the source of sediments. In case of reconstructing past processes these studies must be accompanied by the numerical dating of sediment samples. In this respect optically stimulated luminescence is a widely used technique, by which the time of sediment deposition can be directly dated. Recently, in various fluvial environments it has been shown that certain luminescence properties of minerals, and especially that of quartz, can be applied as indicators of fluvial erosion and/or sediment provenance. These properties are residual luminescence (or residual dose) and luminescence sensitivity of quartz grains. However, the values of the parameters above are affected by various factors, the importance of which is under debate. The present study therefore aims to assess these factors along a ~560 km long reach of River Mureş (Maros) a relatively large river with a compound surface lithology on its catchment. The research focused on the sandy fraction of modern sediments, collected from the main river and from three tributaries alike. This way not only longitudinal downstream changes, but the influence of tributaries could also be studied. Based on the data, both investigated parameters show a great variation, which can be attributed to the lithological differences of subcatchments and geomorphological drivers, such as erosional activity and potential number of sedimentary cycles, and human activity. However, relationships are not entirely clear and are influenced by the maximum grain size of the samples investigated, and the recycling of previously laid deposits with different properties. Still, when performing detailed dating studies, and tracing sediments from certain parts of the catchment luminescence properties can be a useful tool in the future.

Keywords: sediment tracing, luminescence sensitivity, fluvial sediments, erosion, River Mureş

INTRODUCTION

Alluvial deposits are made up of a complex mixture of mineral grains originating from several subcatchments of a river usually with different lithology and erosional intensity. In sedimentary basins with complex river system, the reconstruction of fluvial processes often requires the tracing of sediments in order to assess major avulsion events, channel migration, or the variable activity of catchments, governed by climatic or tectonic processes (Schumm, 1979). Traditionally, sediment tracing is based on geochemical, mineralogical or other physical, such as magnetic properties by which unique fingerprints are aimed to be identified, which can be then attributed to certain parts of the catchment (e.g. Fryirs and Gore, 2013; Walling, 2013; Collins et al., 2020). However, sediment tracing also requires the numerical dating of sediments, as the comparison of fingerprint properties is only viable if the age of deposition is known (Collins et al., 2020). Not just because temporal changes may occur in the activity of catchments, but because the true proportion of sources can be determined if sediments of the same age are investigated (Walling, 2013).

In this respect, a relatively new method for sediment tracing is the investigation of luminescence properties of sedimentary quartz grains, which can be done parallel to the dating of sediments by the means of optically stimulated luminescence (OSL) (Gray et al., 2019). OSL is based on the fact that certain minerals, such as quartz and feldspars function as natural dosimeters recording total environmental radioactivity in their surroundings since their last exposure to sunlight, i.e. since sediment deposition (Aitken, 1998; Bøtter-Jensen et al., 2003). Subsequent to exposure, incident radioactive particles excite the semiconductor natural crystals and charges reaching the valence band are trapped at crystal defects (e.g. vacancies, interstitial ions). The longer time passes since deposition, the more charges are trapped, and the higher luminescence intensity can be measured in the laboratory when charges are artificially detrapped

using light or heat. However, the measured luminescence intensity is depending not only on the age, but also on the charge trapping capacity of the crystals, determined primarily by the number of crystal defects. Consequently, the intensity measured in response to unit radioactive dose is termed as luminescence sensitivity (Preusser et al., 2009; Sawakuchi, 2011; Sharma, 2017; Gray et al., 2019). As luminescence sensitivity is a sample dependent property, thus it has a unique potential in sediment tracing (Gray et al., 2019). This is especially true for quartz, since it can exhibit highly variable sensitivity values, as shown by the study of Bartyik et al. (2021).

Luminescence sensitivity of quartz is primarily determined by the lithology and mineralogy of source rocks. Impurities, developing during the crystallization process, are responsible for the primary charge trapping capacity of the lattice and determine the magnitude of luminescence intensity (Zheng, 2009; Lü and Sun, 2011; Sawakutchi et al., 2011). As pointed out by previous researches, quartz from metamorphic and igneous rocks usually has low sensitivity compared to those originating from sedimentary rocks (Chithambo et al., 2007; Guralnik et al., 2015; Sawakutchi et al., 2018). A difference was also identified based on the formation temperature of rocks (Sawakutchi et al., 2011). Thus, crystallization temperatures can be of significant influence on quartz sensitivity (Sharma, 2017; Sawakutchi et al., 2020).

In the meantime, luminescence sensitivity can increase due to geomorphological processes, most likely as a consequence of recurring sedimentary cycles and long transportation distance, meaning repeated sunlight exposure and natural dosing (Fitzsimmons, 2011; Wintle and Adamiec, 2017). For example, the high luminescence sensitivity of Australian sedimentary quartz is usually explained by the extensive and the repeated reworking of sediments (Pietsch et al., 2008; Fitzsimmons et al., 2010; Fitzsimmons, 2011). Similarly, Preusser et al. (2006) claimed that the low luminescence sensitivity of quartz in sediments of New Zealand is primarily caused by their short sedimentary history. In another study, for Australian river sediments, Gliganic et al. (2017) observed an increase in luminescence sensitivity going downstream. However, no such tendency was detected in terms of the Amazon River Basin (Sawakuchi et al., 2018), where differences and downstream change of quartz sensitivity could rather be related to the lithological background of subcatchments (Sawakuchi et al., 2012). Beside sediment cycling, the mode of sediment transport can also have significant role in determining the natural sensitivity of grains (Li and Wintle, 1991,1992). Though, in her study on Australian quartz from various depositional environments Fitzsimmons (2011) found no systematic sensitivity difference between aeolian and water-lain sediments. The influence of both lithological background and sedimentary prehistory of samples thus proved to be important in the level of luminescence sensitivity.

Beside sensitivity, other OSL properties can also be used to investigate fluvial systems, namely if exposure to sunlight is not of adequate length, residual luminescence signals may be reserved in the crystal lattice (Godfrey-Smith et al., 1988; Tóth et al., 2017; Smedley et al., 2019). This often occurs, since turbulence, together with water depth attenuate the intensity of sunlight reaching the grains and thus lead to reduced bleaching (Gemmell, 1988; Berger, 1990; Rendell et al., 1994). Although residuals can adversely affect the accuracy of the dating procedure and usually lead to age overestimation, they can also be applied to investigate the sedimentary dynamics and erosional capacity of river channels (Fiebig and Preusser, 2007; Sipos et al., 2016; Tóth et al., 2017), as far as high residuals indicate the proximity of the sediment source.

As it has been shown above, the OSL properties of quartz grains can be influenced by many factors, and the understanding of these factors requires the systematic investigation of river systems. From this point of view, River Mureş can be a good choice because sedimentary, igneous and metamorphic rocks are all present on its relatively large drainage basin. Additionally, due to the elongated shape of the catchment the role of subcatchments with different surface lithology can be distinguished relatively well on its upper reaches, while along its lower reaches no major tributaries join the river, primarily geomorphological processes should determine the luminescence properties of quartz grains on this section.

Therefore, the aim of the present research was to investigate the change of some key luminescence properties along an approximately 560 km long section of River Mureş in order to see how subcatchments with different surface lithology, and transportation distance, i.e. repeated reworking of sediments, affect residual doses and luminescence sensitivity of quartz grains. The research also enabled the assessment of the applicability of luminescence properties as a sediment tracer in a relatively large river system.

STUDY AREA AND SAMPLING

River Mureş (Maros) is the fourth largest waterflow in the Carpathian Basin. The area of the its catchment is approx. 30 000 km^2, the majority of which falls in Romania and drains the waters of the Transylvanian Basin (Laczay, 1975). The upstream part of catchment (250x100 km) is rectangular, while the downstream section (200x30 km) starting from Deva is elongated (Urdea et al., 2012). Concerning river morphology and surface lithology, the course of the river can be separated into four major reaches (Fig. 1). The uppermost, steepest upland reach from the source of the river till Deda is dominated by volcanic rocks (Urdea et al., 2012; Pál-Molnár et al., 2015). The next section from Deda to Alba Iulia is characterized by a significantly lower slope as the river enters the hilly landscape of the Transylvanian Basin, built up of Neogene marine and lacustrine sedimentary rocks (Baranyi et al., 2020). The largest tributary of the river, Târnava (Küküllő) is also situated in this lithological domain. However, on the downstream part of this

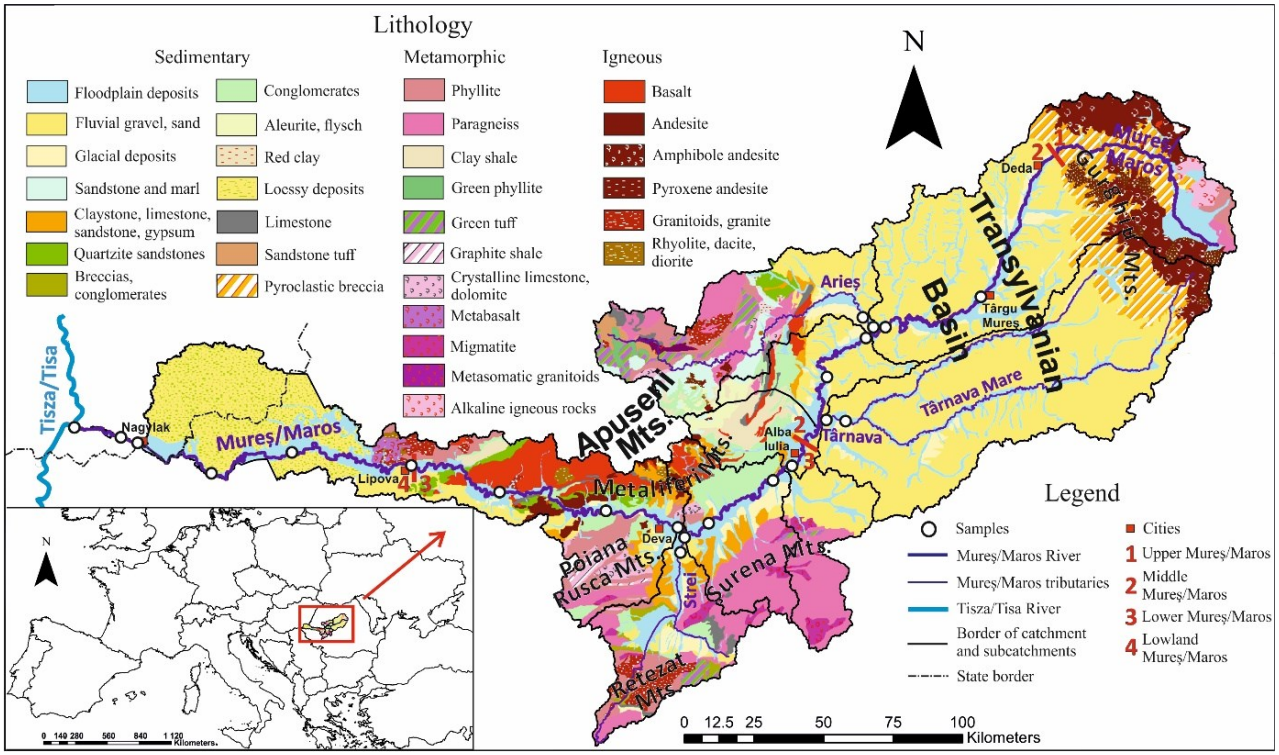

Fig. 1 The surface lithology of the catchment of River Mureş and the location of sampling points (Based on Harta geologică a R. S. România, sc. 1:200.000, 1967 maps).

section tributaries, such as the Arieș (Aranyos), already introduce to the main river sediments produced in the Apuseni Mountains with a complex mixture of surface lithology comprised of metamorphic, magmatic/ plutonic, volcanic and sedimentary rocks of various origin (Kounov and Schmid, 2013; Silye, 2015). Downstream of Alba Iulia, the river flows till Lipova along the tectonic line dividing the Apuseni Mountains and the Southern Carpathians. In this area, small northern tributaries carry the sediments of the Metaliferi (Transylvanian Ore) Mountains, rich in volcanic rocks and ores, to the main river. Larger southern tributaries, such as the Sebeş (Sebes) and Strei (Sztrigy) transport their sediments mostly from the metamorphic and plutonic rocks of the Southern Carpathians (Bojar et al., 2010; Iancu and Seghedi, 2017). On the lowland section, downstream of Lipova the Mureş has built an extensive alluvial fan, on which it has frequently changed its direction even in the Holocene, thus here it reworks its own alluvial deposits (Borsy, 1989; Kiss et al., 2013).

In the present study, a 565 km section between Târgu Mureş and the confluence to the Tisza was studied, along with three of the largest tributaries of the river: Arieș, Târnava, and Strei (Fig. 1).

To investigate the change in luminescence sensitivity, modern sediment samples with similar geomorphological position were collected from the river channel, usually from side bars, point bars or sand sheets on the river bank (Fig. 2A-B). Potential sampling points were pre-selected using satellite images taken at low water periods. Sampling was carried out at 16 locations along the Mureş River, while in the case of tributaries two samples were collected upstream of their confluence at 2-4 rkm and at 8-14 rkm in each case. Thus, we sampled a total of 22 locations in the entire study area (Fig. 1, Table 1). Sampling took place during the autumn low water period. At each point, we aimed to collect samples rich in sand. In the case of the samples on the bank of the channel, sample collection was made using a spatula (Fig. 2C). In case of river bars, sampling was made using a PVC tubes (Fig. 2D).

METHODS

Laboratory processing of the collected samples followed general laboratory techniques (Mauz et al., 2002; Sipos et al., 2016). After removing the light exposed outer layer in the dark laboratory the samples were dried. Then by sieving the 90-150 µm, 150-220 µm and 220-300 µm fractions of samples were separated by wet sieving. In many cases, however, there was enough quartz for the measurements only by mixing the previously separated fractions (Table 1). The carbonate and organic material content of samples were removed by repeated treatment in 10% HCl and 10% H_2O_2. The quartz fraction was separated by using LST (sodium polylungstanate) heavy liquid. This step was followed by a 50 min 40% HF etching to remove unwanted feldspar residues as well as the external shell of quartz grains. For measuring residual doses purified quartz samples were adhered on Ø10 mm stainless steel discs using silicone spray and a 2 mm mask. For sensitivity measurements, Ø10 mm diameter stainless steel cups were used, into which a 6 mg of sample was measured with an analytical balance.

Fig. 2 Typical sample collection sites include point bars (A) and side bars (B). Sampling was performed from the uppermost, thus freshly deposited sediments by spatula (C) or plastic tube (D) for undisturbed samples.

Both residual dose and luminescence sensitivity measurements were performed using a RISØ TL-DA-20 luminescence reader. A $^{90}Sr/^{90}Y$ βsource was used for irradiation, while an EMI ET9107 photomultiplier (PMT) with a Hoya U-340 filter was used for detecting the luminescence signal. The residual dose, i.e. the equivalent dose of modern samples was determined using the single aliquot regeneration (SAR) protocol (Wintle and Murray, 2006).

Sensitivity measurements were performed based on the procedures detailed in Bartyik et al. (2021). First, 5 aliquots from each sample were bleached by using blue LEDs to remove the natural signal. Then each aliquot received a uniform β-dose of 22 Gy. The luminescence response elicited by this dose was measured using the Continuous Wave OSL (CW-OSL) technique during which the LED power was always the same. Background was subtracted using the last 5 s of the decay curve. Results were then normalized by the mass of the samples, measured by an analytical scale. This normalized intensity was considered as the "normalized CW-OSL sensitivity" of the samples.

To examine the lithological background and to delineate the main surface lithological units, 1: 200 000 scale geological maps were used (Harta geologică a R. S. România, 1967). The catchment of the Mureş is covered by 15 map sheets, which were georeferenced using ESRI ArcMap. After georeferencing the map sheets, surface lithology was digitized. The proportion of different rock types was determined for the investigated subcatchments and compared to the luminescence sensitivity values obtained.

RESULTS AND DISCUSSION

Residual dose

Based on the SAR measurements, each sample had a low level of natural luminescence, meaning that grains were well bleached (Fig. 3A-B). In case of one sample (Sample 565 rkm) no curve could be fitted to the plot of laboratory doses and luminescence responses (dose response curve) (Fig. 3C-D). In case of the other samples fitting was successful, and obtained residual doses varied between 0.4 and 3.9 Gy, however results had a high standard error (Table 1). Thus, coarse grain paleo fluvial samples subjected to dating in the area can overestimate the true age of deposition by around 0.2-2.0 ka if a usual 2 Gy/ka dose rate is taken (Kiss et al., 2014; Tóth et al., 2017).

Comparing these results with the residual values measured nearly 417 km long Hungarian section of the Danube by Tóth et al. (2017), it can be seen that much higher values can be observed in the case of River Mureş. In his research the mean residual dose of coarse grain quartz was 0.1±0.01 Gy while the maximum value was only 0.56±0.17Gy, which cause a negligible overestimation between 60 and 120 y in the area. On the other hand, an overestimation of 1.2 -2.3 ka has already been found for the fine grain samples, which is similar to the Mureş coarse grain quartz values. Regarding that Danube, however, Fiebig and Preusser (2007) measured very high residual dose (around 6.1 Gy) in their research on the Vienna section, which were explained by anthropogenic effects.

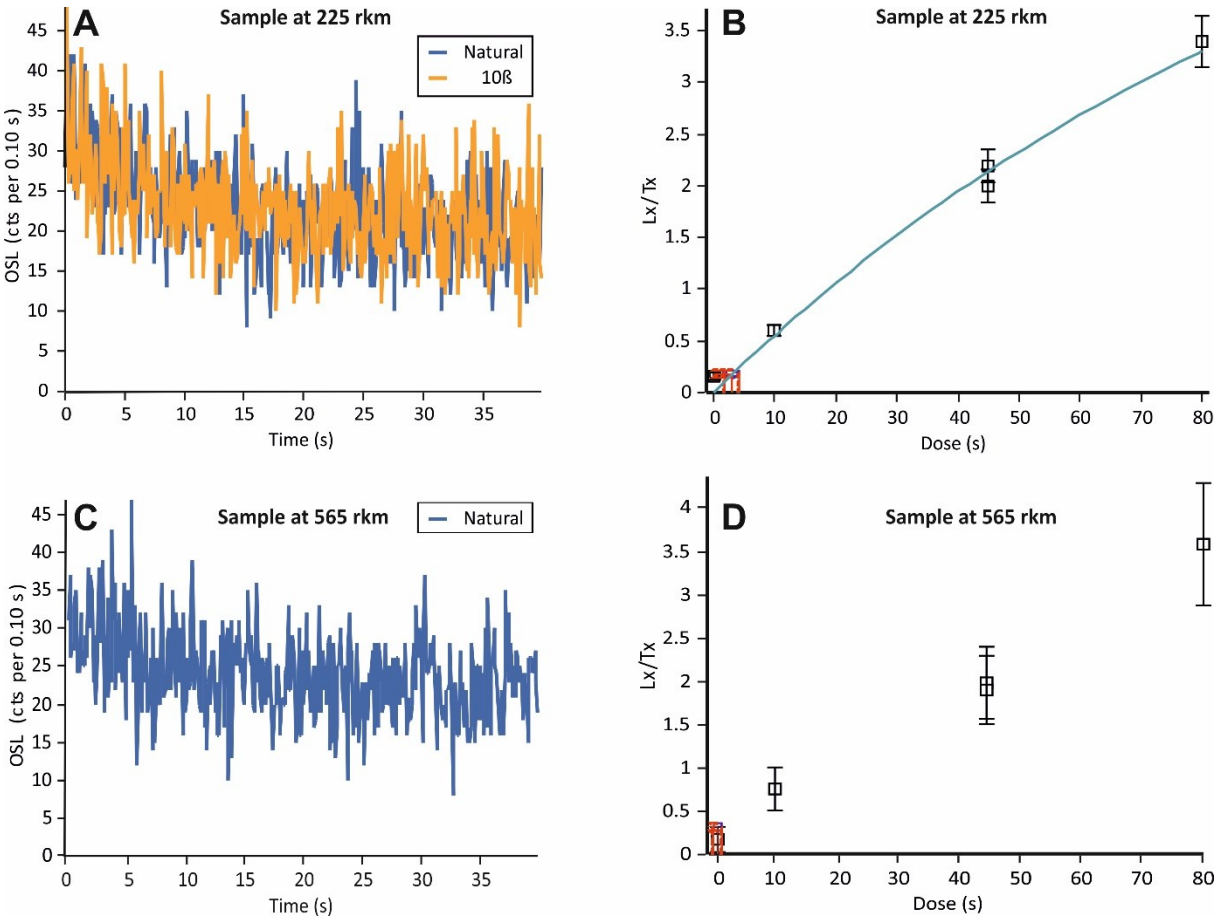

Fig. 3 Dose response curves of two samples. Sample 225 rkm sample (A, B) showed a typical decay with a low signal, while at 565 rkm (C, D) it can be seen that due to a signal close to 0 s, a line cannot be fitted to the data.

If residual doses are analyzed along the longitudinal profile of the river (Fig. 4 and Table 1) it is obvious that in general, there is a decreasing trend in residual dose values. It is in accordance with the fact that channel sediments should be reworked more times towards downstream, and therefore bleaching by sunlight can be more complete. However, local peaks can be observed, and tributaries also show different values. Upstream of the conjunction of River Arieș (Aranyos) the value of the measured residual dose is 2.07±0.60 Gy (Sample 491 rkm), and although the quartz grains of Arieș sediments have a highly variable residual dose they stay in the same range and seemingly do not affect significantly the values measured downstream of the confluence. The first and largest peak can be seen in case of Sample 448 rkm with a value of 3.88±0.79 Gy.

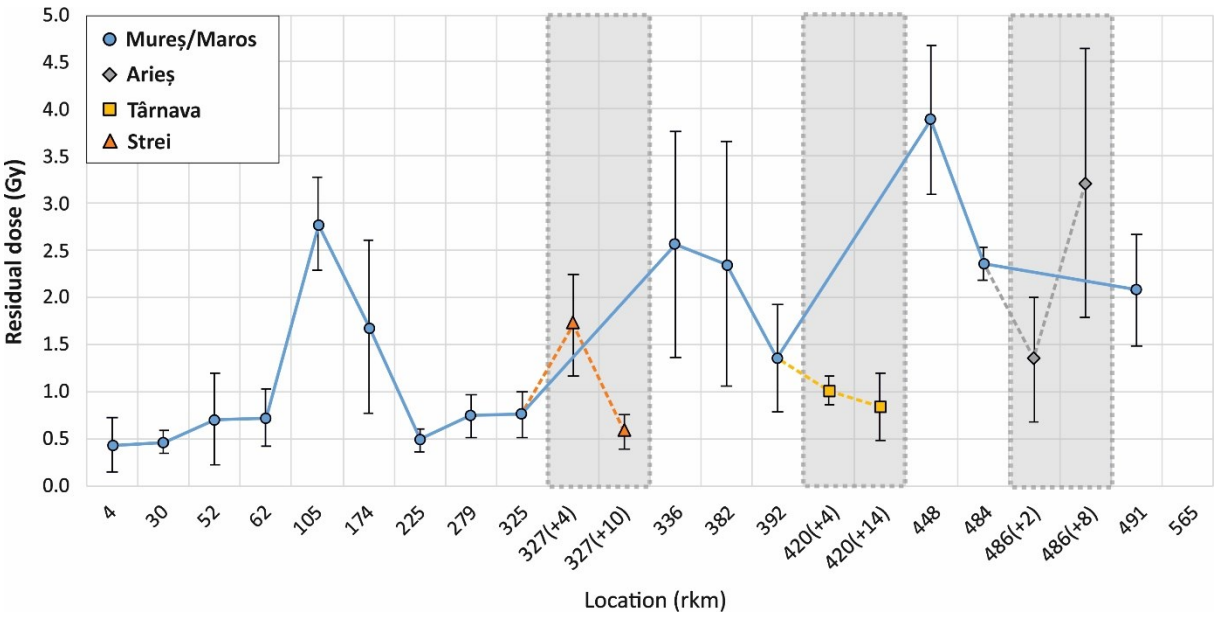

Fig. 4 Residual dose of the tested samples measured by CW-OSL technique.

The sampling site is located on reach where only very short tributaries, mostly arriving from the Apuseni Mountains, join the river, therefore the sediments cannot be resetted completely before reaching the Mureș (Fig. 1 and 4).

Compared to River Arieș the sediments of the Târnava (Küküllő) are bleached more completely and have a more uniform value (Fig. 4). It is possibly related to the fact that the longest tributary of the Mureș has a fairly low gradient, therefore channel sediments can go through several cycles of bleaching before arriving to the confluence zone. Seemingly, the mixing of low residual dose Târnava quartz grains reduces the residual dose level in the sediments of the main river as well, however, that the next sampling point (Sample 392 rkm) is 30 km downstream of the confluence (Fig. 4).

The second, moderate peak in residual dose values (2.56±1.20 Gy and 2.35±1.3 Gy at 382 and 336, rkm, respectively) can be observed downstream of the confluence of River Sebeş (Sebes) on a section where the Mureş is laterally eroding Cretaceous conglomerates and sandstones at the foothills of the Metaliferi Mountains (Fig. 1 and 4). Besides, on this section high gradient and short tributaries join the river, which can also explain the presence of less bleached grains in the sediment mixture. A similar phenomenon was identified by Tóth et al. (2017) along the Danube, where the erosion of loess bluffs resulted an order of magnitude increase in quartz residual doses. On the next 10 km (between 336 and 325 rkm) residual dose values drop by 60-70 %, which can hardly be explained solely by the natural bleaching of grains in the channel, but rather by the entering of River Strei (Sztrigy), which introduces low residual dose sediments to the main river (Fig. 4).

Low values persist till the Lipova Gate, where River Mureș enters the lowlands. Here a third peak of residuals appears, which might be explained either by extensive in-channel gravel mining, mostly on the Lipova section and downstream, and/or the natural erosion of Pleistocene deposits. Nevertheless, by reaching the distal part of the alluvial fan, residual doses decrease to their lowest values along the entire investigated reach (Fig. 4).

Luminescence sensitivity

The downstream change of luminescence sensitivity, that can be affected either by surface lithology or transportation distance show a similar pattern to that of residual dose values on the upstream reaches of River Mureș (Fig. 4 and 5). The first two quartz samples (Sample 565 rkm and 491 rkm) have practically an identical luminescence sensitivity (154±19 and 159±19 cts/mg/Gy). These values fit well to the mean luminescence sensitivity value of five Pleistocene age sediment samples (167±9 cts/mg/Gy) collected from various points on the alluvial fan of the river and investigated by Bartyik et al. (2021). Based on this, it could be expected that there is no significant variation in CW-OSL sensitivity values along the river.

Table 1 Summary of the measured data of quartz extracts. (In case of tributaries the location refers to the distance from the confluence with the Mureș.)

River	Location of sampling points (rkm)	Grain size (μm)	Residualdose (Gy)	Normalized CW-OSL sensitivity (cts/mg/Gy)
Mureș	4	90-300	0.44±0.29	124±22
	30	90-300	0.47±0.13	69±16
	52	90-300	0.71±0.48	37±5
	62	150-220	0.72±0.31	202±60
	105	150-220	2.78±0.49	179±47
	174	90-300	1.69±9.89	71±10
	225	90-150	0.48±0.12	322±34
	279	90-150	0.74±0.23	225±26
	325	90-150	0.74±.023	232±24
	336	90-150	2.56±1.20	132±7
	382	90-220	2.35±1.3	139±27
	392	150-220	1.35±0.57	124±7
	448	90-150	3.88±0.79	587±167
	484	90-220	2.36±0.18	305±72
	491	90-150	2.07±0.6	158±19
	565	90-150	no data	154±19
Arieș	486+2	90-150	1.34±0.66	204±13
	486+8	90-220	3.21±1.43	294±36
Târnava	420+4	90-220	1.01±0.16	146±22
	420+14	90-220	0.84±0.36	173±35
Strei	327+4	90-150	1.71±0.54	179±15
	327+10	150-220	0.57±0.18	118±18

However, values increase considerably going downstream, supposedly by the joining of River Arieș (Fig. 5), since the luminescence sensitivities of Arieș quartz samples are 204±13 cts/mg/Gy and 294±36 cts/mg/Gy and a very similar value is obtained just below the confluence as well (Fig. 5). This way, in the confluence zone the Arieș values almost double the level of quartz luminescence sensitivity. Moreover, at the next sampling site (448 rkm) the sensitivity reaches its maximum on the entire studied reach (Table 1). If surface lithology is considered, the upper catchment of the Mureș is dominated by erodible Neogene sedimentary rocks, and seemingly the quartz fraction of these has a moderate CW-OSL sensitivity. Although, the lower reaches of the Arieș flow across the same Neogene units, its headwaters are in the Apuseni Mountains and its catchment can be characterized by a complex lithology, comprised mostly of various igneous and metamorphic rocks, such as paragneiss, phillite, basalt and metasomatic granitoids (Fig. 1). Although, usually quartz originating from igneous and

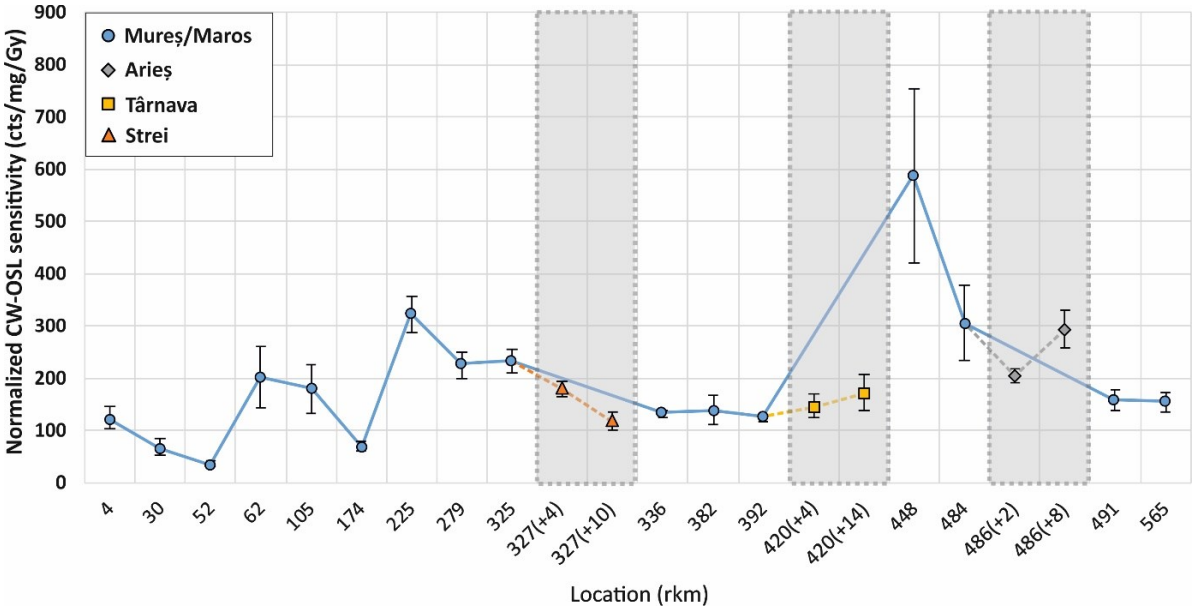

Fig. 5 Normalized CW-OSL sensitivity values of the tested samples.

metamorphic rocks has a relatively low luminescence sensitivity (Chithambo et al., 2007; Guralnik et al., 2015; Sawakutchi et al., 2018), on the other hand Sawakutchi et al. (2011) emphasized that high crystallization temperatures can its value increase. Considering these facts, granitoids affected by metasomatosis, and/or paragneisses metamorphosed from sedimentary rocks can be responsible for the experienced increase in luminescence sensitivity. However, the confirmation of this hypothesis needs further sampling in the area.

Nevertheless, it is also clear from the high standard error of these samples (Fig. 5, Table 1) that high sensitivity of quartz grains originated from the Arieș has limited effect on the overall values of Mureș sediments. This can be the reason for the observation that by the entering of Târnava CW-OSL sensitivity decreases to its original level. The catchment of this tributary is built up by the same Neogene sedimentary rocks as that of the Mureș, consequently, measured sensitivity values (146±22 and 173±35 cts/mg/Gy) are very similar (Fig. 5).

The high erosive capacity of the river, shown by the increase of residual doses downstream of the Târnava is not affecting sensitivity values, thus the quartz of Cretaceous conglomerates supposedly has a similar luminescence sensitivity as that of the Neogene sedimentary rocks. However, three samples (Sample 325, 279 and 225 rkm) collected downstream of the confluence of River Strei show an increasing trend again. Based on the luminescence sensitivity of quartz grains extracted from Strei sediments, this increase cannot be attributed unambiguously to the Strei itself (Fig. 5, Table 1). On the 100 km-long reach represented by the three samples no significant tributaries join the river, and residual doses showed a decreasing trend (Fig. 4). It refers to repeated bleaching of quartz grains. In these circumstances it is appealing to claim that sensitivity increase is due to geomorphological reasons. On the other hand, the jump in sensitivity just 2 rkm downstream of the Strei confluence and the lithological complexity found on both banks of River Mureş points to the possible role of geological reasons. Nevertheless, surface lithology on this section is mostly dominated by volcanic rocks such as andesite and basalt, renown of containing low sensitivity quartz in general (Sawakutchi et al., 2018), and as the most downstream sample of this section (Sample 225 rkm) has the lowest residual dose and the highest CW-OSL sensitivity (322±34 cts/mg/Gy) from all, the significance of geomorphic factors seems also inevitable.

In this sense, the remarkable drop in case of Sample 174 rkm (70±10 cts/mg/Gy) might refer to the mixing of external sediments, possibly as a consequence of in-channel quarrying and related erosion, as it was suggested on the basis of residual dose increase earlier (Fig. 4). It has to be noted also that this sample contained larger quartz grains than any other samples before (Table 1), and by the increased degree of self-absorption during OSL stimulation this may also contribute to reduced sensitivity values.

In case of the following samples (Sample 105 and 62 rkm) values tend to grow again (179±47 and 202±60 cts/mg/Gy), though with a high standard error, referring again to a nonuniform sensitivity of quartz grains. Since, on the basis of residual doses the mixing of palaeo-sediments is suggested on this section, sensitivity increase might be attributed to these. This draws the attention to the potential temporal change in the luminescence sensitivity of channel sediments. It can be explained either by the differential activity of subcatchments under glacial and interglacial climate regimes, or the dynamics of fluvial activity, i.e. the number of sedimentary cycles through which grains arrive to the alluvial fan.

To complicate the picture above, luminescence sensitivity values at the edge of the alluvial fan drop again (Sample 52 rkm) and reach their minimum

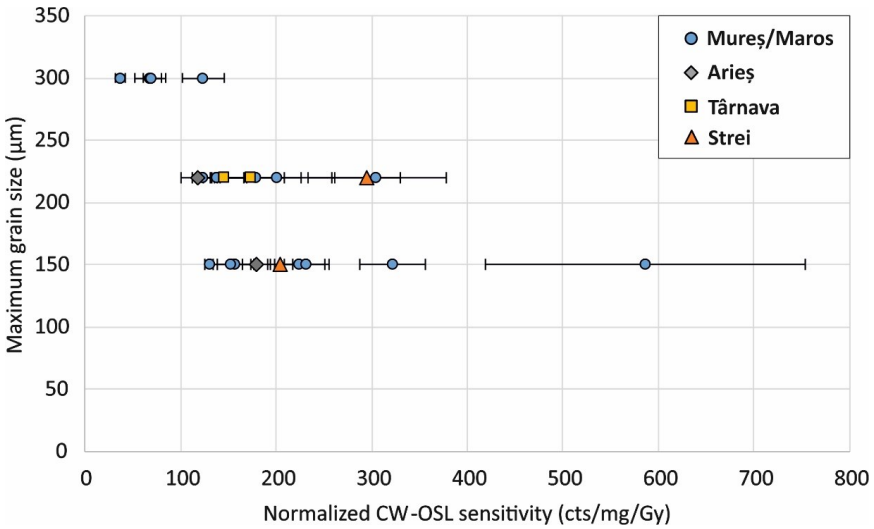

Fig. 6 CW-OSL sensitivity plotted against the maximum grain size of the investigated samples.

(37±5 cts/mg/Gy) on the entire studied section (Fig. 5, Table 1). Just like in the case of Sample 174 rkm, this and the following two samples are composed of larger quartz grains. Consequently, it seems that if maximum grain size of the investigated fraction is above 220 µm then measured values considerably decrease (Fig. 6). However, if fractions between 90-150 µm or 150-220 µm are compared then no such tendency can be identified. The analysis of this parameter needs further measurements on different fractions of the same sample.

CONCLUSIONS

The combined analysis of quartz OSL residual doses, luminescence sensitivity, surface lithology, grain size and transportation distance in terms of modern samples allowed to assess what factors may affect luminescence parameters at most, and if these can be applied late for sediment sourcing and the reconstruction of fluvial processes. In terms of both luminescence parameters it was clearly proven that subcatchment and river reach scale factors can highly influence the downstream variation of luminescence parameters.

Concerning OSL residual doses, in accordance with the general model, by the increase of transportation distance values show a decreasing tendency as a consequence of repeated bleaching. Based on the results, local and reach scale increase in values can be related to either 1) short tributaries carrying sediments undergone limited sedimentary cycles; 2) increased erosion of palaeo-sediments and sedimentary rocks by the main river; or 3) in-channel quarrying. All these processes introduce grains with a high palaeo-dose to the sediment mixture of the main river, which then increases the value of the measured residual dose.

Although, the length of the investigated river reach (565 km) was considerable, no clear downstream increase in luminescence sensitivity was observed as opposed to some previous research (Pietsch et al., 2008; Fitzsimmons, 2011). According to the data of the present study, sensitivity values showed local and reach scale increase in relation with 1) the inlet of Arieş sediments, partly produced from granitoids and paragneiss as opposed to the sediments of the Upper Mureş originating mostly from Neogene sedimentary rocks; 2) repeated sedimentary cycles on reaches where no significant tributaries join the river. Differences in surface lithology, therefore, do affect OSL sensitivity, but this can be used for sediment sourcing only in case of one out of the three investigated tributaries. Meanwhile, the role of transportation distance and sediment recycling cannot be unambiguously confirmed. A major reason for this, is that other parameters, such as the maximum grain size and related self-absorption of investigated quartz extracts can also affect the results. Moreover, especially on the lowland section of River Mureş unexpected drops in values were experienced, drawing attention to the significance of temporal differences in sediment dynamics and its potential effect on quartz luminescence sensitivity. Consequently, reliable sediment sourcing by the means of OSL sensitivity requires further investigations in the study area. However, as shown by the results, the combination of different luminescence properties can help in the assessment of both present and past fluvial processes.

ACKNOWLEDGMENTS

This work was supported by the Hungarian National Research, Development and Innovation Office [grant number: K119309 and K135793].

References

Aitken M. J. 1998. An Introduction to Optical Dating. Oxford University Press. London.

Baranyi V., Bakrač K., Krizmanić K., Botka D., Tóth E., Magyar I. 2021. Paleoenvironmental changes and vegetation of the Transylvanian Basin in the early stages of Lake Pannon (late Miocene, Tortonian). *Review of Palaeobotany and Palynology* 284, 104340. DOI: 10.1016/j.revpalbo.2020.104340

Bartyik T., Magyar G., Filyó D., Tóth O., Blanka-Végi V., Kiss T., Markovic S., Persoiu I., Gavrilov M., Mezősi G., Sipos Gy. 2021. Spatial differences in the luminescence sensitivity of quartz extracted from Carpathian Basin fluvial sediments. *Quaternary Geochronology* 64, 101166. DOI: 10.1016/j.quageo.2021.101166

Berger G. W. 1990. Effectiveness of natural zeroing of the thermoluminescence in sediments. *Journal of Geophysical Research* 95 (B8), 12375–12397. DOI: 10.1029/JB095iB08p12375

Bojar A.-V., Bojar H.-P., Ottner F., Grigorescu D. 2010. Heavy mineral distributions of Maastrichtian deposits from the Haţeg basin, South Carpathians: Tectonic and palaeogeographic implications. *Palaeogeography, Palaeoclimatology, Palaeoecology* 293 (3-4), 319–328. DOI: 10.1016/j.palaeo.2009.10.002

Borsy Z. 1989. Az Alföld hordalékkúpjainak negyedidőszaki fejlődéstörténete (The Quaternary development of the Great Hungarain Plain). *Földrajzi Értesítő* 38 (3-4), 211–224. (in Hungarian)

Bøtter-Jensen L., McKeever S. W. S., Wintle A. G. 2003. Optically Stimulated Luminescence Dosimetry. Elsevier Science, The Netherlands. ISBN: 0-444-50684-5

Chithambo M. L., Preusser F., Ramseyer K., Ogundare F.O. 2007. Time-resolved luminescence of low sensitivity quartz from crystalline rocks. *Radiation Measurements* 42 (2), 205–212. DOI: 10.1016/j.radmeas.2006.07.005

Collins A. L., Blackwell M., Boeckx P. et al. 2020. Sediment source fingerprinting: benchmarking recent outputs, remaining challenges and emerging themes. *Journal of Soils Sediments* 20, 4160–4193. DOI: 10.1007/s11368-020-02755-4

Fiebig M., Preusser F. 2007. Investigating the amount of zeroing in modern sediments of River Danube, Austria. *Quaternary Geochronology* 2 (1), 143–149. DOI: 10.1016/j.quageo.2006.09.001

Fitzsimmons E., Edward J. R., Timothy T. B. 2010. OSL dating of southeast Australian quartz: A preliminary assessment of luminescence characteristics and behaviour. *Quaternary Geochronology* 5 (2-3), 91–95. DOI: 10.1016/j.quageo.2009.02.009

Fitzsimmons E. 2011. An assessment of the luminescence sensitivity of Australian quartz with respect to sediment history. *Geochronometria* 38 (3), 199–208. DOI: 10.2478/s13386-011-0030-9

Fryirs K., Gore D. 2013. Sediment tracing in the upper Hunter catchment using elemental and mineralogical compositions: Implications for catchment-scale suspended sediment (dis)connectivity and management. *Geomorphology* 193, 112–121. DOI: 10.1016/j.geomorph.2013.04.010

Gemmell A. M. D. 1988. Zeroing of the TL signal in sediment undergoing fluvioglacial transport. An example from Austerdalen, Western Norway. *Quaternary Science Reviews* 7(3-4), 339–345. DOI: 10.1016/0277-3791(88)90026-1

Gliganic L. A., Cohen T. J., Meyer M., Molenaar A. 2017. Variations in luminescence properties of quartz and feldspar from modern fluvial sediments in three rivers. *Quaternary Geochronology* 41, 70–82. DOI: 10.1016/j.quageo.2017.06.005

Godfrey-Smith D. I., Huntley D. J., Chen W. H. 1988. Optical dating studies of quartz and feldspar sediment extracts. *Quaternary Science Review* 7 (3-4), 373–380. DOI: 10.1016/0277-3791(88)90032-7

Gray H. J., Jain M., Sawakuchi A. O., Mahan S. A., Tucker G. E. 2019. Luminescence as a sediment tracer and provenance tool. *Reviews of Geophysics* 57 (3), 987–1017. DOI: 10.1029/2019RG000646

Guralnik B., Ankjærgaard J. M., Murray A. S., Müller A., Wälle M., Lowick S. E., Preusser F., Rhodes E. J., Wu T.-S., Herman F. 2015. OSL-thermochronometry using bedrock quartz: a note of caution. *Quaternary Geochronology* 25, 37–48. DOI: 10.1016/j.quageo.2014.09.001

Harta geologică a R. S. România 1967. sc. 1:200.000, Institutul Geologic, Bucureşti.

Iancu V., Seghedi A. 2017. The South Carpathians: Tectono-Metamorphic Units related to Variscan and Pan-African inheritance. *Geo-Eco-Marina* 23, 245–262. DOI: 10.5281/zenodo.1197110

Kiss T., Sümeghy B., Hernesz P., Sipos Gy., Mezősi G. 2013. Az Alsó-Tisza menti ártér és a Maros hordalékkúp késő-pleisztocén és holocén fejlődéstörténete. (Late Pleistocene and Holocene development of the Lower Tisza floodplain and the alluvial fan of the River Maros). *Földrajzi Közlemények* 137, 269–277. (in Hungarian)

Kiss T., Sümeghy B., Sipos Gy. 2014. Late Quaternary paleodrainage reconstruction of the Maros River alluvial fan. *Geomorphology* 204, 49–60. DOI 10.1016/j.geomorph.2013.07.028

Kounov A., Schmid M. S. 2013. Fission-track constraints on the thermal and tectonic evolution of the Apuseni Mountains (Romania). *International Journal of Earth Sciences* 102, 207–233. DOI: 10.1007/s00531-012-0800-5

Laczay I. 1975. A Maros vízgyűjtője és vízrendszere (The catchment area and water system of the Mures). In: Csoma, J., Laczay, I. (ed.). Vízrajzi Atlasz Sorozat 19. kötet. Maros 1. fejezet. *Hidrográfia, geomorfológia.* Budapest, 4–6. (in Hungarian)

Li S. H., Wintle A. G. 1991. Sensitivity changes of luminescence signals from colluvial sediments after different bleaching procedures. *Ancient TL* 9, 50–54.

Li S. H., Wintle A. G. 1992. Luminescence sensitivity change due to bleaching of sediments. *Nuclear Tracks and Radiation Measurements* 20 (4), 567–573. DOI: 10.1016/1359-0189(92)90006-H

Lü T., Sun J. 2011. Luminescence sensitivities of quartz grains from eolian deposits in northern China and their implications for provenance. *Quaternary Research* 76 (2), 181–189. DOI: 10.1016/j.yqres.2011.06.015

Mauz B., Bode T., Mainz E., Blanchard H., Hilger W., Dikau R., Zöller L. 2002. The luminescence dating laboratory at the University of Bonn: Equipment and procedures. *Ancient TL* 20, 53–61.

Pál-Molnár E., Batki A., Ódri Á., Kiss B., Almási E. 2015. Geochemical implications for the magma origin of granitic rocks from the Ditrău Alkaline Massif (Eastern Carpathians, Romania). *Geologia Croatica* 68 (1), 51–66. DOI: 10.4154/GC.2015.04

Pietsch T. J., Olley J. M., Nanson G. C. 2008. Fluvial transport as a natural luminescence sensitiser of quartz. *Quaternary Geochronology* 3 (4), 365–376. DOI: 10.1016/j.quageo.2007.12.005

Preusser F., Ramseyer K., Sclücheter C. 2006. Characterisation of low OSL intensity quartz from New Zealand Alps. *Radiation Measurements* 41 (7-8), 871–877. DOI: 10.1016/j.radmeas.2006.04.019

Preusser F., Makaiko L. Chithambo, Götte T., Martini M., Ramseyer K., Sendezera J. E., Susino J. G., Wintle A. G. 2009. Quartz as a natural luminescence dosimeter. *Earth-Science Reviews* 97 (1), 184–214. DOI: 10.1016/j.earscirev.2009.09.006

Rendell H. M., Webster S. E., Sheffer N. L. 1994. Underwater bleaching of signals from sediment grains: New experimental data. *Quaternary Science Reviews* 13 (5-7), 433–435. DOI: 10.1016/0277-3791(94)90055-8

Sawakuchi A. O., Blair M. W., DeWitt R., Faleiros F. M., Hyppolito T. N., Guedes C. C. F. 2011. Thermal history versus sedimentary history: OSL sensitivity of quartz grains extracted from rocks and sediments. *Quaternary Geochronology* 6, 261–272. DOI: 10.1016/j.quageo.2010.11.002

Sawakuchi A. O., Guedes C. C. F., DeWitt R., Giannini P. C. F., Blair M. W., Nascimento Jr. D. R., Faleiros F. M. 2012. Quartz OSL sensitivity as a proxy for storm activity on the southern Brazilian coast during the Late Holocene. *Quaternary Geochronology* 13, 92–102. DOI: 10.1016/j.quageo.2012.07.002

Sawakuchi A. O., Jain M., Mineli T. D., Nogueira L., Bertassoli Jr. D. J., Häggi C., Sawakuchi H. O., Pupi F. N., Grohmann C. H., Chiessi C. M., Zabel M., Mulitza S., Mazoca C. E. M., Cunha D. F. 2018. Luminescence of quartz and feldspar fingerprints provenance and correlates with the source area denudation in the Amazon River basin. *Earth and Planet. Sci. Lett*. 492, 152–162. DOI: 10.1016/j.epsl.2018.04.006

Sawakuchi A. O., Rodrigues F. C. G., Mineli T. D., Mendes V. R., Melo D. B., Chiessi C. M., Giannini P. C. F. 2020. Optically Stimulated Luminescence Sensitivity of Quartz for Provenance Analysis. *Methods and Protocols* 3 (1), 6. DOI: 10.3390/mps3010006

Schumm, S. A. 1979. Geomorphic thresholds: the concept and its applications. *Transactions of the Institute of British Geographers* 4 (4), 485–515. DOI: 10.2307/622211

Sharma S. K., Chawla S., Sastry M. D., Gaonkar M., Mane S., Balaram V., Singhvi A. K. 2017. Understanding the Reasons for Variations in Luminescence Sensitivity of Natural Quartz Using Spectroscopic and Chemical Studies. *Proceedings of the Indian National Science Academy* 83 (3), 645–653. DOI: 10.16943/ptinsa/2017/49024

Silye L. 2015. Sarmatian foraminiferal assemblages from southern Transylvanian Basin and their significance for the reconstruction of depositional environments. Cluj-Napoca: Presa Universitară Clujeană. ISBN: 978-973-595-852-7

Sipos Gy., Kiss T., Tóth O. 2016. Constraining the age of floodplain levels along the lower section of river Tisza, Hungary. *Journal of Environment Geography* 9 (1-2), 39–44. DOI: 10.1515/jengeo-2016-0006

Urdea P., Sipos Gy., Kiss T., Onaca A. 2012. The Maros/Mureş (A Maros) In: Sipos. Gy. (ed.) Past, Present, Future of the Maros/Mureş River. (A Maros folyó múltja, jelene, jövője). Szegedi Tudományegyetem, Természeti Földrajzi és Geoinformatikai Tanszék, Universitatea de Vest din Timişoara, Departamentul de Geografie. 159–167

Smedley R. K., Buylaert J.-P., Ujvari G. 2019. Comparing the accuracy and precision of luminescence ages for partially bleached sediments using single grains of K-feldspar and quartz. *Quaternary Geochronology* 53, 101007. DOI: 10.1016/j.quageo.2019.101007

Tóth O., Sipos G., Kiss T., Bartyik T. 2017. Variation of OSL residual doses in terms of coarse and fine grain modern sediments along the Hungarian section of the Danube. *Geochronometria* 44 (1), 319–330. DOI: 10.1515/geochr-2015-0079

Walling D. E. 2013. The evolution of sediment source fingerprinting investigations in fluvial systems. *Journal of Soils Sediments* 13, 1658–1675. DOI: 10.1007/s11368-013-0767-2

Wintle A. G., Murray A. S. 2006. A review of quartz optically stimulated luminescence characteristics and their relevance in single-aliquot regeneration dating protocols. *Radiation Measurements* 41, 369–391. DOI: 10.1016/j.radmeas.2005.11.001

Wintle A. G., Adamiec G. 2017. Optically stimulated luminescence. Radiation Measurements signals from quartz: A review. *Radiation Measurements* 98, 10–33. DOI: 10.1016/j.radmeas.2017.02.003

Zheng C. X., Zhou L. P., Qin J. T. 2009. Difference in luminescence sensitivity of coarse-grained quartz from deserts of northern China. *Radiation Measurements* 44 (5-6), 534–537. DOI: 10.1016/j.radmeas.2009.02.013